MAY. - AUG. 2000
Volume VI Number II
ISSN 0859 144X

THE ASEAN JOURNAL OF RADIOLOGY

Published by The Radiological Society and
The Royal College of Radiologists of Thailand,
Bangkok, Thailand

Leading-Edge Technology and Power

Computed Tomography Systems

TOSHIBA

GLOBAL IMAGING • MEDICAL SYSTEMS

Toshiba developed helical scanning which has become the global standard for CT. Other firsts include the real-time reconstruction technology known as AspireCI and other patented innovations creating the heart of the CT scanner. Acting now as a leader in CT technology, Toshiba continues its climb to the top in the area of clinical results.

The half-second CT scanner features a totally new concept in which the gantry has a cylindrical structure. This combines with revolutionary new multislice technology to collect multiple slices simultaneously in a single scan. The result is amazing volume data in a short time over a broad range. The CT has extended its range from diagnosis to treatment, and is now active over a wide range that includes the head region, cardiovascular, lung and abdomen, and limbs. Toshiba will continue to chart new paths in CT technology with new advances.

- 1998 Achieves cumulative global total of 10,000 systems.
- 1998 Development of multislice helical technology and half-second helical CT.
- 1996 Development of subsecond helical CT.
- 1993 Development of AspireCI real time technology.
- 1987 Obtains patent in Europe for helical scanning.
- 1986 Obtains patent in U.S.A. for helical scanning.
- 1979 Starts research on helical technology.

Evolving Step by Step Towards Tomorrow

Half-Second Real-Time Helical CT

- By creating the world's first 0.5 second full scan, Toshiba has realized use in the cardiac region.
- Toshiba has also realized 12 frame/second real-time reconstruction and 0.5 second/frame high-speed reconstruction.
- Equipped with highly definitive 3D display software.
- Designed for multislice technology.

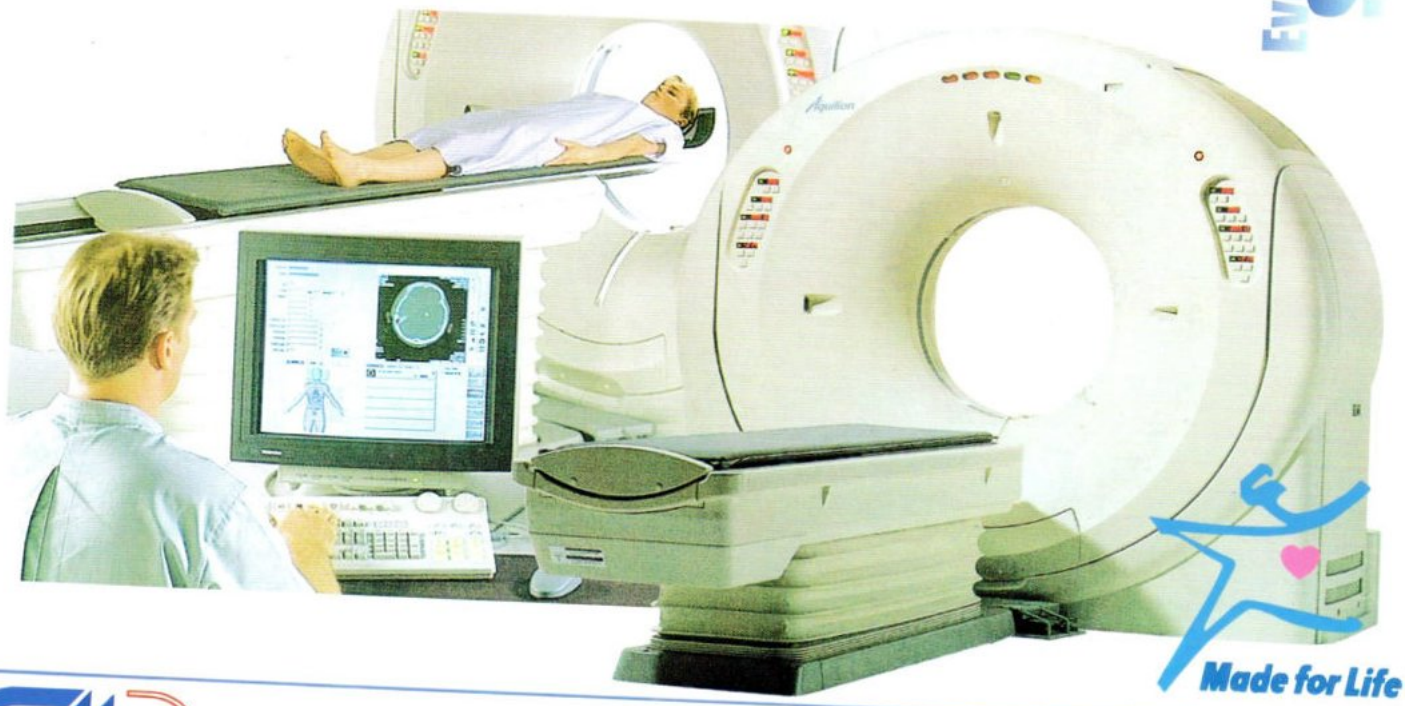

Made for Life

CMC BIOTECH

(SOLE DISTRIBUTOR)

CMC BIOTECH CO., LTD.

364 Muban Town-in-Town, Soi Ladphrao 94, Ladphrao Road, Wangthonglang, Bangkok 10310

Tel.(662) 530-4995-6, 559-2179-80, 538-4102, 538-0710, 559-3261-2 Fax: 539-6903

MAY. - AUG. 2000
Volume VI Number II

ISSN 0859 144X

THE ASEAN JOURNAL OF RADIOLOGY

**Published by The Radiological Society and
The Royal College of Radiologists of Thailand,
Bangkok, Thailand**

Started through an educational grant from

1955

Chief Editor

Professor Kawee Tungsubuttra
Kaweevej Hospital, 318 Taksin Road, Dhonburi, Bangkok 10600, Thailand.

Nippon Electric Glass Co., Ltd.
Radiation Shielding Lead Glass

- ☐ Observation window for CT scanning room
- ☐ Observation window for angiography room
- ☐ Observation window for X-ray diagnosis room

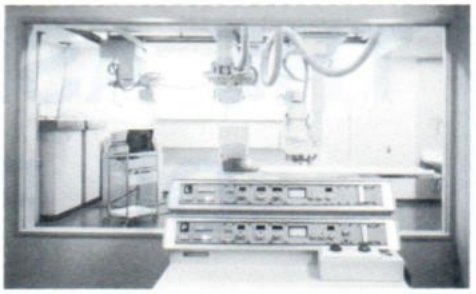

จำหน่าย กระจกตะกั่วกันรังสี แผ่นตะกั่วเรียบหนา 1 มม.-10 มม. รับกรุแผ่นตะกั่วที่ผนังห้องเอ็กซเรย์ รับทำบานประตูไม้อัด ประตูเหล็กบุแผ่นตะกั่ว ยินดีให้คำชี้แนะ

สอบถามได้ที่

ผู้แทนจำหน่ายในประเทศไทย

ห้างหุ้นส่วนจำกัด วิมิตรกิจ เอ็นจิเนียริ่ง
VIMITKIJ ENGINEERING LTD., PART.

42 ซอย 96/3 ถ.จรัญสนิทวงศ์ บางอ้อ เขตบางพลัด กทม. 10700

42 CHARANSANITWONG 96/3, BANG-AW, BANGPLAT, BANGKOK 10700

☎ **(02) 424-9775, 424-1009, 424-0977**

FAX : **435-7870, 424-1009**

E-mail : napana@access.inet.co.th

THE ASEAN JOURNAL OF RADIOLOGY

Volume VI Number II MAY. - AUG. 2000

CONTENTS

THE ASEAN JOURNAL OF RADIOLOGY

Volume VI Number II MAY. - AUG. 2000

CONTENTS

TECHNETIUM-99M SESTAMIBI (^{99M}TC MIBI) SINGLE-PHOTON EMISSION COMPUTERIZE TOMOGRAPHY IN THE DETECTION OF NASOPHARYNGEAL CARCINOMA

Sunanta CHIEWVIT, MD.[1] Supatra SANGRUCHI, MD.[2] Vutisiri VEERASARN, MD.[2] Nan SUNTORNPONG, MD.[2] Mongkol UIPRASERTKUL, MD.[3] Ruentip TIPPAROJ, B.sc.[1] Vacharin RATANAMART, MD.[1]

ABSTRACT

Nasopharyngeal carcinoma is a radiosensitive tumor. Recurrence after radiotherapy is a common cause of treatment failure. Early diagnosis and accurate identification of residual/ recurrent disease are essential for proper patient management. It is radiobiologically necessary to booster the irradiation dose or using combined therapy for the persistent tumor after the initial course of radiotherapy. CT and MRI cannot be used in the evaluation of response to therapy in NPC. Positron Emission Tomography (PET) have proved to be valuable as metabolic imaging tracer, however, their restricted availability and high cost are inherent limitations to their uses. We evaluated ^{99m}Tc MIBI in identifying primary tumor, neck node metastases, distance metastasis and recurrence of the diseased after therapy in NPC patients. The sensitivity and specificity in identifying primary tumor were 100% and 33% respectively. ^{99m}Tc MIBI scintigraphy can detect neck nodes metastasis 13 of 15 cases. One case of lung metastases and two cases of liver metastases can be detected by ^{99m}Tc MIBI scintigraphy in our study. The sensitivity and specificity in identifying recurrence or residual tumor in pre and post treatment group and post-treatment group were 100%, 80% and 100%, 60% respectively.

The incidence of of nasopharyngeal carcinoma (NPC) in statistical report 1997 from Tumor Registry Siriraj Cancer Center is 3.11 %[1] of all cancer. NPC is a potentially curable disease using combined modality treatment. Radiotherapy is the primary treatment modality for all locally and regionally confined stages. Systemic chemotherapy has been added to radiotherapy in locoregionally advanced and systemic metastasis diseases. Follow up after treatment of NPC are important in improving of survival rates. Early diagnosis and accurate identification of residual/ recurrent disease in patient with NPC are essential for proper patient management. Proper assessment of primary and metastatic NPC requires clinical/ fiberoptic examination followed by biopsy. Computed tomography (CT) or Magnetic resonance imaging (MRI) are the imaging to outline the anatomical planes involved by disease. CT/ MRI is the investigation of choice for accurate locoregional staging at initial presentation. CT cannot differentiate between inflammation, post-radiation fibrosis and recurrent disease. Although MRI may be useful in distinguishing between radiation fibrosis and recurrent disease, inflammatory changes and infection may simulate tumor recurrence. The presence of residual masses is 45% - 65% of

[1] Division of Nuclear Medicine, Department of Radiology, Faculty of Medicine, Siriraj Hospital, Mahidol University.
[2] Division of Radiotherapy, Department of Radiology, Faculty of Medicine, Siriraj Hospital, Mahidol University.
[3] Department of Pathology, Faculty of Medicine, Siriraj Hospital, Mahidol University. Bangkok Thailand, 10700.

patients after therapy.[2] Incomplete eradication of locoregional disease results in further tumor growth and mutation that may lead to high metastatic propensity. It is radiobiologically necessary to retreat persistent tumors after the initial course of radiotherapy.[3] The target volume and required radiation dose will be smaller.[4,5] Thus more precise imaging modalities that could be used as a gold standard for differentiating viable tumor from post-therapy changes may detect those patients requiring additional therapy so that both unnecessary further treatment options and suboptimal therapy can be avoided. Unnecessary further treatment may cause early or late morbidity that can significantly reduce patient's quality of life. Positron emission tomography (PET) tracers such as fluorine-18-fluorodeoxy-glucose and carbon-11 methionine have proved valuable as metabolic imaging tracer, however, their restricted availability and high cost are inherent limitations to their uses.[6,7] Technetium 99m methoxyisobyltyl isonitile (^{99m}Tc MIBI) and Thallium-201 (Tl-201) single photon emission computerize tomography (SPECT) were accurated in detecting regional recurrence and distance metastasis.[8] ^{99m}Tc MIBI is taken up by cancer cells by an active transport mechanism and stored in the mitochondria and cytoplasm. Mitochondrial and plasma membrane potentials of tumor cell, and cellular mitochondrial content can play a significant role in tumor uptake of ^{99m}Tc MIBI or uptake may be caused by an indirect phenomenon such as increased tumor blood flow and capillary permeability.[9] The study evaluated ^{99m}Tc MIBI as a potential agent for the diagnosis of primary tumors, lymph node metastases, distance metastases and local recurrence in nasopharyngeal carcinoma.

MATERIALS AND METHODS

PATIENTS

Thirty-three patients with histologically proven nasopharyngeal cancer and 3 patients with histologically proven metastatic squamous cell carcinoma to neck nodes were included in the study. Six patient were studied in both pre and post treatment. There were 22 patients studied prior to radiation treatment only. Eight patients were studied after treatment. The detail statuses of the patients were presented in table 1

Table 1 The detail status of the patients in 3 groups (pre and post treatment group, pre treatment group, and post treatment group)

Group	Sex		Histologic cell type		mean age (year)
	Male (case)	Female (case)	Squamous cell carcinoma (case)	Undifferentiated carcinoma (case)	
Pre and post treatment	4	3	2	5	42.86
Pre-treatment	16	5	11	10	42.38
Post- treatment	5	3	2	6	55.50

IMAGING STUDIES

All studies were performed on a Toshiba SPECT digital gamma camera GCA-901A , equipped with a low-energy high-resolution collimator. All patients underwent dynamic blood flow, static image, whole body and SPECT of head and neck following the administration of 20 mCi of ^{99m}Tc MIBI. The SPECT was performed in a step and shoot mode at 360° for 64 frames with

an imaging time 30 sec/view.

INTERPRETATION

Physiologic uptake in the head and neck area was noted in the pituitary gland, nasal and oral cavity, parotid, submandibular and sublingual salivary glands. Any uptake other than physiologic uptake was considered positive for primary or residual/recurrent or metastatic disease depending on the location of uptake.

RESULT OF ^{99M} TC MIBI FOR NASOPHARYNGEAL CANCER

Table 2 The result of pre and post treatment group.

STUDY	SEX	AGE (YEAR)	CELL TYPE	SCAN FINDING			RESULT OF BIOPSY	T.N.M. status
				PRIMARY	NECK NODE	DISTANCE METASTASIS	-	
1-1	M	43	Undiff CA	+	+	-	+	
1-2	M	43	Undiff CA	-	-	-	-	
2-1	F	33	Squamous cell CA	+	+	-	+	T1N2aMx
2-2	F	33	Squamous cell CA	+	+(improve)	-	-	
3-1	M	43	Undiff CA	+	+	-	+	T4N3Mx CT : NPC with lymphadenopathy
3-2	M	43	Undiff CA	+	-	-	+	Squamous cell CA (post Px)
4-1	F	48	Undiff CA	+	-	Lung	+	T4N1M1 CXR positive
4-2	F	48	Undiff CA	+	-	Lung	+	CT +
5-1	M	36	Squamous cell CA	+	+	-	+	T1N2bMx bone scan: multiple bone metastasis
5-2	M	36	Squamous cell CA	-	-	-	-	
6-1	M	49	Undiff CA	-	-	-	+	
6-2	M	49	Undiff CA	-	-	-	-	
7-1	F	48	Undiff CA	+	+	-	+	T2N1M0
7-2	F	48	Undiff CA	-	-	-	-	

Table 3 The result of pre-treatment group.

STUDY	SEX	AGE (YEAR)	CELL TYPE	SCAN FINDING			RESULT OF BIOPSY	T.N.M.status
				PRIMARY	NECK NODE	DISTANCE METASTASIS		
1	M	79	Squamous cell CA	+	-	Liver	+	CT: suggested multiple liver metastasis T2N2 Mx
2	F	47	Undiff CA	+	-	-	+	
3	F	33	Squamous cell CA	+	+	-	+	CT: NPC with intracranial extension, lymph node negative.
4	F	31	Squamous cell CA	+	+	-	+	Bilat. Lymphadenopathy rt. 1.5 lt. 4cm.
5	M	23	Undiff CA	+	+	-	+	loss radiation treatment
6	M	61	Undiff CA	+	+	-	+	T1N3M1 loss radiation treatment
7	M	30	Meta. Undiff CA	-	+	-	-	CT: no mass at nasopharynx, multiple lymphadenopathy jugular chain.
8	M	51	Meta.squamous cell CA	+	-	-	-	study post cervical LN biopsy, scalp : squamous cell CA
9	M	23	Undiff CA	+	+	-	+	T3N1M0
10	F	35	Undiff CA	+	+	-	+	
11	M	49	Undiff CA	+	+	-	+	
12	F	47	Undiff CA	+	-	-	+	
13	M	66	Meta. Squamous cell CA	+	+	-	-	biopsy at nasopharynx is negative CT: bilat. NPC, enlarge left cervical node.
14	M	41	Undiff CA	+	+	-	+	T3N3Mx
15	M	15	Squamous cell CA	+	+	-	+	T2N2Mx
16	M	46	Undiff CA	+	+	Liver	+	T4N2M1 U/S multiple liver meta, Bone scan multiple bone meta
17	M	36		+	+	-	+	
18	M	48	Squamous cell CA	+	+	-	+	T4N2bMx
19	M	24	Squamous cell CA	+	+	-	+	
20	M	56	Squamous cell CA	+	+	-	+	
21	M	49	Squamous cell CA	+	-	-	+	

Table 4 The result of post-treatment group.

STUDY	SEX	AGE (YEAR)	CELL TYPE	SCAN FINDING			RESULT OF BIOPSY	T.N.M.status
				PRIMARY	NECK NODE	DISTANCE METASTASIS		
1	M	63	Undiff CA	+	-	-	-	MRI: positive tumor mass at base of skull
2	M	61	Undiff CA	+	+	-	-	Lt. LN 3Cm.
3	M	60	Undiff CA	+	-	-	+	
4	F	43	Undiff CA	-	-	-	-	
5	M	72	Undiff CA	+	+	-	+	biopsy at neck node and primary :recurrent NPC
6	F	58	Squamous cell CA	+	+	-	+	
7	F	38	Squamous cell CA	-	-	-	-	
8	M	49	Undiff CA	-	-	-	-	

Table 5 The Statistical analysis in the pre-post treatment group, pre-treatment group and post treatment group

Group of patients	True positive (case)	True negative (case)	False positive (case)	False negative *(case)	Total (case)
Pre and post treatment group	2	4	1	-	7
Pre treatment group	18	1	2	-	21
Post treatment group	3	3	2	-	8

*There were no false negative studies for primary disease

Table 6 The Sensitivity and specificity of pre and post treatment group, pre-treatment group and post treatment group.

Study	Cases	Sensitivity %	Specificity %
Pre and post treatment group	7	100	80
Pre treatment group	21	100	33
Post treatment group	8	100	60

Table 7 The comparative sensitivity and specificity of our study and Lale et al. study.

		No of patients	Sensitivity %	Specificity %
Lale Kostakoglu[11]	3 month F/U	5	100	85
	6 month F/U	3	100	93
Sunanta	3-9 month F/U	6	100	80
Lale Kostakoglu[10]	Pre-treatment	22	100	67
	Post-treatment	16	100	67
Sunanta	Pre-treatment	22	100	33
	Post-treatment	8	100	60

Fig. 1,2 Case of undifferentiated nasopharyngeal carcinoma,

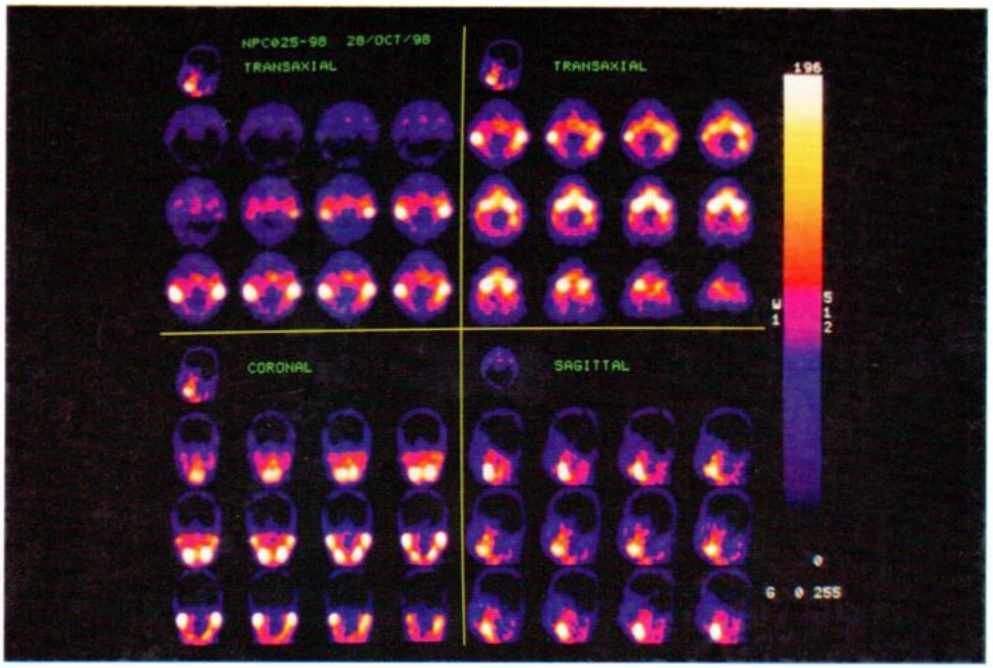

Fig. 1 (pre-treatment) reveals increased uptake of the radioactivity at left nasopharynx.

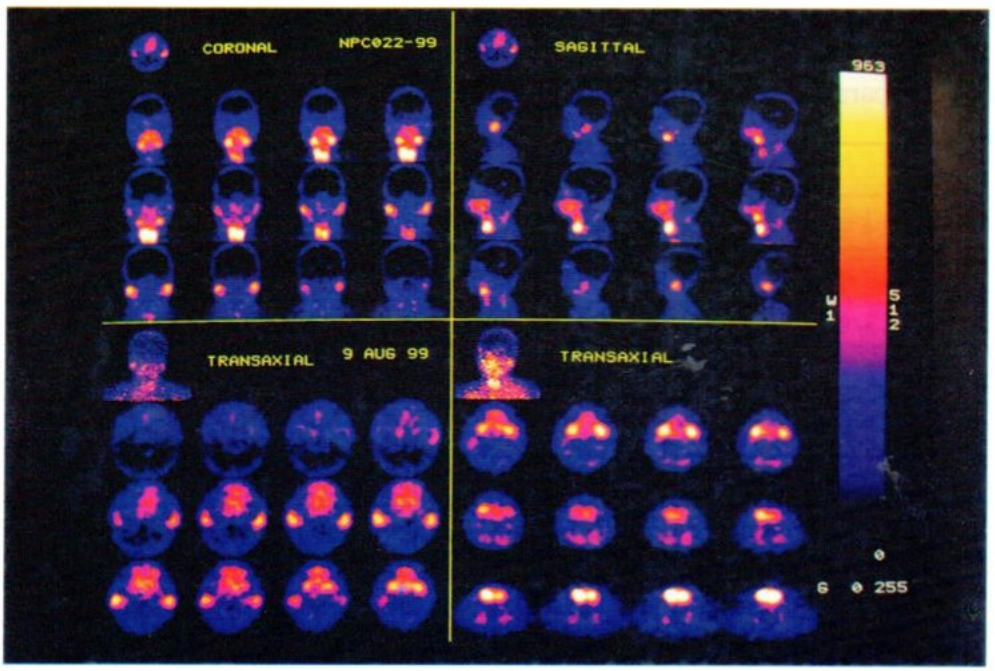

Fig. 2 (post-treatment) shows no abnormal increased uptake at nasopharynx.

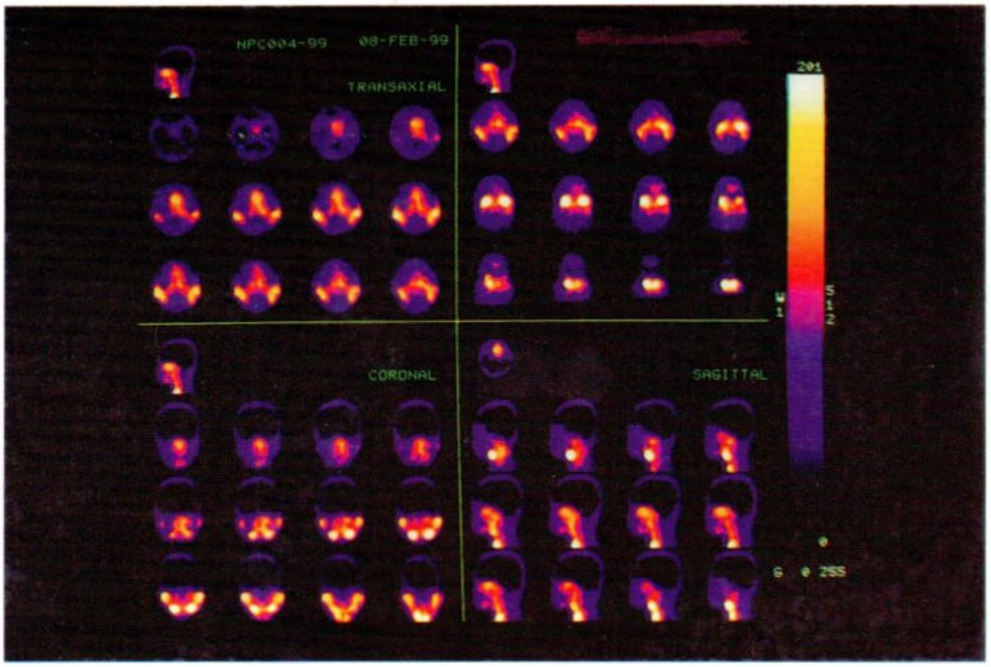

Fig. 3 Case of squamous cell nasopharyngeal carcinoma reveals increased uptake of the radioactivity at nasopharynx. There are multiple areas of increased uptake of the radioactivity at both upper cervical nodes.

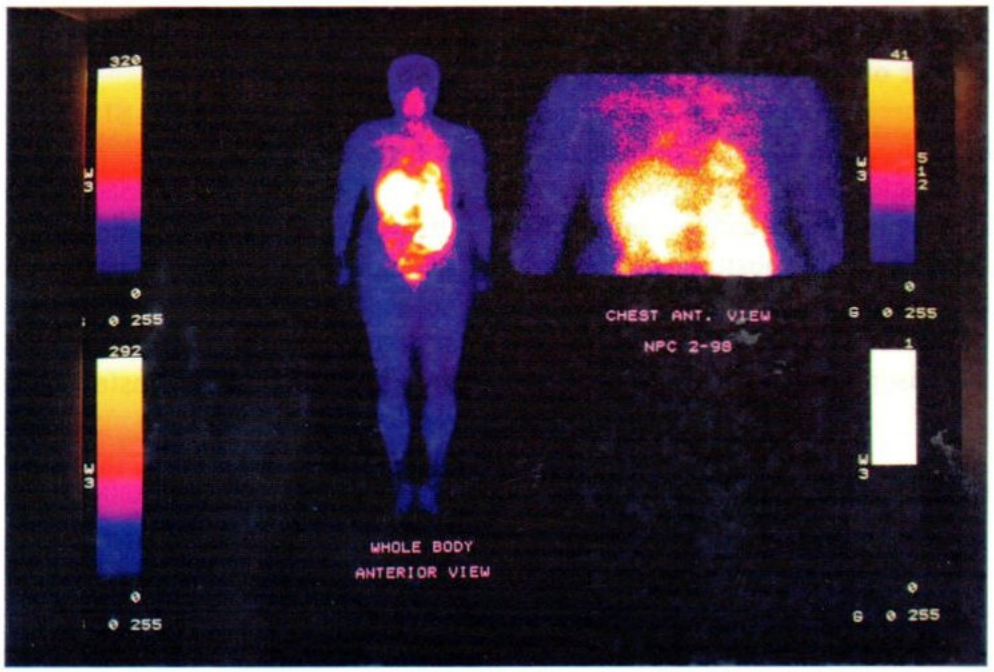

Fig. 4 Whole body image shows increased uptake of ^{99m}Tc MIBI at right chest. CA Nasopharynx with lung metastasis is suggested.

Fig. 5 Multiple areas of decreased uptake of the tracer in the liver compatible with liver metastases

The result of the study is based on histological confirmation. There were no false-negative studies for primary cancer in pre and post treatment group, pre-treatment group, and post-treatment group. Four of five cases of false positive finding in the three groups of our study were chronic inflammation in histological diagnosis. Chronic inflammation could be postulated that the high blood flow might account for the positive finding. One case of the positive finding was squamous cell carcinoma of scalp with neck node metastasis. Two of five cases with negative histology had nasopharyngeal mass by CT and MRI.

NECK NODES METASTASIS

We evaluated 15 cases of known cases of Nasopharyngeal Carcinoma with neck node metastases. ^{99m}Tc MIBI scintigraphy detected 13/15 cases of the metastatic lymph nodes, missing two cases which were possibly obscured by the physiologic uptake in the adjacent salivary glands. Lale et al.[11] studied in 18 cases of nasopharyngeal cancer with neck nodes metastasis and found a sensitivity of 94.7%. There was no true negative study to determine specificity.

DISTANCE METASTASIS

One case of lung metastasis and two cases of liver metastasis can be detected by ^{99m}Tc MIBI scintigraphy. Two cases of positive bone scan were not seen by ^{99m}Tc MIBI scintigraphy. Bone scan is superior than ^{99m}Tc MIBI scintigraphy in the detection of bone metastasis. False-negative results obtained for bone metastases may be due to the lower extraction fraction of radiotracer by the skeletal or obscured by the physiologic uptake in the adjacent organ such as liver, bowel and urinary bladder.

DISCUSSION

Nasopharyngeal carcinoma is a radiosensitive tumor. Recurrence after radiotherapy is a

common cause of treatment failure.[5] Incomplete eradication of loco-regional disease results in further tumor growth and mutation that may lead to high metastasis propensity. It is radiobiologically necessary to booster the radiation doses or combined therapy for the persistent tumor after the initial course of radiotherapy. Histological confirmation is the currently approved gold standard for the present of residual tumor, however biopsy may be misleading due to sampling errors. Therefore a specific functional imaging (Tl-201, ^{99m}Tc MIBI) modality is important to differentiate physiologic from pathologic uptake in NPC. The limitation of ^{99m}Tc MIBI scintigraphy is physiologic uptake at salivary glands, nasal and oral cavity and false positive study in chronic inflammation ^{99m}Tc MIBI could detect metastasis in the lymph node and distance metastasis. ^{99m}Tc MIBI scintigraphy is useful in the detection of distance metastases such as lung and liver metastases. Cold nodules were seen in case of liver metastases. Bone scan is superior than ^{99m}Tc MIBI scintigraphy in the detection of bone metastasis. MIBI is recognised as a transport substrate of P-glycoprotein, which is encoded by multidrug-resistance gene. Lale et al[10] reported no influence of P-glycoprotein pump on MIBI accumulation. There was no patient whose disease had progressed over the duration of 12-15 month when MIBI was negative.

CONCLUSION

^{99m}Tc MIBI scintigraphy was found to be sensitive in detecting residual/ recurrent tumor, lymph nodes and distance metastases. Therefore, ^{99m}Tc MIBI scintigraphy may be incorporated after therapy to evaluate the persistent masses or confirmation of diagnosis in case of false negative biopsy caused by sampling error.

ACKNOWLEDGMENT

The authors are indebted to Syncor International for providing ^{99m}Tc MIBI.

REFERENCE

1. Tumor registry Siriraj cancer center. Statistical report 1997. Faculty of Medicine, Siriraj Hospital Mahidol University: page 3
2. International Nasopharynx Cancer Study Group VUMCA I Trial preliminary results of a randomized trial comparing neoadjuvant chemotherapy (cisplatin, epirubicin, bleomycin) plus radiotherapy versus radiotherapy alone in Stage IV (≥N2, M0) undifferentiated nasopharyngeal carcinoma a positive effect on progression free survival. Am J Radiat Oncol Biol Phys 1996;35:463-469.
3. Taifu L. Trend in the clinical management of NPC. Int J Radiat Oncol Biol Phys 1992; 23:469-471.
4. Wither HR, Peter s LJ. Basic principles of radiotherapy: biological aspects of radiation therapy. In: Fletcher GH, ed. Textbook of radiotherapy, 3rd edn. Philadelphia: Lea and Febiger.1980:103-108.
5. Sham JST, Wei WI, Kwan WH, Chan CW, Kwong WK, Choy D. Nasopharyngeal carcinoma: pattern of tumor regression after radiotherapy. Cancer 1990;65:216-220.
6. Rege S, Maas A, Chaiken L. et al. Use of positron emission tomography with fluorodeoxyglucose in patients with extracranial head and neck cancers. Cancer 1994;73: 3047-3058.

7. Lindholm P, Leskinen-Kallio, Grenman R. et al. Evaluation of response to radiotherapy in head and neck cancer by positron emission tomography and (^{11}C) methionine. Int J Radiat Oncol Phys 1995; 32:787-794.
8. Abdel-Dayem H, Scott AM. Macapinlac HA, El- Gazzar AH, Larson SM. Role of Tl-201 chloride and Tc-99m-sestamibi in tumor imaging. In: Freeman LM, ed. Nuclear medicine annual. New York: raven press; 1994:181-234.
9. Cumali Aktolun, Hikmet Bayhan, and Metin Kir. Clinical Experience with Tc-99m MIBI imaging in patients with malignant tumors preliminary results and comparison with Tl 201. Clin Nucl Med 1992;17:171-176.
10. Lale Kostakoglu, Ugur Uysal, Enis Ozyar et al. A comparative study of technetium-99m sestamibi and technetium-99m tetrofosmin single-photon tomography in the detection of nasopharyngeal carcinoma. Eur J Nucl Med 1997;24:621-628.
11. Lale Kostakoglu, Ugar Uysal, Enis Ozyar et al. Monitoring response to therapy with Thallium-201 and Technetium-99m-sestamibi SPECT in nasopharynxgeal carcinoma. J Nucl Med 1997; 38: 1009-1014.

CHILDHOOD THYROTOXICOSIS

Dr. M.A. TAHER[1]

ABSTRACT

Most of the thyrotoxic patients are adult and it is rare (about 1% of adult) in childhood. This rarity prompts us to report these two cases (both girl, age 10 & 12 years) found recently, confirmed by radioiodine uptake (RAIU), radioassay of thyroid related hormones (T_3, T_4 TSH levels) and both of them had been followed upto clinical cure by carbimazole and radioiodine (I-131) therapy.

CASE REPORTS

(1) A young girl aged 12 years, referring from Lalmonirhat Al-Nahiyan Shishu Paribar (Orphanage) on 22-09-93 complained of palpitations, weight loss inspite of increased appetite, insomnia and trembling. On examination, her pulse rate was 120min, both eye-balls were protruded (bilateral exophthalmos), skin was warm and moist, thyroid gland was enlarged diffusely (grade 1b), radioiodine uptake (RAIU) was high with rapid turnover, (2h 20%, 24h 46%, 48h 30%) radioimmunoassay of thyroid hormones (T_3 = triiodothyronine, T_4 = thyroxine) showed elevated serum levels (Table-1). She was treated with carbimazole 10mg/day up to 29-11-96 with little improvement, then she was given radioiodine (I-131) therapy (5mCi) and was found euthyroid on 06-06-97. Long - term follow-up is being done.

(2) Another girl aged 10 years from Adorshapara, Rangpur complained of generalized weakness, palpitations, insomnia and trembling. On examination, her pulse rate was 128/min. both eye-balls were slightly prominent, skin was warm, thyroid gland was slightly enlarged (grade 1a.) Her thyroid hormone levels (T_3, T_4) were high and thyrotropin (thyroid stimulating hormone, TSH) level was low (Table-1). She was treated with carbimazole 20mg/day, evaluated several times and gradually tapered down over about six months (Sep. 94 to Feb. 95) & now confirmed euthyroid by RIA and clinical examinations (T_3 = 2.67 nmol/L, T4 = 104.7 nmol/L). Long - term follow-up is being done.

Table-1 Hormone levels*

Pt. No.	T_3 normal ranges 0.8--2.7 n mol/L	T_4 normal ranges 62--165 n mol/L	TSH normal ranges 0.48--4.8 μ IU/ml
01.	11.2	320	--------
02.	13.8	240	<0.2

* Done at N.M.C. Dinajpur.

[1] Director. Nuclear Medical Center, Post Box No. -16. Rangpur-5400 Bangladesh

DISCUSSION

Most of the northern districts of Bangladesh are iodine-deficient and endemic goitre area.

Cretinism (congenital hypothyroidism) are widely prevalent, but the clinicians should be aware that some children even on the contrary may be thyrotoxic (hyperthyroid) even,[1] as demonstrated in the present cases. Older textbooks mentioned that children and adolescents should not be treated with radioiodine for thyrotoxicosis, but recent research works are in favour of radioiodine therapy,[2-6] rather antithyroid drugs may give rise to serious adverse reactions which may reach as high as 40% in children and the incidence of surgical complications is higher than other modalities.[7] Leukemia and other cancers apparently do not increase after radioiodine treatment.[8] Long - term follow-up is important to check recurrence of hyperthyroidism and/or hypothyroidism.

REFERENCES

1. Galaburda M, Rosman NP, Haddow JE : Thyroid storm in an 11-year old boy managed by Propranolol. Pediatrics 53: 920-922, 1974.
2. Safa AM, Schumacher OP, Rodriguez-Antunez A : Long term follow-up results in children and adolescents treated with radioactive iodine for hyperthyroidism. N. Eng. J. Med. 292:167-171, 1975.
3. Starr P, Jaffe HL, Oetinger L Jr. : Later results of 131-I treatment of hyperthyroidism in 73 children and adolescents : 1967 follow-up. J Nucl Med 10:586-590, 1969.
4. Becker DV : The role of radioiodine treatment in childhood hyperthyroidism. J Nucl Med 20:890-892, 1979.
5. Freitas JE, Swanson BP, Gross MD et al. Iodine-131 ; optimal therapy for hyperthyroidism in children and adolescents ? J N M 20:847, 1979.
6. Gotlin RW, Kappy MS, Slover RH. Endocrine Disorders. In Hay WW, Groothuis JR, Hayward AR, Levin MJ (eds.) Current Pediatric Diagnosis and Treatment 13th ed. 1997. Appleton & Lange. Stamford CT, pp, 818-856.
7. Amrhein JA, Kenny FM, Ross D. Granulocytopenia, lupus-like syndrome and other complications of propylthiouracil. J Pediatr 76:54-55, 1970.
8. Saha GB. Fundamentals of Nuclear Pharmacy 4th ed. 1998, Springer, New York, pp. 320-323.

IS RADIOIODINE (I-131) TERATOGENIC ?

Dr. M. A. TAHER

Use of radioiodine is absolutely contraindicated during pregnancy,[1] although dose to fetal thyroid is small, but sensitivity and untoward effect may be of medicolegal consequence. However, gonadal exposure is extremely low (less than a diagnostic radiograph), genetic effects are unlikely, extensive studies have failed to show I-131 related neoplasm or birth defects.[2 to 7]

No significant increase in genetic abnormalities has been documented in children of Japanese parents exposed to atomic radiation,[8] and there is an increased tendency to treat young patients with I-131 in recent years.[9] In human beings, organogenesis does not begin until the third week after conception. There is no evidence that radiation of a conceptus in the early weeks of pregnancy is more dangerous than irradiation of the ovary before fertilization. The International Commission on Radiological Protection (ICRP) withdrew support for the 10-day rule in 1984. Many agree that pregnancy be allowed to continue after known exposure of less than 10 centi-Gray (cGy), but some would reduce the upper limit to 5 cGy in the second trimester[10] (1 cGy = 1 rad). We found a healthy daughter born to a woman who inadvertently received radioiodine therapy during early pregnancy, and would like to report considering its rarity.

CASE REPORT

A woman of age 30 years complained of increased sweating, weight loss inspite of increased appetite, palpitations, insomnia and was diagnosed as thyrotoxic in February, 1995. She took carbimazole (neomercazole) 45 mg/day for a month with little improvement and received I-131 therapy (10 milli-Curie) on 18-5-95 at Nuclear Med. Institute, Dhaka. At first follow-up, she disclosed that her last menstrual period (LMP) started on 25-5-95 and ultrasonography revealed gestational sac of 10 weeks 2 days. She was advised therapeutic abortion but she did not agree and gave birth to a healthy daughter on 12-3-96. The baby is in good health till the last follow-up in 27-9-99, however, her mother is now hypothyroid and on thyroxine (100 microgram daily) therapy (Table 1).

Table 1. Hormone levels

Date	T_3 NR 0.8-3.16 nmol/L	T_4 NR 64.5-152 nmol/L	TSH NR 0.3-6 mIU/L
19-3-95	8.89	214	0.09
13-4-95	5.39	213	0.02
5-9-95	0.3	60	0.17
31-3-98	0.48	20	49.9
7-9-99	2.5	50	17.75

NR = Normal Range

Director. Nuclear Medical Center, Post Box No. -16. Rangpur-5400 Bangladesh

DISCUSSION

We do not recommend the use of radioiodine during pregnancy and lactation, however, the present case shows that radioiodine is not teratogenic.

REFERENCES

1. Robertson J S, Gorman C A. Gonadal radiation dose and its genetic significance in radioiodine therapy of hyperthyroidism. J Nucl Med 17:826, 1976.
2. Safrit H F, Thyroid disorders. In Fitzgerald P A (ed.) : Handbook of Clinical Endocrinology. Jones Med. Pub. Chicago, 1986 pp. 122-169.
3. Sarker S D, Beierwaltes W H, Gill S P et al. Subsequent fertility and birth histories of children and adolescents treated with I-131 for thyroid cancer. J Nucl Med 17:460, 1976.
4. Gotlim RW, Kappy MS, Slover RH. Endocrine Disorders. In Hay WW, Groothuis JR, Hayward AR, Levin MJ (eds.) Current Pediatric Diagnosis and Treatment 13th ed. 1997. Appleton & Lange. Stamford CT, pp, 818-856.
5. Stoffer S S, Hamgurger J L. Inadvertent, ^{131}I therapy for hyperthyroidism in the first trimester of pregnancy. J Nucl Med 17: 146, 1976.
6. Stoffer P, Jaffe H L, Oetinger L Jr. Later results of ^{131}I treatment of hyperthyroidism in 73 children and adolescents : 1967 followup, J Nucl Med 10:586, 1969.
7. Becker DV. The role of radioiodine treatment in childhood hyperthyrodism J Nucl Med 20:890, 1979.
8. Ritenour E R, Health effects of low level radiation : carcinogenesis, teratogenesis and mutagenesis. Sem Nucl Med 16:109-117, 1986
9. Safa A M, Schumacher O P, Rodriguez-Antunez A : Logn-term follow-up results in children and adolescents treated with radioactive iodine (I131) for hyperthyrodism. N Eng J Med 292:167, 1975.
10. Russell JGB. The rise and fall of the ten rule. Br. J Radiol 59:3-6, 1986.

MEASURMENT OF TUMOR UPTAKE OF ^{99M} TC-DTPA – ^{10}B-CARBORANE COMPLEX IN BRAIN TO EVALUATE ^{10}B ABSORBED DOSE FOR NCT.

Nisarut RUKSAWIN MS. Med. Physics

ABSTRACT

Although neutron capture therapy (NCT) is a very promising technique for the treatment of brain tumors, it is very difficult to clearly evaluate the dose absorbed by the brain tumor. This paper will show how to use nuclear medicine to evalutate the ^{10}B dose aborbed by the brain tumor. ^{10}B carborane gadolinium complex was labelled with ^{99m}Tc and quality control showed 95 % of radiochemical purity. Scinticamera can tell the %uptake of ^{99m}Tc-DTPA – ^{10}B-carborane complex in brain tumor by selecting area of interest on tumor, the count rate was read and divided by the activity injected. Using %uptake of ^{99m}Tc-DTPA –^{10}B-carborane complex of the tumor in brain, dose of ^{10}B absorbed by brain tumor can be evaluated. Nuclear medicine can be used instead of in vivo quantitation of boron using MRI only for the compound which can be labelled with suitable radionuclide. ^{99m}Tc is at the present time the most popular radionuclide for this purpose.

Keywords: BNCT, NCT, label, radionuclide, area of interest, tumor uptake.

INTRODUCTION

A factor limiting the development of NCT is the lack of drugs which will give tumor:brain uptake ratio higher than two popular compounds, Na2 B12 H11 SH (BSH) and p-dihydroxyborylphenylalanine (BPA) which have been authorised for clinical trials. So researhers from different countries are seeking ideal boron compounds which are suitable for NCT1-4. Working in nuclear medicine I can imagine, if chemists can synthesize something with optimum selectivity for cancer cells people in nuclear medicine will labell it with suitable radionuclide and inject it into the patients. Cancer can be eliminated as easy as ^{131}I has been used for some thyroid cancer.[5] Why do you still need NCT at that moment?

At present time brain tumor scan in Figure 1 shows the uptake of ^{99m}Tc-DTPA beautifully. This agent is rapidly filtered by the kidney, which is a disadvantage, so that it necessitates the injection of a larger amount of radioactivity, but its advantage is that, it provides a higher tumor-to-brain activity ratio.

Section of Nuclear Medicine, Department of Radiology, Siriraj Hospital, Bangkok 10700, Thailand.
E-mail: sinrs@mucc.mahidol.ac.th

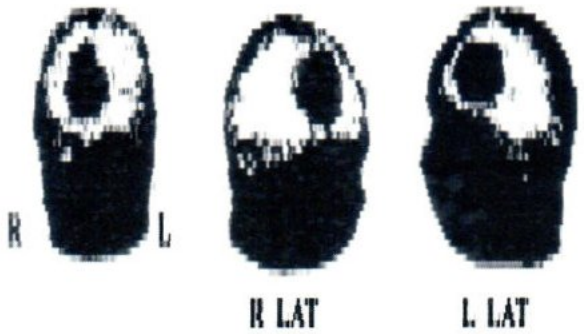

Fig. 1 Brain scintiphotographs obtained with ^{99m}Tc-DTPA in different projections 1 hour after injection. Diagnosis: glioblastoma multiforme.

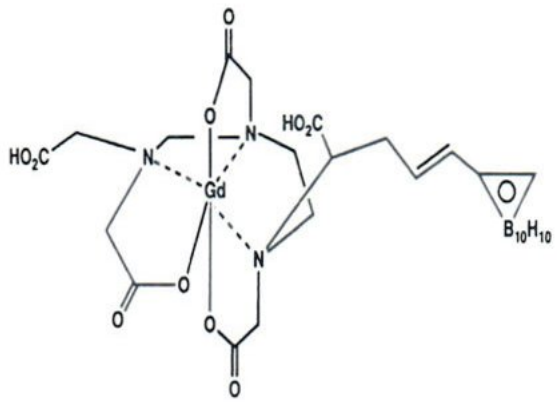

Fig. 2 ^{10}B carborane Gd-DTPA complex.

Since ^{99m}Tc-DTPA provides a higher tumor-to-brain activity ratio. Labelling ^{10}B carborane Gd-DTPA complex with ^{99m}Tc was performed aseptically. ^{10}B carborane Gd-DTPA complex can be labelled with ^{99m}Tc but it is not the same as labelling DTPA. So I would like to present this paper how to label ^{10}B carborane Gd-DTPA complex with ^{99m}Tc and how to use ^{99m}Tc-DTPA ^{10}B carborane complex in NCT.

MATERIALS

1. Cation exchange resin.
2. Sterile distilled water.
3. ^{10}B carborane Gd-DTPA complex from Department of Chemistry, Graduate School of Science, Tohoku University, Sendai 980-77, Japan.
4. Stannous chloride dihydrate, E-Merck, Darmstadt, Germany.
5. Calcium chloride, Anhydrous, J.T. Baker chemical Co., Phillipsburg, N.J. 08865.
6. Sodium hydroxide pellets, E-Merck, Darmstadt, Germany.
7. Nuaire larminar flow biological safety cabinet.
8. Hetosicc Freeze dryer type CD-13.2
9. Sterile disposible syringes were used in all procedures.

METHODS

1. Cleaned glassware and equipment were wrapped in wrapping paper, and sterilized in autoclave.
2. Dissolve ^{10}B carborane Gd-DTPA complex 0.5 g in 50 ml of Sterile distilled water and let it stand in room temperature for 6 hours then pass the solution through cation exchange resin.
3. Put 0.55 g of $CaCl_2$ in the solution from 2, stir until the solution is clear. Add 40% NaOH 0.35 ml pH = 8
4. Dissolve $SnCl_2.2H_2O$ 1 g in 5 ml of concentrated HCl. Filter the solution through 0.22 mm millipore filter. Stir the filtered solution at least 30 minutes.
5. To the solution in 3, add 0.15 ml of solution from 4, the pH is 4
6. Sterilize the solution by 0.22 mm membrane filtration into pre-sterilized evacuated vials. Aseptically transfer 1 ml each of this solution to sterile 7 ml serum vials. Freeze dry for 24 hour, seal under vacuum after freeze drying, each vial contains 0.6 mg stannous chloride.
7. Take one vial from 6 and add 1.5 ml=35 mCi of ^{99m}Tc, shake well.
8. Find the radiochemical purity using instant thin-layer chromatography (ITLC-SG) as shown in Figure 3

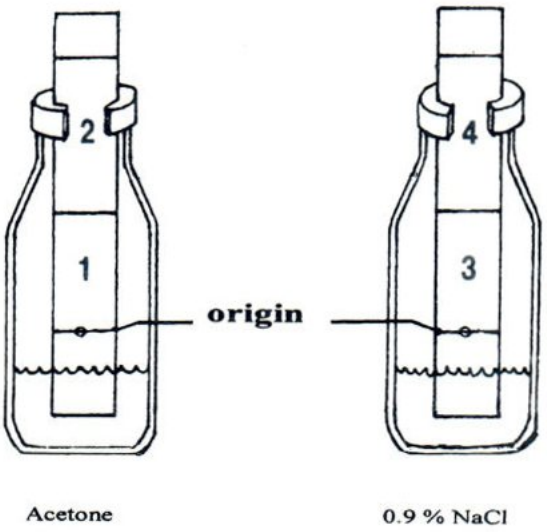

Fig. 3 Two strip mini- instant thinlayer chromatography system (Left) $^{99m}TcO_4^-$ sepa ration, (right) ^{99m}Tc-hydro lyzed reduced technetium (R-^{99m}Tc) separation.

A. Put about 1 ml of acetone into the left vial and 1 ml of 0.9% NaCl into the right vial.
B. Spot 2 µl of solution from 7 at the bottom pencil lines of the two strips.
C. Immediately place the bottom of the strips in the appropriate solvents and allow the solvents to migrate until they reach the top pencil lines.
D. Cut each strips at its central pencil line into sections1, 2, 3 and 4.
E. Count each section in a well scintillation counter.
F. Calculate % $^{99m}TcO_4^-$:

$$= \frac{\text{net activity of section 2}}{(\text{net activity of section 1}) + (\text{net activity of section 2})} \times 100$$

Calculate % R-^{99m}Tc:

$$= \frac{\text{net activity of section 3}}{(\text{net activity of section 3}) + (\text{net activity of section 4})} \times 100$$

Calculate %bound

$$= 100 - (\%\,^{99m}TcO_4^- + \%\ R\text{-}^{99m}Tc).$$

RESULT AND DISCUSSION

After labellingThe ^{99m}Tc be in place of ^{157}Gd as shown in Figure 4.

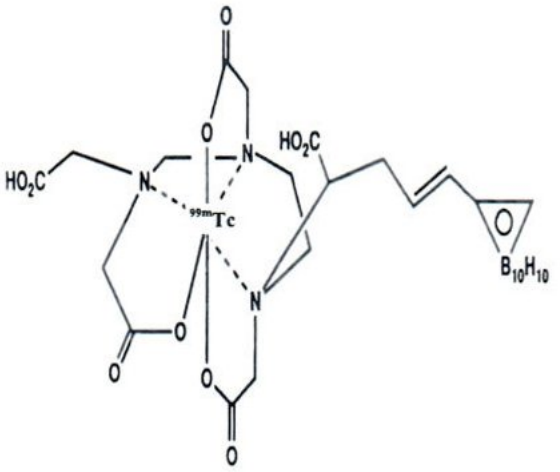

Fig. 4 Shows structure of ^{99m}Tc-DTPA-^{10}B-carborane complex.

When ^{99m}Tc-DTPA-^{10}B-carborane complex 20 mCi is injected to glioma patients the doctor can tell which patient is suitable for NCT. So it will be very useful. After injection the counts from the camera should be recorded not only at the brain, but also the counts of the wholebody should be recorded in order to get % brain tumor uptake.

A key requirement of NCT is the selective delivery of an adequate concentration of ^{10}B to tumors (15-30 mg ^{10}B/ g tumor).[6] For the 7 gram tumor need at least 105 mg of ^{10}B, if % brain tumor uptake is 1% at least 10.5 g of ^{10}B must be given to the patients. So the key requirement of NCT can be solved by nuclear medicine method.

REFERENCES

1. Barth RF, Soloway AH, Fairchild RG, Brugger RM. Boron neutron capture therapy for cancer. Cancer 1992;70:2995-3007.
2. Gabel D. BSH as a boron carrier for glioma BNCT: overview and update. Advances in Neutron Capture Therapy. Elsevier Science B.V.1997;149-52.
3. Girard F, Nakamura H, Fukuda H, Yamamoto Y, Yoshida K. Rat tumor imaging with B-10 carborane gadolinium complex. Recent Advances in Biomedical Imaging. Elsevier Science B. V. 1997 ; 201-207.
4. Yamamoto Y. Hiroshi Hatanaka Lecture : Search for new tumor-seeking boron compound in Japan. Advances in Neutron Capture Therapy. Elsevier Science B.V.1997 ; 22-29.
5. Maisy Mn, Fogelman I. Thyroid cancer. In : Maisy MN, Britain KE, Gilley DL, eds. Clinical Nuclear Medicine. London: Chapman and Hill Ltd. 1983:222-5.
6. Fairchild RG, Bond VP, Current status of ^{10}B-neutron capture therapy: enhancement of tumor dose via beam filtration and dose rate: and the effects of these parameters on minimum boron content: a theritical evaluation. Int J Radiat Oncol Biol Phys 1985;11:831-40.

COMPARISON OF SERUM THYROGLOBULIN MEASUREMENTS BY RADIOIMMUNOASSAY AND IMMUNORADIOMETRIC ASSAY

Vipa BOONNAMSIRI, Ph.D.[1]
Panee JAMPATHONG, M.Sc.[2] **Busara SATAYABAN, M.Sc.**[1]
Boontham AMORNGITTICHAROEN, M.Sc.[1]

ABSTRACT

Serum thyroglobulin (Tg) concentrations are widely used as a tumour marker for monitoring the patients with differentiated thyroid carcinoma. Precise and reproducible Tg measurements are critical, especially when patients are judged to have a high risk for recurrence. The clinical utility of two different Tg methods (RIA and IRMA) was compared and evaluated focusing on measurement methodology. Therefore, complete quality control profiles were performed and assessed. The results revealed that the sensitivity (low detection limit) of the assays for Tg-RIA (DPC) and Tg-IRMA (CIS) was 2.28 ng/ml and 0.62 ng/ml, respectively. The assay precision of both intra-and inter-assays had coefficient of variation (C.V.) of 5.49-15.63% for Tg-RIA and 5.56-8.27% for Tg-IRMA. The accuracy of the two assays was 96.9-121.3% for Tg-RIA and 97.6-104.3% for Tg-IRMA. No cross-reaction and no drift effect were obtained in both assays. The results showed complete parallelism between Tg standards and serial dilutions of Tg-containing serum. The hook effects were indicated with both assays at very high concentration of Tg. The quality of Tg-IRMA (CIS) was proved to be superior to Tg-RIA (DPC).

Quantitation of thyroglobulin (Tg) in the circulation is considered to be a good diagnostic test for the detection of the presence of metastases or recurrence of differentiated thyroid carcinoma (papillary and follicular).[1,2,3,4,5,6] It is well established that serial Tg measurements are usefully employed in the management of the patients following removal of the thyroid gland by surgery and radioablation, if successful, should result in circulating Tg stabilizing at very low or undetectable levels; higher levels, on the other hand, are suggestive of remnent thyroid tissue or metastasis. Numerous methods have been developed to measure Tg in serum, including radioimmunoassay (RIA), immunoradiometric assay (IRMA) and enzyme immuno-assay.[7,8,9,10,11,12,13]

The detection limit is an important characteristic because the main interest of the assay is the follow-up of differentiated thyroid cancer. It is critical to be able not only to detect small amounts of Tg, but also to observe a change in Tg concentration. Thus the objective of this study is to compare the two commercial assays for thyroglobulin : a competitive-binding RIA by Diagnostic Products Corporation (DPC) and the 'CIS' IRMA-type assay utilizing quality control (Q.C.) profiles such as sensitivity, precision, accuracy, specificity, drift test, parallelism and hook effect.

[1] Division of Nuclear Medicine, Department of Radiology, Faculty of Medicine, Siriraj Hospital, Mahidol University, Bangkok 10700, Thailand.
[2] Department of Radiology, Sappasittiprasong Hospital, Ubonrajchathani, Thailand.

MATERIALS AND METHODS

BLOOD SAMPLES FOR DILUTION TEST AND HOOK EFFECT

Very high Tg concentrations from the sera of patients with differentiated thyroid carcinoma were selected, mixed and pooled. The serum mixture was then made to the dilutions of 1:10, 1:100, 1:1,000 and 1:10,000 for the test of hook effect.

STOCK AND WORKING Tg STANDARDS

One milligram of purified Tg from human thyroid glands was kindly obtained from Dr. S. Damrongpisuttikul,[14] weighed and dissolved in a few drops of 10.0 M sodium hydroxide, and then diluted to 100 ml with 0.05 M phosphate buffer pH 7.4 containing 0.05%BSA to give the concentration of Tg about 10,000 ng/ml. For the hook effect test, the stock Tg solution was further diluted to the serial two-fold dilutions with the 0.05 M phosphate buffer pH 7.4 giving the working Tg standard of 0-5,000 ng/ml.

MEASUREMENT OF SERUM Tg

1. TG RIA (DIAGNOSTIC PRODUCTION CORPORATION OR DPC, U.S.A.)

The serum Tg was measured by a double antibody (Donkey anti-goat gamma-globulin) and diluted polyethylene glycol (PEG) in saline as precipitating agent. 200 µl of the zero calibrator for maximum binding tubes and for non-specific binding (NSB) tubes, Tg standards at different concentrations,Q.C.sera at low and medium concentrations, and unknown samples were pipetted into 12×75 mm polypropylene tubes. 100 µl Tg antiserum was added to all tubes except the 'NSB' tubes and mixed. After 2 hours incubation at room temperature, 100 µl of ^{125}I-Tg was added, mixed and incubated for 2 hours at room temperature. 1.0 ml of the cold precipitating solution was added, mixed and incubated for 30 minutes. The tubes were centrifuged at 3,000 g for 15 minutes. Supernatant was discarded and counted the precipitate in a gamma counter. Tg concentrations for the unknown samples were read out from the calibration curve.

2. TG IRMA (CIS-BIOINTERNATIONAL, FRANCE)

The assay was performed by dispensing 300 µl of the buffer into each ELSA-tube. 100 µl of Tg standards, controls and serum samples was added and mixed on a horizontal shaker for 3 hours at room temperature. The tubes were then washed twice with 3 ml of the washing solution. After addition of 300 µl of ^{125}I anti-Tg monoclonal antibody, the tubes were incubated for 18-24 hours at room temperature and then washed twice with 3 ml of the washing solution. The radioactivity bound to the tubes was measured in a gamma counter. The concentrations of the samples were read directly from the standard curve.

STATISTICAL ANALYSIS

The mean, standard deviation, percentage and coefficient of variation (CV) were determined by the program of SPSS 7.5 for window.[15]

RESULTS

The validation of Tg RIA and Tg IRMA was carried out and compared as follows :

1. RESPONSE STANDARD CURVE

The typical standard curves of both assays were constructed and shown in Figures 1 and 2.

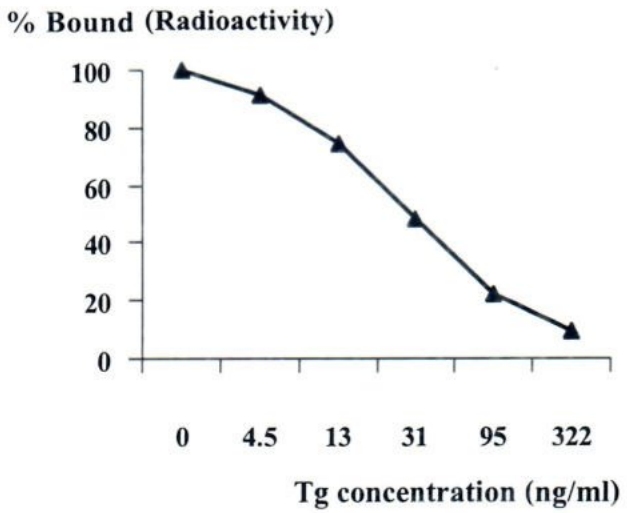

Fig. 1. Response standard curve for Tg RIA (DPC)

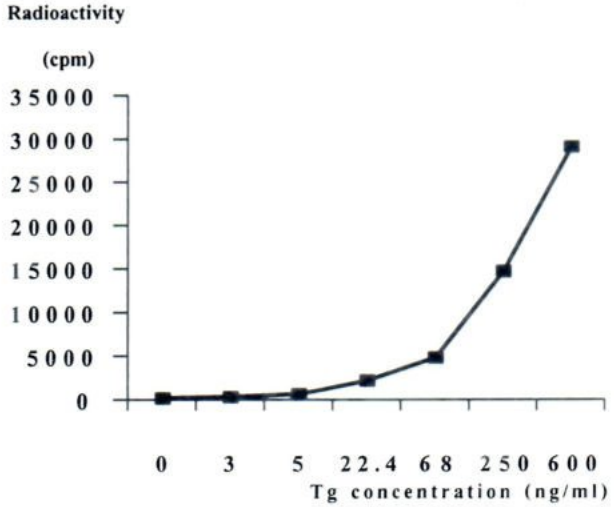

Fig. 2. Response standard curve for Tg IRMA (CIS)

2. SENSITIVITY TEST

Twenty zero calibrator tubes were processed in a single assay, along with a set of nonzero calibrators. Mean and standard deviation were calculated and two standard deviations were subtracted from mean counts at zero point. The detection limit (minimal detectable dose) of Tg RIA and Tg IRMA was 2.28 ng/ml and 0.62 ng/ml, respectively.

3. PRECISION TEST

The reliability of 2 assay kits was performed by examining their reproducibility on control sera to represent a range of Tg levels. The coefficient of variation (C.V.) was determined for each of two control sera from the results of 20 pairs of tubes in a single assay for intra-assay precision and in 20 different assays for inter-assay precision. Better inter-assay reproducibility was obtained from the IRMA Tg kits (CIS) as summarized in Tables 1 and 2.

4. ACCURACY TEST

Known amounts of Tg were added to human sera and then assayed. The accuracy of the test was expressed in percentage of recovery (observed value / expected value). Analytical recovery varied between 96.9%-121.3% for the RIA Tg kits and 97.6%-104.3% for the Tg IRMA as provided in Tables 3 – 4.

Table 1. Assay reproducibility of Tg RIA

Assay precision	Tg RIA (DPC)			
	No.	Mean	SD	%CV
Intra-assay				
Control serum 1	20	8.80	0.48	5.49
Control serum 2	20	62.57	3.62	5.78
Inter-assay				
Control serum 1	20	9.72	1.52	15.63
Control serum 2	20	63.22	8.16	12.90

Table 2. Assay reproducibility of Tg IRMA

Assay precision	Tg IRMA (CIS)			
	No.	Mean	SD	%CV
Intra-assay				
Control serum 1	20	7.81	0.43	5.56
Control serum 2	20	48.49	2.82	5.78
Inter-assay				
Control serum 1	20	8.48	0.70	8.27
Control serum 2	20	50.43	3.73	7.39

Table 3. The percentage of recovery for the Tg RIA (DPC)

Number of samples	Observed value (ng/ml)	Expected value (ng/ml)	%Recovery
1	11.6	11.4	101.8
2	21.7	22.4	96.9
3	52.6	53.2	98.9
4	37.0	30.5	121.3
5	46.0	39.8	115.6
6	78.0	74.0	105.4
		Mean ± SD = 106.7 ±9.7	

Table 4. The percentage of recovery for the Tg IRMA (CIS)

Number of samples	Observed value (ng/ml)	Expected value (ng/ml)	%Recovery
1	2.1	2.0	103.5
2	5.7	5.5	104.2
3	14.6	14.0	104.3
4	44.9	46.0	97.6
5	136.4	138.0	98.8
6	497.5	490.0	101.5
		Mean ± SD = 101.7 ±2.9	

5. SPECIFICITY TEST

The quality of Tg antibodies for two commercial kits was assessed by cross-reactivity tests with monoiodothyronine (T_1), diiodothyronine (T_2), triiodothyronine (T_3), thyroxine (T_4) and thyrotropin (TSH). The results indicated that the Tg antibodies used in the both assays did not present any cross-reaction with these analogues as illustrated in Figures 3 and 4

RADIOACTIVITY OF

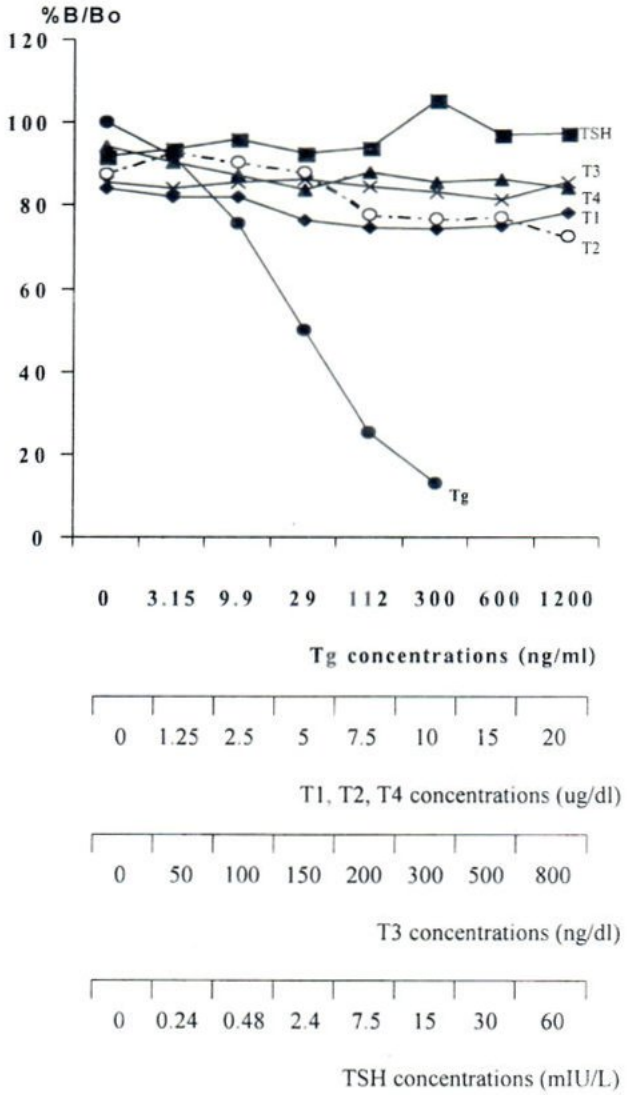

Fig. 3. Specificity of Tg antibody for Tg RIA (DPC)

6. PARALLELISM TEST

This test was carried out by adding the serum sample (A) to each concentration of the

standard Tg, giving a final dilution of 1:1. The two response curves were plotted and compared. Parallelism between sample and standard of the two methods was observed as seen in Figures 5 and 6.

7. DRIFT TEST

Pairs of three different Tg concentra-tions were spaced throughout a long assay of RIA and IRMA. There were any position effect due to delay in the addition of the reagents as listed in Tables 5 and 6.

Table 5. Drift test for Tg RIA (DPC)

Tg RIA	Concentrations of Tg in the samples (ng/ml)		
	A	B	C
• Tube No.			
21 - 26	13.10	65.81	89.60
65 - 70	13.12	68.95	90.31
95 - 100	13.69	72.86	93.15
• Mean	13.30	69.21	91.02
• SD	0.27	2.89	1.53
• % CV	2.06	4.17	1.69

Table 6. Drift test for Tg IRMA (CIS)

Tg IRMA	Concentrations of Tg in the samples (ng/ml)		
	A	B	C
• Tube No.			
21 - 26	6.58	56.07	837.55
51 - 56	6.67	57.58	847.07
91 - 96	6.86	59.75	852.23
• Mean	6.70	57.80	845.62
• SD	0.11	1.51	6.08
• % CV	1.74	2.61	7.19

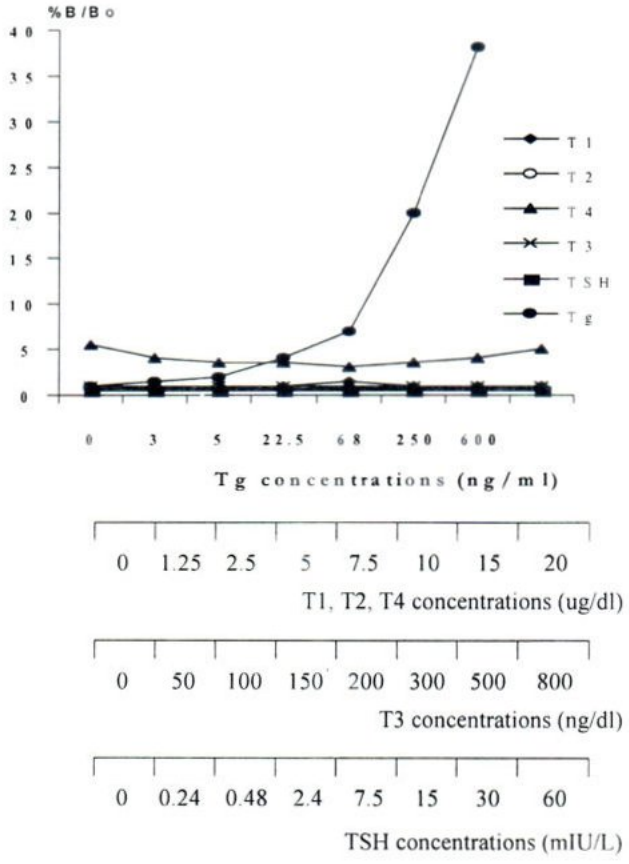

Fig. 4. Specificity of Tg antibody for Tg IRMA (CIS)

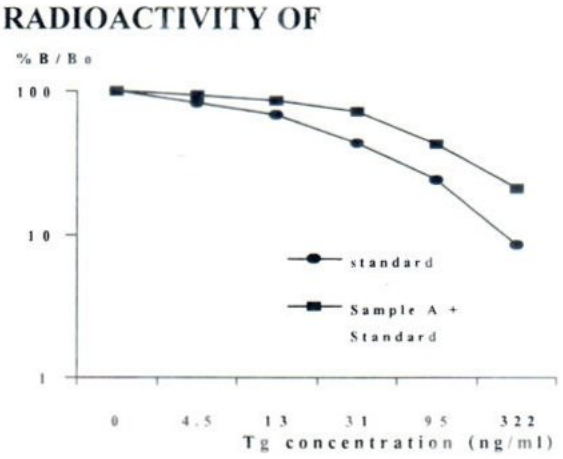

Figure 5. Parallelism test for Tg RIA (DPC

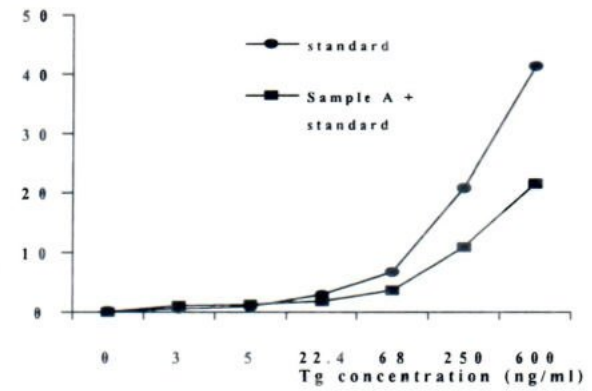

Fig. 6. Parallelism test for Tg IRMA (CIS)

8. HOOK EFFECT TEST

The tests were made in two selected patient sera with very high Tg concentrations utilizing the RIA and IRMA. In order to establish the final Tg values, serum Tg concentrations were determined in the undiluted and diluted sera at dilutions of 1:10, 1:100 and 1:1000. The hook effect results were given in Tables and Figures 7 and 8.

Table 7. Hook effect at different dilutions of the patient sera for Tg RIA

Serum dilutions	Tg concentrations (ng/ml)
Sample A	
Undiluted serum	390.68
1 : 10	2445.08
1 : 100	9151.00
1 : 1000	2017.30
Sample B	
Undiluted serum	395.11
1 : 10	2851.59
1 : 100	9601.10
1 : 1000	2679.30

Table 8. Hook effect at different dilutions of the patient sera for Tg IRMA

Serum dilutions	Tg concentrations (ng/ml)
Sample A	
Undiluted serum	480.11
1 : 10	6024.73
1 : 100	20739.10
1 : 1000	29438.00
Sample B	
Undiluted serum	423.76
1 : 10	4701.05
1 : 100	70368.40
1 : 1000	82193.00

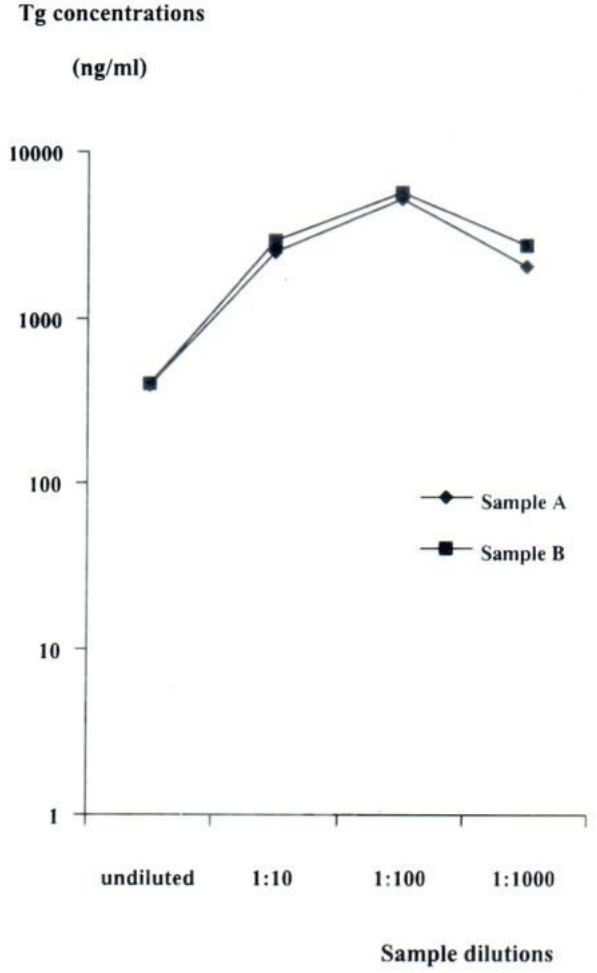

Fig. 7. Hook effect at different dilutions of Sample A and B for Tg RIA

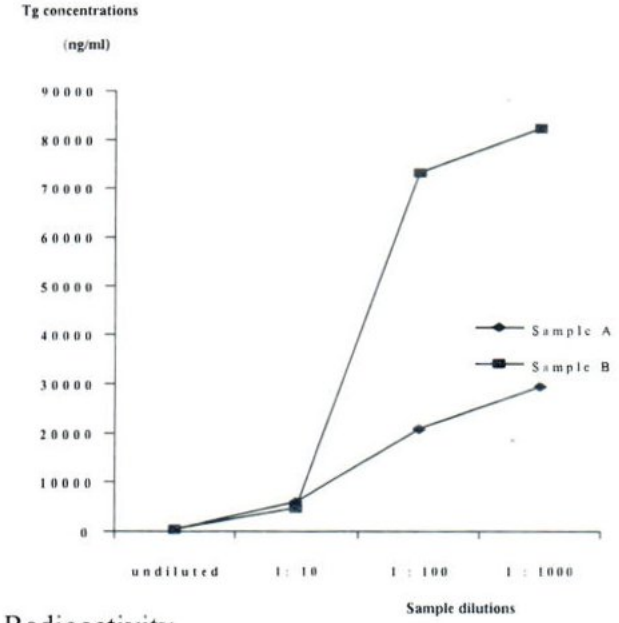

Fig. 8. Hook effect at different dilutions of Sample A and B for Tg IRMA

Purified preparations of human Tg were kindly offered by Dr. S. Damrongpisuttikul. Therefore, the standard curve of Tg at very high concentratios was performed by IRMA technique, and hook effect was obtained as illustrated in Figure 9.

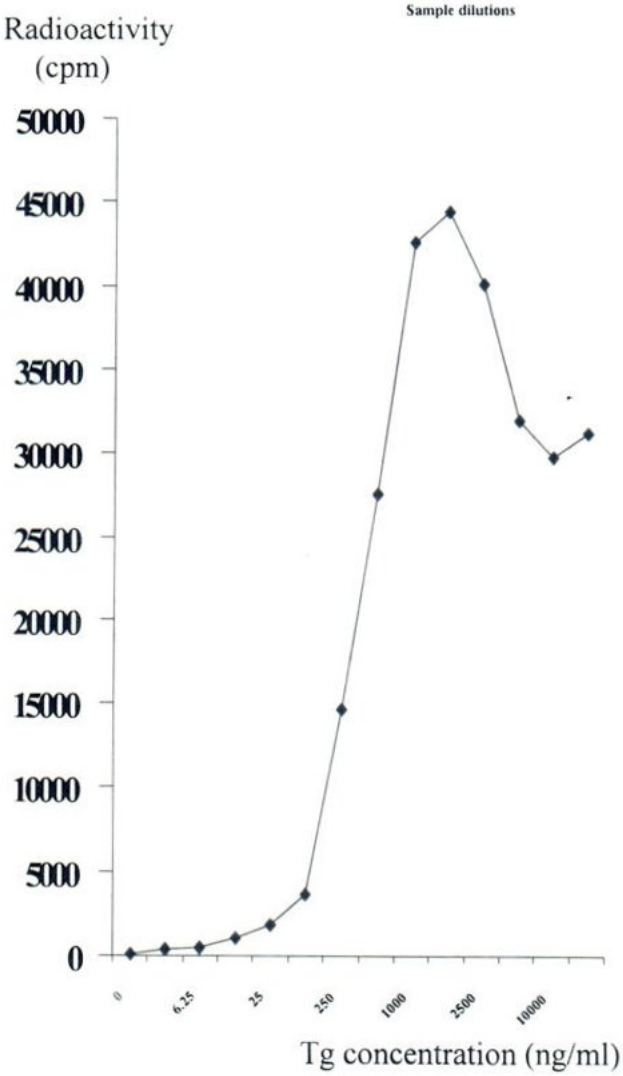

Fig. 9 Hook effect at high concentrations of standard Tg

DISCUSSION

The measurement of Tg in serum is technically challenging and now widely accepted as a sensitive and specific alterna-tive to radioiodine scans in the detection of residual, recurrent or metastatic disease in patients with differentiated thyroid cancer.[3,4,16] The first haemagglutination techniques were replaced by RIA.[7,8,9] Subsequently, monoclonal antibody technology has led to the development of IRMA[10,11] and ELISA.[12,13] Therefore, it is interesting to compare the quality of two commercial assays between Tg RIA (DPC) and Tg (CIS), and to choose the best one of the assay kit since incorrect results can lead to diasterous effects for the patients.

The typical response standard curves for a competitive-binding RIA by Diagnostic Production Co. (DPC) and a noncompetitive-binding IRMA by CIS bio international (CIS) were illustrated in Figures 1 and 2, respectively.

The minimal detectable concentration or sensitivity is an important characteristic because the main interest of the assay is the follow-up of patients with differentiated thyroid carcinoma, so it is critical to be able not only to detect small amounts of Tg but also to observe a change in Tg concentration.[17] The sensitivity was determined using the calculated error at zero concentration. Two standard deviations were subtracted from the mean counts at zero point and

the corresponding Tg concentration was read off from the standard curve. The sensitivity of Tg RIA (DPC) was found to be 2.3 ng/ml which were similar to those found earlier by previous authors.[5,18,19] The higher sensitivity was also reported by Ashcraft et al.[20] and Charles et al.[21] However, the lower sensitivity of Tg was obtained by the previous studies at 5.0 and 15 ng/ml.[22,23]

The Tg assay should be sensitive enough to detect concentrations as low as 1.0 to 2.0 ng/ml which can use in the follow-up of patients with differentiated thyroid cancer. The more sensitive assays are capable of distinguishing the lower limit of euthyroid range from the functional sensitivity limit. The sensitivity of Tg IRMA (CIS) was found to be 0.6 ng/ml giving the higher sensitivity than Tg RIA (DPC). Marquet and co-workers reported the highest sensitivity of 0.2 ng/ml for Tg IRMA[24] but the lowest sensitivity of 3.0 ng/ml was presented by the previous authors.[25,26]

The reproducibility or precision is the error associated with assay results. Therefore, the intra- and inter-assay precision was carried out using two control sera with different Tg concentrations. The coefficients of variations (CVs) of intra-assay precision were determined in the same series of Tg assays. The results of intra-assay CVs for Tg RIA (DPC) and Tg IRMA (CIS) were 5.49%-5.78% and 5.56%-5.78%, respectively. The inter-assay precision is a measure of variability associated with test results in different series of assays. The inter-assay CVs for Tg RIA (DPC) and Tg IRMA (CIS) were found to be 12.90%-15.63% and 7.39%-8.27%, respectively. The acceptable intra- and inter-assay CVs should be less than 10% for good precision of assay results which showed that Tg IRMA (CIS) had better assay precision than Tg RIA (DPC) especially inter-assay CVs as summarized in Tables 1 and 2.

Accuracy of the assay is the ability of an assay to detect all of the substances being assayed that is present in the sample. Analytical recovery test was made by adding known amounts of Tg to serum samples. The percentage of recovery of Tg RIA (DPC) and Tg IRMA (CIS) in six samples were 96.9%-121.3% with the mean (±SD) of 106.6 ± 9.7% and 97.6 – 104.3% with the mean of 101.7 ± 2.9%, respectively as given in Table 3 and 4. Better recovery results were also noted in Tg IRMA (CIS).

Specificity of the Tg antibodies was performed by cross-reactivity tests with different thyroid analogues such as T1, T2, T3, T4 and TSH. The results demonstrated that the antibodies used in the both assays did not present any cross-reaction with their analoques as illustrated in Figures 3 and 4.

In a valid assay, it is essential to test that the standard and unknown sample react identically with the same antibody binding sites. Thus, parallelism test between serum sample and standard was made because it can be done to assess interfering factors and for comparing the molecular integrity of the standard and sample. The results revealed that parallelism between the two curves of the both methods was observed as seen in Figures 5 and 6.

Drift test was also performed in order to determine whether there is any position effect due to delay in the addition of reagents. Three different concentrations of Q.C. sera were spaced throughout along the assays. There was no significant position effects in the both assays even in assays involving as many as 100 tubes (Tables 5 and 6).

The hook effect is referred as the phenomenon of a falling dose-response at very high analyte concentrations. The IRMA techniques were found to be more often subjected to hook effect than RIA methods.[17,27] The hook effect can lead to inappropriately low- or euthyroid-range Tg values in sera

with very high serum Tg concentrations, which require dilution. The hook effect appears to result when a massive excess of antigen (10 to 10,000 times the upper limit of the assay range) exhausts the binding capacity of the Tg capture antibody on the solid support. The hook effect test is necessary since concentration of tumour marker can be exceedingly high and the consequence of such an error has serious medical implication. [28] It is interesting to demonstrate whether these assays exhibited a high-dose hook effect in which a high concentration produced values lower than the value of the highest standard concentrations. Therefore, two selected serum samples with very high Tg concentrations were assayed in undiluted and diluted samples at 1:10, 1:100 and 1:1,000 dilutions to establish the final Tg value, which was based on the dilutions that produced parallelism within the assay working range. Hook effects were obtained in both different methods when Tg values were over 1,000 ng/ml as defined in Figures and Tables 7 and 8.

The purified preparation of human Tg was kindly provided by Dr. Sunetra Damrongpisuttikul[14] so a wider working range of the standard (0-10,000 ng/ml) could be performed according to Tg IRMA (CIS) method. A falling dose-response or hook effect occurred at very high Tg concentration of 1,250-2,500 ng/ml as presented in Figure 9.

Spencer and their co-workers[27] suggested the elimination of hook effect that the users of RIA methods should periodically validate the upper assay limit by diluting specimens having concentrations close to the upper limit with patients' specimens. Thus, the users of IRMA methods should run every serum specimen at two dilutions (undiluted and 1:10 dilution) to detect hook problems.

CONCLUSION

The quality of two different Tg methods was assessed and compared by using complete Q.C. profiles. This study revealed that different methods have different sensitivities which were 2.3 ng/ml for Tg RIA (DPC) and 0.6 ng/ml for Tg IRMA (CIS). The CVs of the assays both intra- and inter-assay precisions were 5.49-15.63% for Tg RIA (DPC) and 5.56-8.27% for Tg IRMA (CIS). The accuracy of the two assays was determined by recovery tests which were 96.9-121.3% for Tg RIA (DPC) and 97.6-104.3% for Tg IRMA (CIS). No cross-reaction between Tg antiserum and their analogues in both assays was observed. Parallelism between Tg standard and serial dilutions of Tg-containing serum sample was obtained, and no drift effects occurred in both assays. The hook effects of both assays were noted at very high Tg concentrations.

In conclusion, the quality of Tg IRMA (CIS) was proved to be superior to Tg RIA (DPC) for detecting residual, recurrent of metastatic patients with differentiated thyroid cancer.

ACKNOWLEDGEMENT

The authors express their appreciation to Dr. Sunetra Damrongpisuttikul for the gift of purified preparations of human thyroglobulin, and Ms. Nucharee Putraseranee for her excellent photographic and computergraphic work.

REFERENCES

1. Van Herle AJ, Uller RP. Evaluated serum thyroglobulin : A marker of metastases in differentiated thyroid carcinomas. J Clin Invest 1975;56:272-7.
2. Lo Gerfo P, Stillman T, Colacchio D, Feind C. Serum thyroglobulin and recurrent thyroid cancer. Lancet 1977;23:881-2.

3. Ronga G, Fiorentino A, Paserio E, Signore A, et al. Can I-131 whole body scan be replaced by thyroglobulin measurement in the post-surgical follow-up of differentiated thyroid carcinoma?. J Nucl Med 1990;31:1766-71.
4. Castagnoli A, Cappelli G, D'Agata A, Forni S, Milani S, Pupi A. Can thyroglobulin assay really supplant radioiodine scans in patients with differentiated thyroid cancer?. Lancet 1982; 6:573-4.
5. Barsano CP, Skosey C, DeGroot LJ, Refetoff S. Serum thyroglobulin in the management of patients with thyroid cancer. Arch Intern Med 1982;142:763-7.
6. Blahd WH, Drickman MV, Porter C, Hill VA, Baumgartner WA. Serum thyroglobulin, a monitor of differentiated thyroid carcinoma in patients receiving thyroid hormone suppression therapy : concise communication. J Nucl Med 1984;25:673-6.
7. Falk U, Schmidt-Gayk H, Hufner M. Radioimmunoassay for serum thyroglobulin designed for early detection of metastases and recurrences in the follow-up of patients with differentiated thyroid carcinoma. J Clin Chem Biochem 1984;22:661-70.
8. Lemish I, Benneth F, Martin C, Warwick A, Quinlan M. A sensititive human thyroglobulin radioimmunoassay to define clearly presence or absence of function ing thyroid tissue. J Nucl Med 1984;25: 49-55.
9. Schneider AB, Pervos R. Radioimmunoassay of human thyroglobulin : effect of antithyroglobulin autoantibodies. J Clin Endocrinol Metab 1978;47:126-37.
10. Mariotti S, Cupini C, Giani C, Lari R, Rolleri E, et al. Evaluation of a solid-phase immunoradiometric assay (IRMA) for thyroglobulin : effect of anti-thyroglobulin autoantibody. Clin Chim Acta 1982; 123: 347-55.
11. Plechaczyk M, Baldet L, Pau B, Bastide JM. Novel immunoradiometric assay of thyroglobulin in serum with use of monoclonal selected for lack of cross-reactivity with autoantibodies. Clin Chem 1989;35: 422-4.
12. Kastrup J, Feldt-Rasmussen U, Bartram HR, Witten J, San Hansen H. An enzyme linked immunosorbent assay (ELISA) for measurement of serum thyroglobulin : evaluation of the influence of thyroglobulin autoantibodies. Scan J Clin Lab Invest 1985;45:471-6.
13. Erali M, Bigelow RB, Meikle AW. ELISA for thyroglobulin in serum : recovery studies to evaluate autoantibody interference and reliability of thyroglobulin values. Clin Chem 1996;42:766-70.
14. Damrongpisuttikul S, Nuclear Medicine Section, Department of Radiology, Thai Royal Army Hospital, Bangkok 10400, Thailand, Personal communication, 1998.
15. SPSSâBase 7.5 for Windowâ SPSS Inc. United States of America 1997.
16. Ng Tang Fui SC, Hoffenberg R, Maisey MN, Black EG. Serum thyroglobulin concentrations and whole body radioiodine scan in follow-up of differentiated thyroid cancer after thyroid ablation. Br Med J 1979; 2: 298-300.
17. Cole TG, Johnson D, Eveland BJ, Nahm MH. Cost-effective method for detection of hook effect in tumour marker immunometric assay [Letter]. Clin Chem 1993; 39: 695-6.
18. Feldt-Rassmussen U, Holten I, Sand Hansen H. Influence of thyroid substitution therapy and thyroid auto-antibodies on the value of serum thyroglobulin in recurring thyroid cancer. Cancer 1983;51:2240-4.

19. Grant S, Luttrel B, Reeve T, Wiseman J, Wilmshurst E, Stiel J, et al. Thyroglobulin may be undetectable in the serum of patients with metastatic disease secondary to differentiated thyroid carcinoma. Cancer 1984;54:1625-8.
20. Asheraft MW, Van Herle AJ. The comparative value of serum thyroglobulin measurements and I-131 total body scan in the follow-up study of patients with treated differentiated thyroid cancer. Am J Med 1981;71:806-14.
21. Charles MA, Dodson LE Jr., Waldeck N, Hofeldt F, Chaed N, Telepak R, et al. Serum thyroglobulin levels predict total body iodine scan findings in patients with treated well-differentiated thyroid cancer. Am J Med 1980;69:401-7.
22. Hufner M, Stumpf JP, Grussendort M. A comparison of the effectiveness of ^{131}I whole body scan and plasma thyroglobulin determinations in the diagnosis of metastatic differentiated carcinoma of the thyroid : A retrospective study. Acta Endocrinol 1983;104:327-32.
23. Echenique RL, Kasi L, Haynie TP, Glenn HJ, Samaan NA, Hill CS. Critical evaluation of serum thyroglobulin levels and I-131 scans in post-therapy patients with differentiated thyroid carcinoma : concise communication. J Nucl Med 1982;23:235-40.
24. Marquet PY, Daver A, Sapin R, Bridgi B, Muratet JP, Hartmann DJ, et al. Highly sensitive immunoradiometric assay for serum thyroglobulin with minimal interference from autoantibodies. Clin Chem 1996;42:258-62.
25. Pacini F, Lari R, Mazzeo S, Grasso L, Taddei D, Pinchera A. Diagnostic value of a single serum thyroglobulin determination on and off thyroid suppressive therapy in the follow-up of patients with differentiated thyroid carcinoma. Clin Endocrinol 1985;23:405-11.
26. Girelli ME, Busnardo B, Amerio R, Casara D, Betterle C, Piccolo M. Critical evaluation of serum thyroglobulin levels during thyroid hormone suppression therapy versus thyroglobulin levels after hormone withdrawal and total body scan : results in 291 patients with thyroid cancer. Eur J Nucl Med 1986; 11: 333-5.
27. Spencer CA, Takeuchi M, Kazarosyan M. Current status performance goals for serum thyroglobulin assays. Clin Chem 1996;42:164-73.
28. Vaidya HC, Wolf BA, Garrett N, Catalona WJ, Clayman RV, Nahm MH. Extremely high values of prostate-specific antigen in patients with adenocarcinoma of the prostate : demonstration of " hook-effect". Clin Chem 1988; 34: 2175-7.

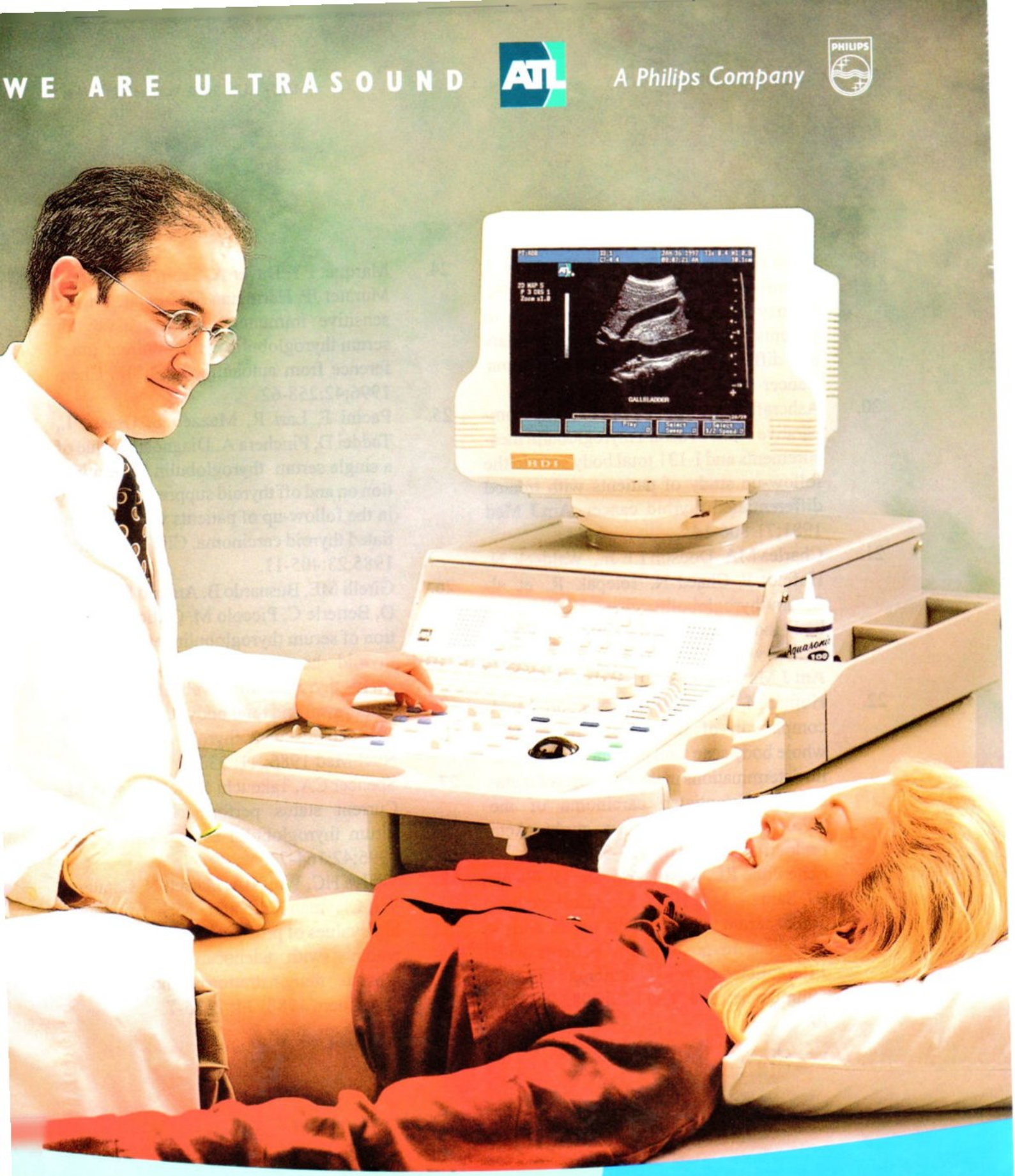

FOR MORE INFORMATION PLEASE CONTACT

PHILIPS MEDICAL SYSTEMS

- TEL. 745-4090 Ext. 3332
- FAX. 398-0792

Philips Electronics (Thailand) Ltd.
209/2 Sanpavuth Road, Bangna, Bangkok 10260

ฆพ. 78/2542

PHILIPS

Let's make things better.

ABSENT SEPTUM PELLUCIDUM : IS IT IMPORTANT

Orasa CHAWALPARIT, Nasuda SUCHATO, Anchalee CHUROJANA, Pipat CHIEWVIT, Suthisak SUTHIPONGCHAI

ABSTRACT

The absent septum pellucidum on imaging was thought to be normal variation when present alone. On the review of reported cases, however, it has been reclaimed that this finding alone is very rare. We reviewed the 204 reported cases of absent septum pellucidum (ASP) with other associated anomalies from 1978 through 1998. There are only six cases reported to have ASP alone. Two of them were schizophrenic. Most of the cases were associated with septo-optic-hypothalamic dysplasia. There were 26 cases associated with other anomalies of mid-line defect and 4 cases with migrational or differentiation anomalies of neurones. Some authors claimed that the findings may only indicate the timing of a congenital insult. Many reports showed cases of only ASP on imagings in patients with clinically proven to have optic nerve hypoplasia and/or hypothalamic-pituitary dysfunction. This implied that the abnormality of optic nerve and hypothalamic-pituitary axis are out of sensitivity of the imagings to be demonstrated. We believe that when an ASP is found on the imaging, the searching for other associated anomalies should be done carefully eventhough nothing else are demonstrated, emphasizing clinician to evaluate clinical abnormalities of optic nerve and hormonal dysfunction should be done.

Radiologists, who work in the field of neuroimagings either computed tomography (CT) or magnetic resonance imagings (MRI) of brains, at least once have seen the septum pellucidum loss. They might have a question whether it is important. If there are other associated anomalies, the question may be easy. But if it is found alone, the other questions will follow. In the past, the absent septum pellucidum (ASP) alone on CT was thought to be normal variation or not to have any significant in clinical course. After studying by MRI, it has been found that ASP alone is very rare. This article is emphasized in the significant of the septum pellucidum in human nervous system and radiologic points to help the clinicians dealing with these patients.

ANATOMY

The septum pellucidum (SP) is a thin structure. The word "pellucidum" means transparent. In fact, it consists of two thin translucent membranes stretching between corpus callosum about 1.5 – 3 mm. Andy and Stephen used the term septum telencephali meaning the thin membrane at the proximal end of the telencephalon. They separated the membrane into two parts : the thin part located superiorly consists of glial cells and fiber bundles called septum pellucidum. This part is found only in higher mammals. The inferior part called septum verum consists of nuclei found also in the lower animals. The septum verum cannot be separated from the

Department of Radiology, Siriraj Hospital, Faculty of Medicine, Mahidol University, Bangkok, Thailand.

SP and joins with the subcallosal or paraterminal gyrus. In the septum verum, there are many fiber systems passing. It works like the delayed stations between the hypothalamus and hippocampus. So the septum verum (or SP. in general meaning) controls the signals between the diencephalon and the limbic system.

EMBRYOLOGY

SP is developed from the primitive lamina terminalis, the so call "commissural plate", at about 10 - 12 weeks gestational age. It develops along with the corpus callosum, the anterior and hippocampal commissure until adult-like at 17 weeks gestation.

The lamina terminalis is the central membranous tissue at the cephalic end of the neuropore. It develops from closure of the neural tube and determines the location of the prosencephalon. At both sides, the budding telencephalon is expanded to be future cerebral hemisphere. The midline thickening structure develops to be the corpus callosum, hippocampal and the anterior commissure. The much more development and the growing of the corpus make the connection with the anterior and hippocampal commissure spread out to be a thin membrane.

Rakic and Yakovlev postulated that each membrane of the SP is developed from cavitation of the medial inferior commissural plate during the growing of the corpus. The cavity inside is the cavum septum pellucidum. After birth, the cavum septum will be closed from posterior to anterior direction.

EVOLUTION

The evolution of SP is inevitably along with corpus callosum which has been detected first in the placental mammals. The more development of frontal lobe means the more clever of the animals. The more enlarged frontal lobe makes the more arch of corpus callosum and the thinner of the SP. In contrast, the olfactory system is the down evolution structure in higher mammals.

FUNCTION

Because the SP is the delayed station between hypothalamus and hippocampus, it is a part of the limbic system controling consciousness, neuroendocrine, autonomic function, sleeping cycle, environmental response and memmory. The fiber tract runs from olfactory bulb to the preoptic area passing the SP but not stopping..

From the anatomic and functional points, one could recognize the important of the SP. We have reviewed 42 medical articles from 1978 through 1998 reporting patients with ASP.[1-42] The total patients was 204 and the associated anomalies were summarized in the table 1. Most of the reported cases were septo-optic dysplasia (125 cases). In this group, nearly half had no other associated anomalies (79 cases). The rest of this group (46 cases) and the non-septo-optic dysplasia cases (79 cases) had other associations such as holoprosencephaly, agenesis of corpus callosum, schizencephaly, migrational and organization disorder, associated destructive causes and cerebellar anomalies. There were only 6 patients reported with ASP alone (2.9%). In these 6 patients, two had psychological disorder. No other information about the other four was reported. This implies that the ASP is significant enough for radiologist to search for other associated anomalies.

IMAGING FINDINGS OF ASP.

The characteristic findings on both CT and MRI are no SP and squared frontal horn of the lateral ventricle (Fig.1). This squared frontal horn is not found in secondary septal necrosis from chronic severe hydrocephalus (Fig.2). The fornix is normally hung above the verum interpositum by the SP. In ASP, the fornix is sinking into the verum interpositum.

Table 1 Reported cases of ASP from 1979-1998

I.	Septo-optic dysplasia	=	125 (61.2 %)
	- Alone	=	79
	- Medial midline defect	=	18
	- Migration / organization disorder, Schizencephaly	=	9
	- Destructive causes (Hypoplasia white matter, thin gray matter, Porencephaly)	=	16
	- Cerebellum disorder	=	1
	- Olfactory bulb agenesis	=	1
II.	Holoprosencephaly	=	13
III.	Agenesis of Corpus callosum	=	12
IV.	Destructive causes (Porencephaly, hydrocephalus, hydranencephaly)	=	9
V.	Migration / organization disorder, Schizencephaly	=	4
VI.	Cerebellum, Chiari II	=	14
VII.	Cephalocele	=	3
VIII.	Absent septum pellucidum alone	=	6 (2.9%)
	- II + III	=	1
	- III + V	=	7
	Total cases	=	**204**

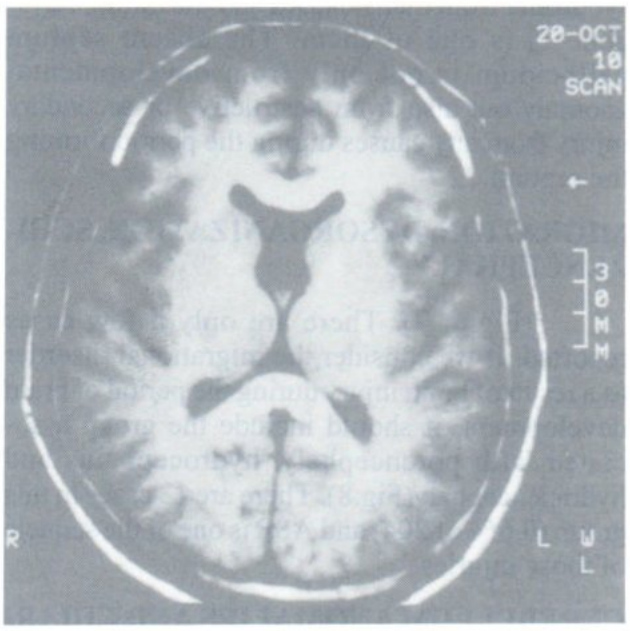

Fig. 1. Axial T1-wi shows absent septum pellucidum and square shape of the frontal horn of lateral ventricle.

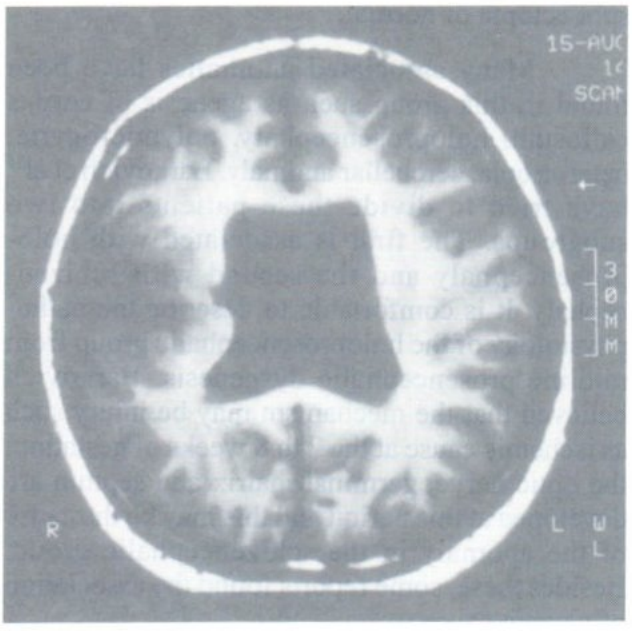

Fig. 2. Axial T1-wi demonstrated partial absent septum possible from pressure necrosis from severe hydrocephalus. Note the shape of the frontal horn of lateral ventricle.

ASSOCIATED ANOMALIES SEPTO-OPTIC DYSPLASIA

The syndrome consists of hypoplasia of optic nerve and ASP (Fig.3). It was first described by Reeves in 1941[45] and 36 cases were reported by de Morsier in 1956.[46] In 1970, Hoyt[34] reported high incidence of hypothalamic-pituitary dysfunction. The following reports have found that there were spectrums of abnormalities in three systems: visual function, hormonal function and seizure. The typical visual abnormality is congenital blindness, nystagmus and optic nerve hypoplasia. Some cases have small optic nerve with normal vision or normal size optic nerve. The common hormonal abnormality is hormonal deficit especially the growth hormone and thyroid stimulating hormone (TSH) with spectrum of variable degree. In the part of ASP, variable degree of abnormality is also found from complete absent, some residual remnant and normal septum. On imagings, ASP may be the only finding ; optic nerve, chiasm and tract may be small or normal and not correlate with the patient's vision ; the hypothalamus and pituitary gland may be hypoplasia, posterior bright spot ectopia or normal.

Many associated anomalies have been found in this group such as agenesis of corpus callosum, holoprosencephaly, polymicrogyria, heterotropia, cerebellar anomaly. Barkovich et al[35] have tried to divide these patients into two subgroups. The first is associated with holoprosencephaly and the second with schizencephaly. It is comfortable to describe the pathophysiology of the holoprosencephalic group from midline prosencephalic dysgenesis. Barkovich believed that the mechanism may be injury such as ischemic cause at the 7 to 8 weeks of gestation, the optic nerve, germinal matrix and septum are developed at this period and this may be the cause of the anomaly in the schizencephalic group. Besides these, some reports found the association of genetic cause.

However, if we find the ASP in patient either with clinical evidence of visual abnormality or not, we should suggest the clinician to search for the possible hormonal abnormality especially GH and TSH deficiency so that the patients could be prevented from the mental retardation.

HOLOPROSENCEPHALY AND AGENESIS OF CORPUS CALLOSUM

As described above, ASP may be caused by midline dysgenesis. It is not surprised to have these two conditions associated in many reported cases. From reviewed papers, there are 26 (12.1 %) cases not included in the septo-optic dysplasia. Imagings of the holoprosencephaly can be divided into 3 subgroups : alobar, semilobar and lobar type by the degree of development of falx cerebri (Fig.4). However, ASP is found in all groups. The corpus callosum may be normal, partial or complete agenesis (Fig.5).

When we look back to the septo-optic dysplasia associated with holoprosencephaly, there are only 18 cases (14.4 % of 125) reported. It could be concluded that the septo-optic dysplasia is the syndrome from many causes and the midline dysgenesis is one of them. The absent septum pellucidum is not only from developmental anomaly but also from destructive or secondary injury from any causes during the period forming the septum.

MIGRATION, DYSORGANIZATION, SCHIZENCEPHALY

(Fig.6, 7). There are only a few cases reported. If we consider the migrational disorder as a result of brain injury during the period of brain development, it should include the group associated with porencephaly, hydrocephalus and hydranencephaly(Fig.8). There are 13 cases in this group (0.6 % of 204) and ASP is one of the sequele of those injuries.

CEREBELLUM ANOMALIES AND CHIARI 2 MALFORMATION

(Fig.9, 10). There is 14% reported. Most of them have associated hydrocephalus. The ASP may be from pressure necrosis.

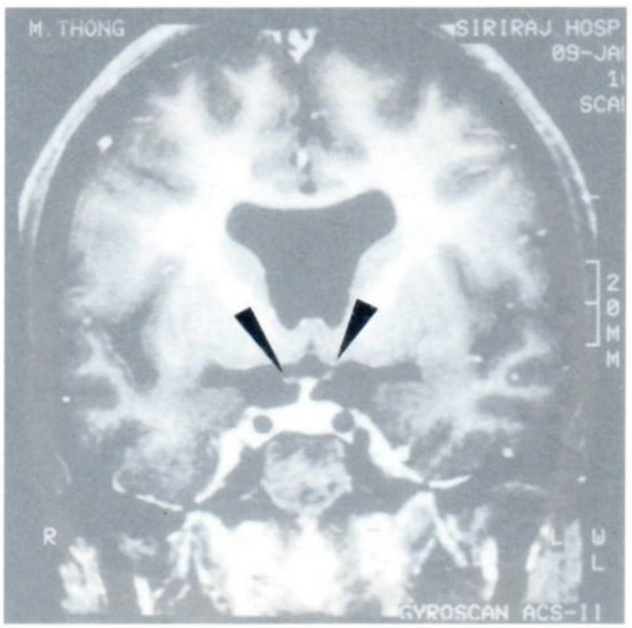

Fig. 3. Coronal T1-wi postenhancement shows the absent septum with hypoplasia of optic nerve and chiasm (arrows).

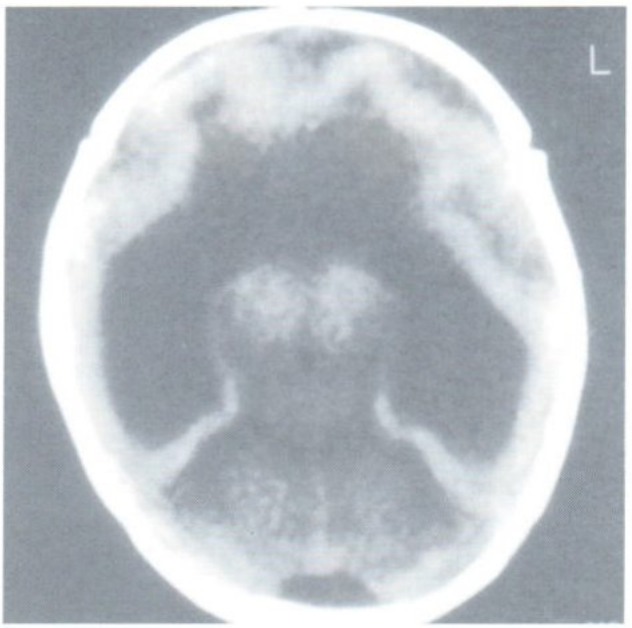

Fig. 4. Axial NECT brain of a baby with cleft lip and palate shows non-separated cerebrum with dilated lateral ventricle and absent septum.

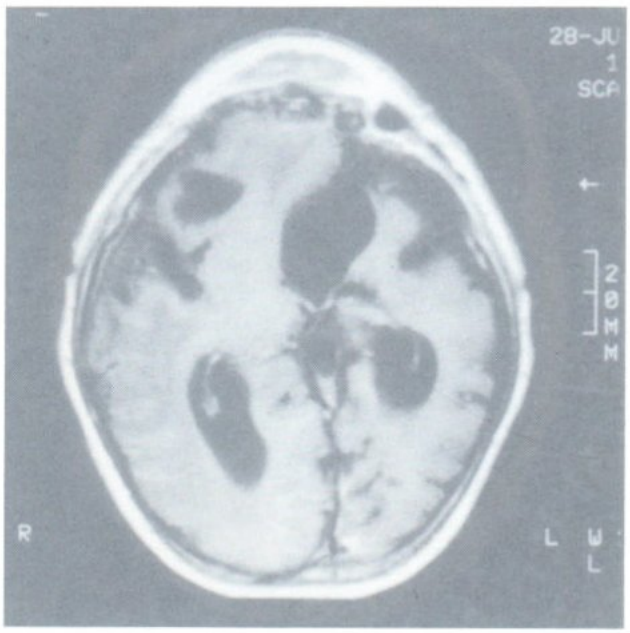

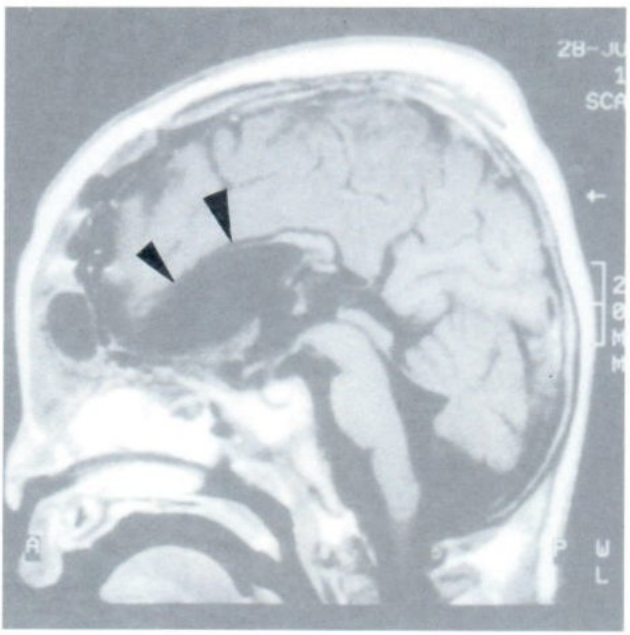

5A **5B**

Fig. 5. T1-wi in axial (A) and sagittal (B) planes of a patient with previous closure of frontal meningocele show absent septum and partial agenesis of corpus callosum from rostrum through body (arrow).

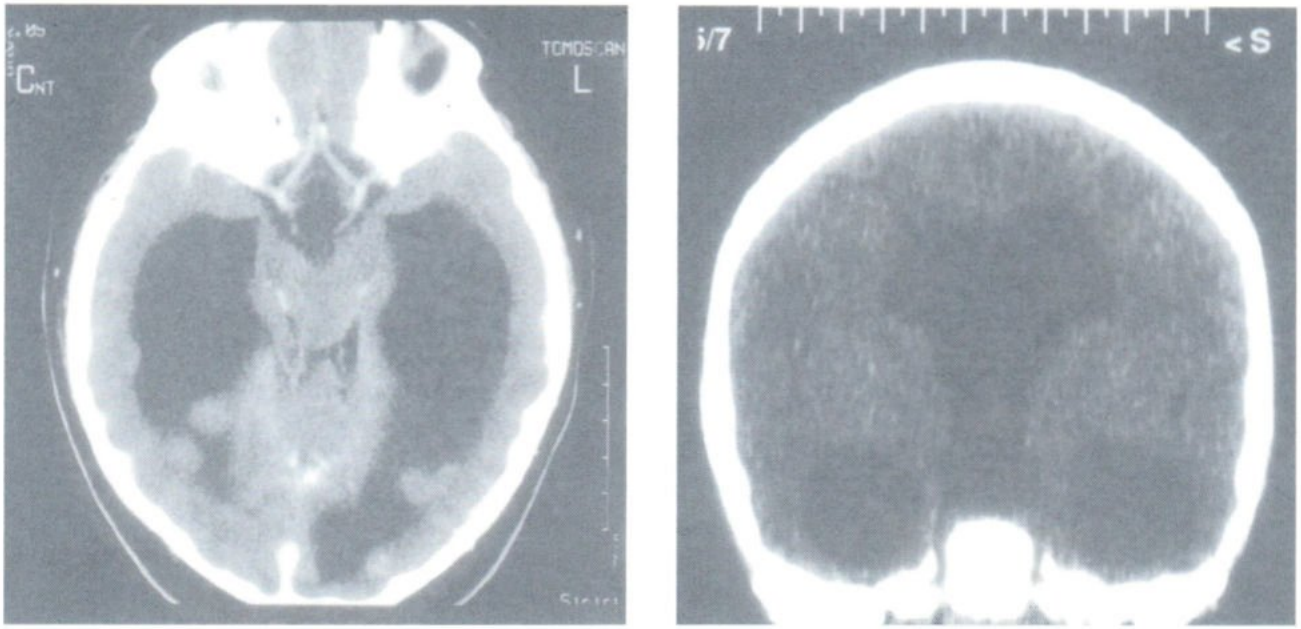

6A 6B

Fig. 6. CT brain in axial (A) and reconstructed coronal (B) planes of a boy with frontoethmoidal meningoencephalocele demonstrate absent septum and heterotropia at subependymoid region (A).

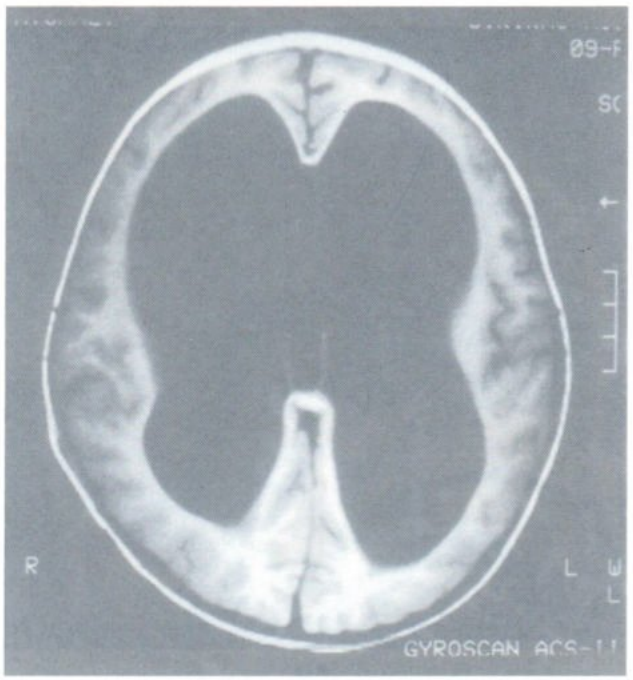

Fig. 7. Axial T1-wi of a patient with absent septum demonstrates right schizencephaly. Note the polymicrogyria of the cortex outlining the cleft.

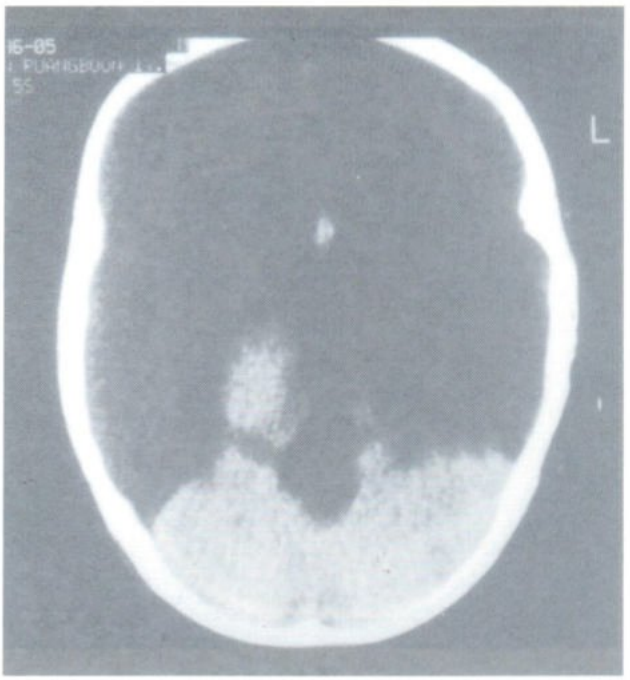

Fig. 8. Axial CT brain of a patient with hydranencephaly shows absent septum.

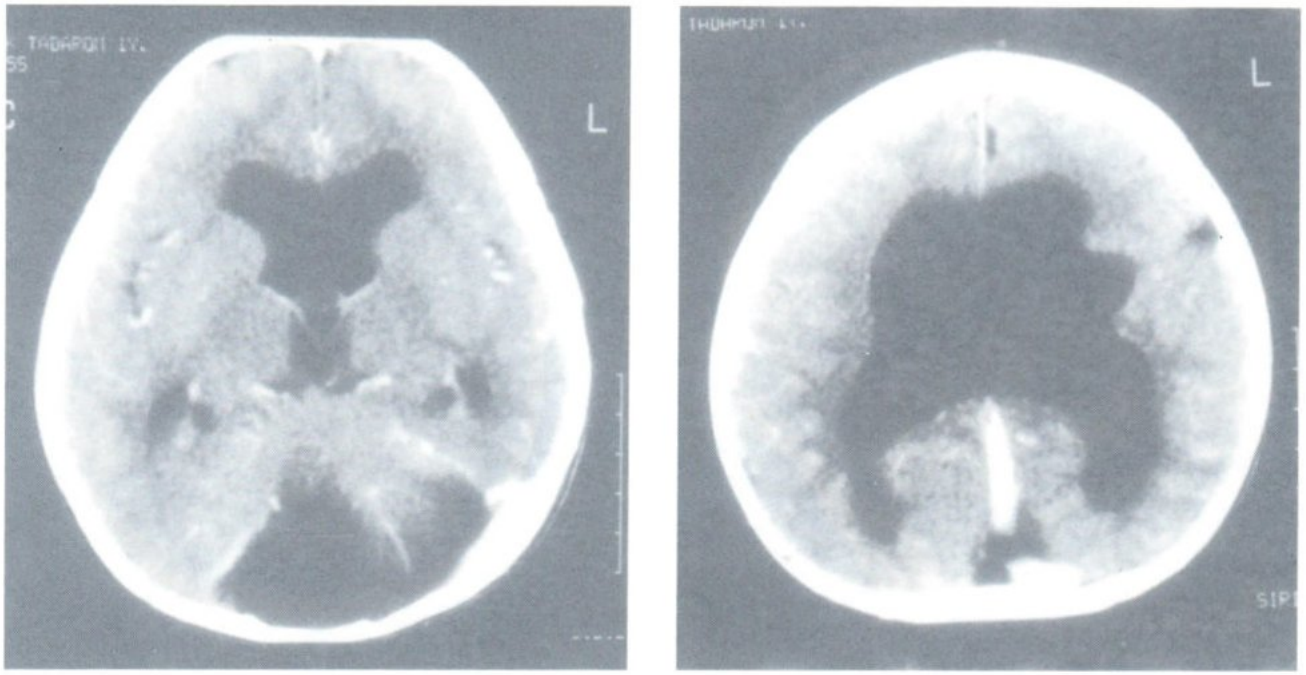

9A 9B

Fig. 9. Axial CT of a patient with cerebellar hypoplasia (A) shows absent septum and left cerebral cleft (B).

CONCLUSION

We can conclude that ASP is the abnormal finding of the brain either from primary or secondary developmental causes. It is the indicator or marker for radiologist to search for other associated anomalies. CT scan may give lower resolution to see other abnormalities. MRI should be done in the available places. If MRI is not available or no other abnormalities could be found, suggestion to the clinician to search for neurological and psychological disorder should be given, especially in the pediatric septo-optic dysplasia. The early treatment of GH or TSH deficiency will prevent mental retardation and the associated abnormalities may predict the prognosis of the patients.

REFERENCES

1. Stangel M., Vogeley KT., Jandeck C., et al. Septo-optic dysplasia (de Morsier syndrome). Nervenargt, 1998;69(4):352-6.
2. Takahashi S., Makita Y., Okamoto N., et al. L1CAM mutation in a Japanese. Brain & Development, 1997;19(8):559-62.
3. Nuri Sener R. Septo-optic dysplasia associated with cerebral cortical dysplasia (cortico-septo-optic dysplasia). J. of Neuroradiology, 1996;23(4):245-7.
4. Ramos Fernandez JM., Martinez San Millan J., Barrio Castellano R. et al. Septo-optic dysplasia. Anales Espanoles de Pediatria, 1996;45(6):614-8.
5. Guduz K., Gunalp I., Saatci I. Septo-optic dysplasia associated with bilateral complex microphthalmos. Ophthalmic Genetics, 1996;17(3):109-13.

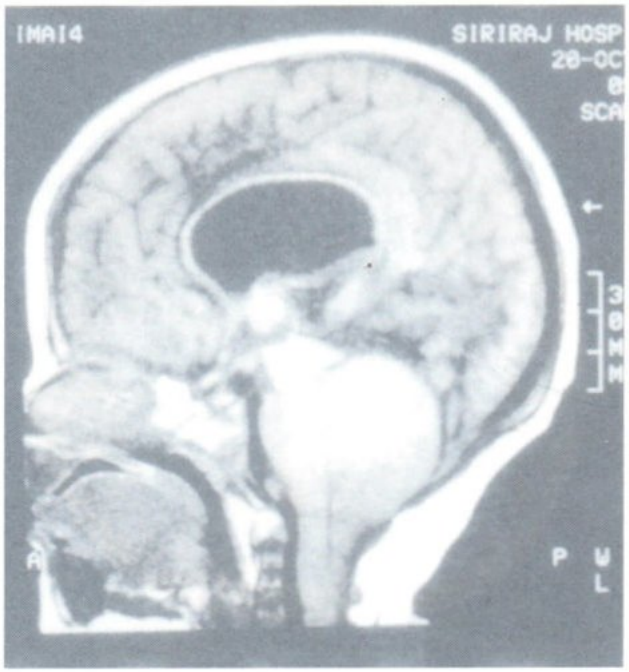

10A

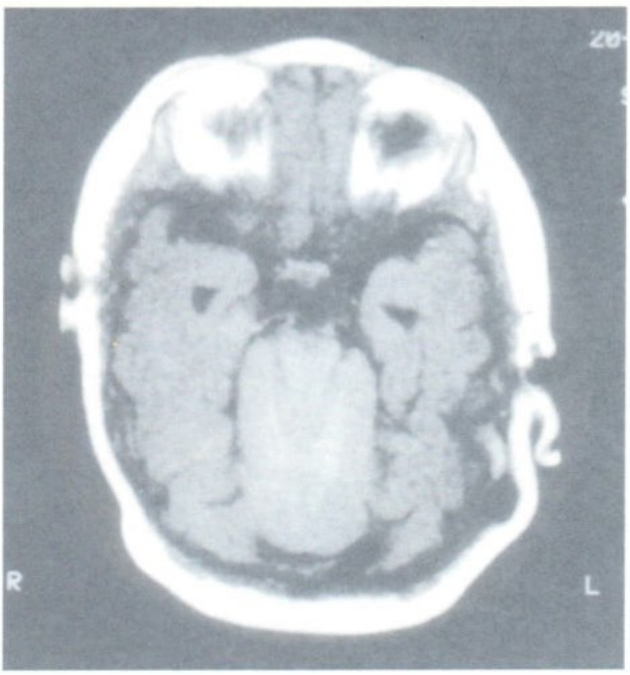

10B

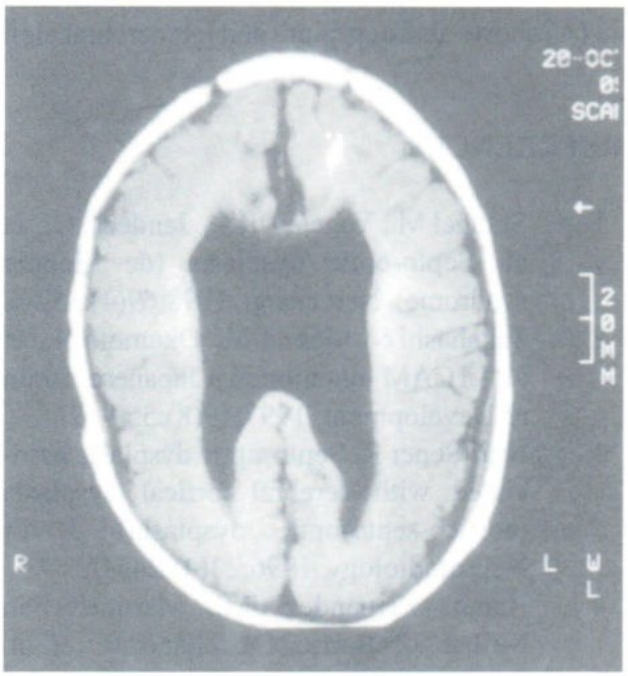

10C

Fig. 10. T1-wi of a patient with Chiari II malformation demonstrate typical beaked tectum and tonsillar herniation (A), triple peak sign of cerebellum (B) and absent septum (C). Note the normal shape of fronfal horn of lateral ventricle.

REFERENCES (CON'T)

6. Jabourian AP., Benhamou PA., Bitton R. Clinical imaging in psychiatrys. Annales Medico-Psychologiques, 1996;154(1):74-7.
7. Groenveld M., Pohl KR., Espezel H., et al. The septum pellucidum and spatial ability of children with optic nerve hypoplasia. Developmental Medicine & Child Neurology, 1994;36(3):191-7.
8. Badawy SZ., Pisarska, MD., Wasenko JJ., et al. Congenital hypopituitarism as part of suprasellar dysplasia. Journal of Reproductive Medicine, 1994;39(8):643-8.
9. Wolf SS., Hyde TM., Weinberger DR. Malformations of the septum pellucidum. Journal of Psychiatry & Neuroscience, 1994;19(2):140-4.
10. Coulter CL., Leech RW., Schaefer GB., et al. Department of Neurology, Creighton University, Omaha, NE 68131. Archives of Neurology, 1993;50(7):771-5.

11. Williams J., Brodsky MC., Griebel M., et al. Septo-optic dysplasia : The clinical insignificance of an absent septum pellucidum. Developmental Medicine & Child Neurology, 1993;35(6):490-501.
12. Nayak V., Bhat KR. Septo-optic dysplasia (case report). Indian Journal of Ophthalmology, 1991;39(4):186-7.
13. Benner JD., Preslan MW., Gratz E. et al. Septo-optic dysplasia in two siblings. American Journal of Ophthalmology, 1990;109(6):632-7.
14. Teng RJ., Wang PJ., Wang TR. et al. Apert syndrome associated with septo-optic dysplasia. Pediatric Neurology, 1989;5(6): 384-8.
15. Gualdi G., Dibiasi C., Pingi A. et al. MR in the evaluation of schizencephalys. Radiology Medical, 1989;78(4):311-3.
16. Knudtzon J. Aarskog D. Growth hormone deficiency associated with the ectrodactyly-ectodermal dysplasia-clefting syndrome and isolated absent septum pellucidum. Pediatrics, 1987;79(3):410-2.
17. Nowell M. Ultrasound evaluation of septo-optic dysplasia in the new born. Neuroradiology, 1986;28(5-6):491-2.
18. Deeg KH., Bundscherer F., Bowing B. Cerebral ultrasound diagnosis in brain abnormalitiess. Monatsschrift Kinderheilkunde. 1986;134(10):738-47.
19. Morishima A., Aranoff GS. Syndrome of septo-optic –pituitary dysplasia : the clinical spectrum. Brain & Development, 1986;8(3):233-9.
20. Morgan SA., Emsellem HA., Sandler JR. Absence of the septum pellucidum. Archives of Neurology, 1985;42(8):769-70.
21. Wilson DM., Enzmann DR., Hintz RL. et al. Computed tomographic findings in septo-optic dysplasia ; discordance between clinical and radiological findings. Neuroradiology, 1984;26(4):279-83.
22. Marechal JC., Boniface L., Clarisse J. et al. Septo-optic dysplasia. Archives Francaises de Pediatric, 1983;40(4):323-5.
23. Michaud J., Mizrahi EM., Urich H. Agenesis of the vermis with fusion of the cerebellar hemispheres, septo-optic dysplasia and associated anomalies. Acta Neuropathologica, 1982;56(3):161-6.
24. Cagianut B., Sigg P., Isler W., et al. Dysplasia opticoseptaliss. Klinische Monatsblatter fur Augenheilkunde, 1980; 176(4):699-703.
25. Krause-Brucker W., Gardner DW. Optic nerve hypoplasia associated with absent septum pellucidum and hypopituitarism. American Journal of Ophthalmology, 1980;89(1):113-20.
26. Manelfe C., Rochiccioli P. CT of septo-optic dysplasia. AJR. American Journal of Roentgenology, 1979;133(6): 1157-60.
27. Piper HF., Bastian GO., Warecka K. Nystagmus giratoire and optic nerve hypoplasia in combination with absence of the septum pellucidum (author's transl). Klinische Monatsblatter fur Augenheilkunde, 1979;174(5):663-75.
28. Fukushima N., Konno M., Sato T., et al. A case of septo-optic dysplasia. Tohoku Journal of Experimental Medicine, 1978; 126(2):193-7.
29. Arslanian SA., Rothfus WE., Foley TP. Jr., Becker DJ. Hormonal, metabolic and neuroradiologic abnormalities associated with septo-optic dysplasia. Acta Endocrinologica, 1984;107:282-288.
30. Izenberg N., Rosenblum M., Parks JS. The endocrine spectrum of septo-optic dysplasia. Clin. Pediatrics, 1984;23(11):623-636.
31. Skarf B., Hoyt CS. Optic nerve hypoplasia in children associated with anomalies of the endocrine and CNS. Arch Ophthalmol, 1984;102:62-67.

32. Brodsky MC., Glasier CM. Optic nerve hypoplasia : clinical significance of associated central nervous system obnormalities on MRI. Arch Ophthalmol, 1993; 111:66-74.
33. Stanhope R., Preece MA., Brook CGD. Hypoplastic optic nerves and pituitary dysfunction. Arch. Dis. In Childhood, 1984;59:111-114.
34. Hoyt WF., Kaplan SL., Grumbach MM. et al. Septo-optic dysplasia and pituitary dwarfism. The Lancet, 1970;25:893-4.
35. Barkovich AJ., Fram EK., Norman D. Septo-optic dysplasia : MR imaging. Radiology, 1989;171:189-192.
36. Wales JKH., Quarrell OWJ. Evidence for possible Mendelian inheritance of septo-optic dysplasia. Acta Paediatr, 1996; 85:391-2.
37. Barkovich AJ., Norman D. Absence of the septum pellucidum : A useful sign in the diagnosis of congenital brain malformations. AJR, 1989;152:353-360.
38. Meyer BU., Roricht S, Niehaus L. Morphology of acallosal brains as assessed by MRI in six patients leading a normal daily life. J. Neurol, 1998;245:106-110.
39. Zeke SM., Hollman AS., Dutton GN. Neuroradiological Features of patients with optic nerve hypoplasia. J Pediatr. Ophthalmol & Strabis, 1992;29:107-112.
40. Truwit CL, Barkovich AJ., Shanahan R., Maroldo TV. MR imaging of rhombencephalosynapsis : report of three cases and review of the literature. AJNR, 1991;12: 957-965.
41. Kuhn J., Swenson LC., Youssef H. Absence of the septum pellucidum and related disorders. Comput. Med. Imaging and Graphics, 1993;17(2):137-147.
42. Bonnemann CG., Meinecke P. Bilateral Porencephaly cerebellar hypoplasia and internal malformations : Two siblings representing a probably new autosomal recessive entity. A. J of Med. Genetics, 1996;63:428-433.
43. Sarwar M. The septum pellucidum : Normal and abnormal AJNR, 1989;10: 989-1005.
44. Fitz CR., Holoprosencephaly and related entities. Neuroradiology, 1983;25:225-238.
45. Reeves DL. Congenital absence of the septum pellucidum : case diagnosed encephalographically and associated with congenital amaurosis. Bull Johns Hopkins Hosp, 1941;69:61-71.
46. De Morsier G. Etudes aur les dysraphes cranioencephaliques. III. Agenesie du septum lucidum avec malformation du tractus optique; la dysplasie septo-optique. Schweiz Arch Neurol Neurochir Psychiatr, 1956;77:267-292.

DIAGNOSIS AND DESCRIPTION OF MITRAL VALVE PAPILLARY FIBROELASTOMA BY MRI: A CASE REPORT

Suvipaporn SIRIPORNPITAK, MD[1], Sarana BOONBAICHAIYAPRUCK. MD,[2] Montien NGAONGAMTHAWEESUK, Bsc,.MD[3]

ABSTRACT

Papillary fibroelastoma is a rare primary tumor of the heart and is usually found incidentally at autopsy. The tumor is considered as benign but it may cause potential fatal event such as stroke and cardiac obstruction. In this case report, we describe a mitral valve papillary fibroelastoma detected by magnetic resonance imaging. A 28 year-old-female presented with cardiac syncope and chest pain and a small mass was detected by transthoracic echocardiography. The mass was further characterized by MRI and was described here. Complete surgical excision was performed. A mitral papillary fibroelastoma was diagnosed histologically. This case illustrated the value of MRI as an alternative non-invasive diagnostic tool in establishing the diagnosis.

Cardiac papillary fibroelastoma is a rare primary cardiac tumor, which is considered as endocardial in origin and is usually found incidentally at autopsy.[1] It is the third most common primary cardiac tumor but is the most common primary tumor of the heart valve.[2] Characteristically, it is small, solitary and usually not resulting in clinical problem. However, it can cause important clinical implications.[3-5] Echocardiography, particularly with transesophageal echocardiography, is the primary diagnostic procedure. It provides information regarding characteristic, location and other associated abnormality.[6] Magnetic resonance imaging (MRI) is useful as an adjunct diagnostic tool. It has the potential to provide the more precise delineation in term of size, shape, location and surface as well as some tissue characteristic.[7]

In this case report, we described the mitral valve papillary fibroelastoma diagnosed by MRI.

CASE REPORT

A 28 year-old-female with no previous medical history presented 4- week history of intermittent chest pain and one episode of syncope while she was walking. Chest pain was characterized as tightness at substernal area with radiation to left mandible and left arm, lasting approximately 15 minutes. The pain was relieved by rest. She did not experience any dyspnea or fever.

Physical examination revealed only a grade I-II diastolic murmur at left upper sternal border.

Chest X-ray showed mild cardiomegaly without pulmonary venous congestion. Electrocardiogram revealed symmetrical inverted T wave in lead V1 to V5 with occasional paroxysmal ventricular contraction. Transthoracic echocardiography demonstrated a 2x2x2 cm. mass of homogeneous echogenicity attached to the ventricular aspect of the anterior leaflet of the

1 Department of Radiology
2 Cardiology unit, Department of Internal Medicine
3 Cardiovascular and Thoracic Surgery Section, Department of Surgery Faculty of Medicine, Ramathibodi Hospital.

mitral valve (Fig.1). Doppler examination revealed mild mitral regurgitation secondary to the mass interfering with the valve function. There was mild left ventricular enlargement with poor left ventricular ejection function (35%).

Further evaluation with MRI revealed a 2x2x2 cm. mobile, multilobulated frond-like mass attached to the ventricular side of the anterior leaflet of mitral valve. The mass has a central core of hyposignal on and peripheral frond-like appearance of iso to slight hypersignal on T1W , hypersignal on T2W (Fig.2) with moderate peripheral enhancement after intravenously administered gadolinium (Fig3). On GRE T2W, the mass had the signal higher than the myocardium, which suggested tumor rather than thrombus. Mild mitral regurgitation and enlargement of left ventricle were also noted. There was no other cardiac mass.

Patient did not undergo for the cardiac catheterization due to the less likelyhood of coronary artery disease in this age group.

Laboratory evaluation revealed no leukocytosis.

The patient underwent surgery with excision of a bead-liked mass from ventricular side of anterior leaflet of mitral valve and the reconstruction of the mitral valve was performed. Histology confirmed the diagnosis of papillary fibroelastoma. The patient did not have any post-operative complications. She remained asymptomatic in a 5-month followed-up period.

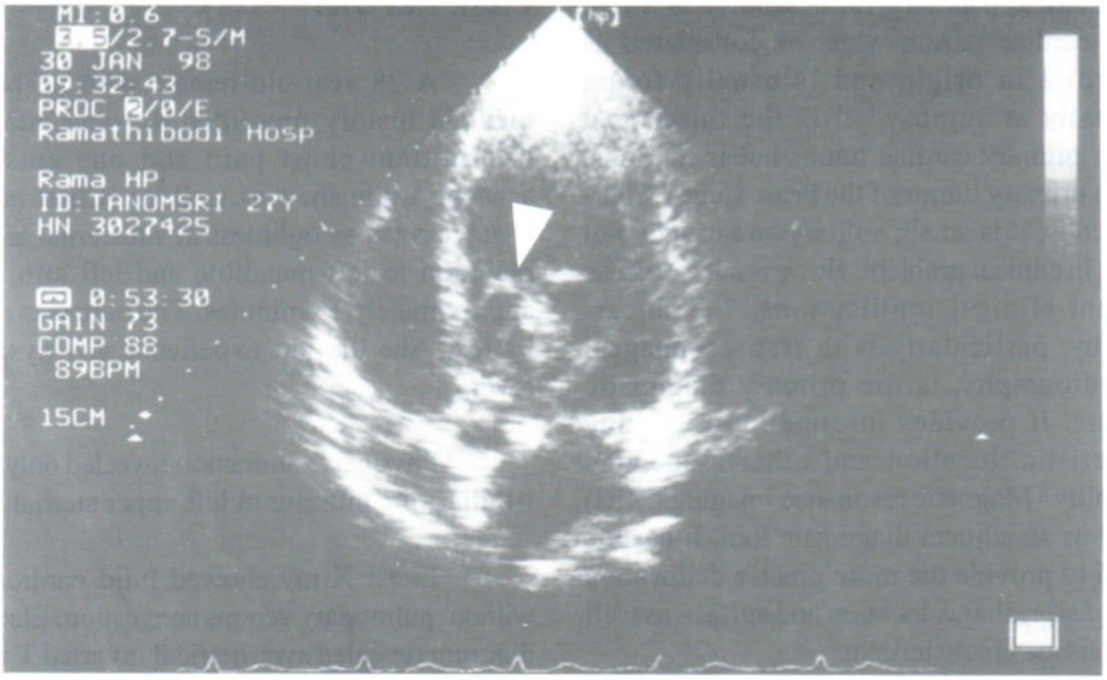

Fig. 1. Transthoracic echocardiography demonstrated an echogenic mass at anterior leaflet of mitral valve.

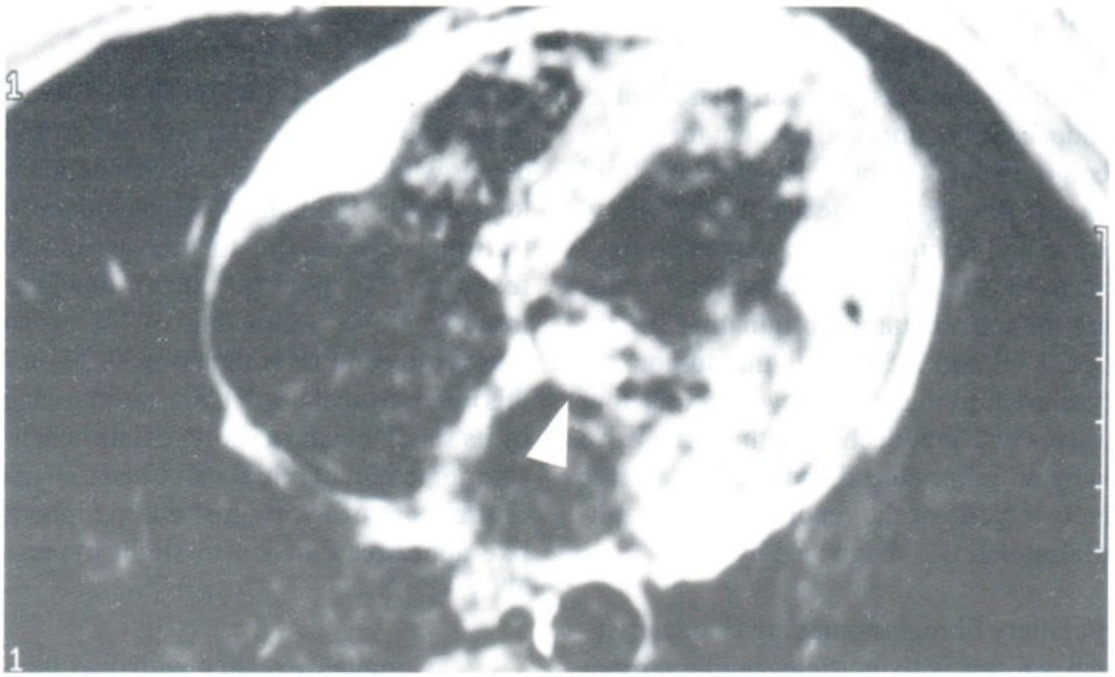

Fig. 2. MRI SE T1W in axial plane revealed a small, well-defined mass of isosignal to slight hypersignal, attaching to the anterior leaflet of the mitral valve. Note the characteristic of the frond-like appearance of the tumor.

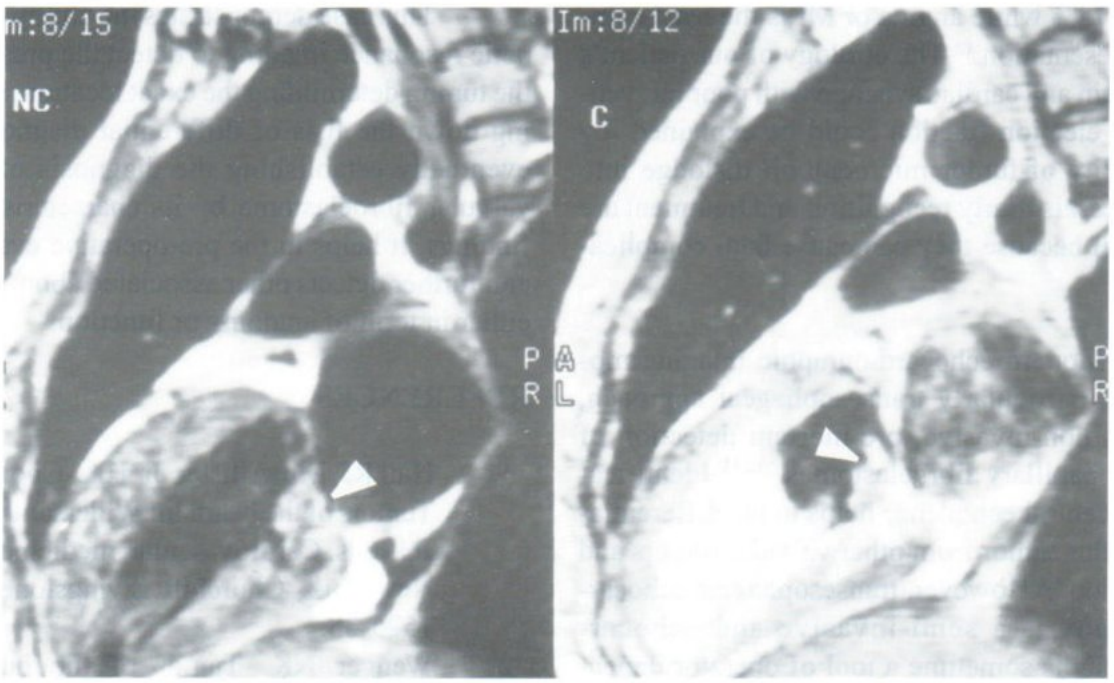

Fig. 3. MRI SE T1W pre gadolinium (left) and post gadolinium (right) in sagittal oblique plane demonstrated further details of the mass which showed a central core of hyposignal and peripheral frond-like appearance of iso to slight hypersignal on T1W (left). Gadolinium SE T1W revealed a peripheral enhancing frond-like peripheral part (right).

DISCUSSION

Papillary fibroelastomas are classified as benign endocardial tumors and account for 5-10% of all benign cardiac tumors.[1] They are the third most common primary cardiac neoplasm, following myxoma and lipoma.[3,5] They may arise from anywhere in the endocardium, however, cardiac valves are the most common originating site.[3,8,9] In addition, 88% and 71% of valvular tumors are papillary fibroelastomas.[10,11] They affect all four cardiac valves with predilection on the aortic valve followed by mitral, tricuspid and pulmonic valve respectively.[12] None of the reported mitral papillary fibroelastoma was diagnosed by MRI.

Papillary fibroelastomas are characteristically small, solitary with multiple papillary fronds and usually are attached to the endocardium by a short pedicle.[3,8] Neurologic symptoms such as stroke are the most common symptoms, accounting for 75% while angina or MI is the least common presentation.[12] The etiology of our patient's chest pain and cardiac syncope with poor left ventricular ejection fraction could be explained by possibility of tumor microemboli dislodge into great vessels. Early recognition and treatment are essential because they can cause fatal complication.[12,13]

Modern echocardiographic imaging modalities, particularly transesophageal approach, allow a non-invasive, pre-mortem detection of cardiac papillary fibroelastomas.[6,12,13] Identification of central echodense helps in the differentiation of this tumor from other valvular tumors and vegetation.[6,8] However, transesophageal echocardiography is a semi-invasive and echocardiography is sometime a tool of operator dependence.

Various MRI techniques allow a non-invasive diagnosis of papillary fibroelastomas. MRI is also useful in evaluation of valvular function. Spin echo T1W technique provides anatomical details while cine MRI provides functional physiologic details. Using the GRE technique, differentiation between the thrombus and tumor is feasible.[14] In general, thrombus has signal intensity lower than that of the surrounding muscle, in contrast with tumor. Differentiation of this tumor from the valvular myxoma can be made by its small, having a short pedicle attached to the anterior leaflet of mitral valve and a characteristic central core of hyposignal and peripheral frond-like appearance of iso to slight hypersignal on T1W.

Complete excision with or without valvular repair is the mean of eliminating the source and potential of fatal embolization.[15]

This case demonstrates the ability of magnetic resonance imaging to detect the presence of the tumor, determining the exact location, narrowing down the lists of differential diagnosis and eventually establishing the diagnosis of mitral valvular fibroelastoma by its characteristic MR findings. It helps in the pre-operative evaluation and further detects other associated abnormalities either in term of anatomy or function.

REFERENCES

1. Hall RJ, Mc Allister Jr HA, Cooley DA. Tumors of the heart. In: Willerson JT, Cohn JN, eds. Cardiovascular medicine. 1st ed. New York, Churchill Livingstone, 1995; 1525-38.
2. Wenger NK. Tumor of the heart. In: Gravanis MB, eds. Cardiovascular disorders: pathogenesis and pathophysiology. 1st ed. St Louis, Mosby, 1993;270-98.

3. Mc Allister HA Jr, Fenoglio JJ Jr. Tumors of the cardiovascular system. In: Atlas of tumor pathology. Fasc 15, 2nd series. Washington DC: Armed Forces Institute of Pathology, 1978;20-5.
4. Abu Nassar SG, Parker JC Jr. Incidental papillary endocardial tumors: its potential significance. Arch Pathol 1971;92:370-6.
5. Chitwood WR Jr. Cardiac neoplasm: current diagnosis, pathology and therapy. J cardiac Surg 1988;3:119-54.
6. Klarich KW, Enriquez-Sarano M, Gura GM, Edwards WD, Tajik AJ, Seward JB. Papillary fibroelastoma: echocardiographic characteristics for diagnosis and pathologic correlation. J Am Coll Cardiol 1997;30:784-90.
7. Link KM, Lesko NM. MR evaluation of cardiac/juxtacardiac masses. Topics Magn Reson Imaging 1995;7(4):232-45.
8. Shahian DM, Labib SB, Chang G. Cardiac papillary fibroelastoma. Ann Thorac Surg 1995;59:538-41.
9. Lichtenstein HL, Lee JC, Stewart S. Papillary tumor of the heart: incidental finding at surgery. Hum Pathol 1979;10: 473-5.
10. Ryan PE Jr, Obeid AL, Parker FB Jr. Primary cardiac valve tumors. J Heart Valve Dis 1995;2:222-6.
11. Edwards FH, Hale D, Cohen A, Thompson L, Pezzella AT, Virmani R. Primary cardiac valve tumors. Ann Thorac Surg 1991;52:1127-31.
12. Grinda J-M, Couetil JP, Chauvaud S, et al. Cardiac valve papillary fibroelastoma: surgical excision for revealed or potential embolization. Cardiovasc Surg 1999;117: 106-10.
13. Bhagwandien NS, Shah N, Costello JM Jr, Gilbert CL, Blankenship JC. Echocardiographic detection of pulmonary valve papillary fibroelastoma. J Cardiovasc Surg 1998;39:351-4.
14. Seelos KC, Caputo GR, Carrol CL et al. Cine gradient refocused echo (GRE) imaging of intravascular masses: differentiation between tumor and nontumor thrombus. J Comput Assist Tomogr 1992; 16:169-75.
15. McFadden PM, Lacy JR. Intracardiac papillary fibroelastoma: an occult cause of embolic neurologic deficit. Ann Thorac Surg 1987;43:667-9.

THE BOARD OF EDITORS OF THE AAR JOURNAL ,
THE JOURNAL OF THE RADIOLOGICAL SOCIETY OF THAILAND ,
AND THE ROYAL COLLEGE OF RADIOLOGISTS OF THAILAND.

WE WOULD LIKE TO EXTEND OUR GRATITUDE AND APPRECIATION FOR THE KIND CONSIDERATIONS TO BE HELPFUL IN THE PUBLISHING OF THE JOURNAL OF THE RADIOLOGICAL SOCIETY OF THAILAND IN THAI LANGUAGE AND THE ASEAN JOURNAL OF RADIOLOGY IN ENGLISH, TO THOSE COMPANIES OF DIFFERENT BUSINESSES IN THAILAND AND ABOARD.

IF THERE IS ANY THING WE CAN DO TO PROMOTE YOUR BUSINESSES IN THAILAND, PLEASE DON'T HESITATE TO LET US KNOW.

THE BRACCO INTERNATIONAL CO.,LTD.
INTERNATIONAL PHARMACEUTICAL CO.,LTD. (BRACCO)
C.M.C. BIOTECH CO.,LTD. (TOSHIBA)
PHILIPS ELECTRICAL CO. OF THAILAND LTD.
VIMITKIJ LTD. PARTNERSHIP
SCHERING (BANGKOK) CO.,LTD.
KONGSAK X-RAY MEDICAL INDUSTRY CO.,LTD.
HOPE THAI MEDICAL CO.,LTD.
PACIFIC HEALTH CARE (THAILAND) CO.,LTD.
THAI TECHNOMED CO.,LTD.
SUPREME PRODUCTS CO.,LTD.
KAMOL SUKOSOL ELECTRIC CO.,LTD.
BERLI JUCKER CO.,LTD. (AGFA)
RADIOLOGICAL EQUIPMENT CO.,LTD.
U.S. SUMMIT CO.,LTD.
FUJI PHOTO FILM (THAILAND) CO., LTD.
KODAK (THAILAND) CO.,LTD.
VIDHAYAKOM CO.,LTD.
SIEMENS CO.,LTD.
OXO CHEMIE CO.,LTD.
KYUOWA HAKKHO (THAILAND) CO.,LTD.
JEBSEN & JESSEN CO.,LTD.
MEDICAL INTENSIVE CARE CO.,LTD.
THAI POLY MEDIC CO.,LTD.
INTERNATIONAL COSMETICS CO.,LTD.
TERUMO (THAILAND) CO.,LTD.
ZUELLIG PHARMA CO.,LTD. (NYCOMED)
UDOM MEDICAL EQUIPMENT CO.,LTD.
SCIENCE TECH CO.,LTD.
S.I. MEDICAL (DU PONT FAR EAST INC.)
THAI HOSPITEX CO.,LTD.
S.J. MEDICAL TRADING CO.,LTD.
G.E. INTERNATIONAL OPERATIONS CO.,LTD.
UNITED 4 CO.,LTD.
THANETPATTANA CO.,LTD.
BIO JINITECH CO.,LTD.
TRANMEDIC CO.,LTD.
UNIMED CO.,LTD.
XOVIC CO.,LTD.
BORNEO (THAILAND) CO.,LTD.
THAI INDUSTRIAL GLASS CO.,LTD.
MEDICAL INDUSTRIAL DOMESTIC CO.,LTD.
THAI GL. CO.,LTD.
PHATUMKARNCHANG X-RAY PARTNERSHIP
B-GRIMM HEALTH CARE CO.,LTD.
ANGLO-THAI (THAILAND) CO.,LTD.
JOHNSON & JOHNSON (THAILAND) CO.,LTD.
OREX TRADING CO.,LTD.
MAY & BAKER CO.,LTD.
DELTA LABORATOIRE CO.,LTD.
NAMSIN TRADING CO.,LTD.
HARIKUL LTD. PARTNERSHIP
SIAM PHARMACEUTICALS CO.,LTD.
3M (THAILAND) CO.,LTD.
DIAMOND FIELD CO.,LTD.
STERLING DRUG INTERNATIONAL INC.
S.B. MEDICO CO.,LTD.
PICKER INTERNATIONAL (THAILAND) CO.,LTD.
THAI UNIQUE CO.,LTD.
THAI GAUZE CO.,LTD.
PRAMUANMIT CO.,LTD.
SURIYA & GALAXY GROUP LTD. PARTNERSHIP
DIETHELM CO.,LTD.
MEDICAL MEDIA PRODUCT CO.,LTD.
THAIMED TECH CO.,LTD. (SCHNEIDER)
J.F. ADVANCE MED CO.,LTD.
PRIME MEDICAL CO.,LTD.
APEX MEDICAL TECHNOLOGY (THAILAND) CO.,LTD.
MEDITOP CO.,LTD.

CALCIUM PYROPHOSPHATE DIHYDRATE CRYSTAL DEPOSITION IN THE LIGAMENTUM FLAVUM OF THE CERVICAL SPINE

Daranee PITANUPONGSA [1], Jarturong TAPARHUDEE [2], Hatcha SRIPLUNG [3]

ABSTRACT

A 73 – year-old woman with cervical myelopathy was shown to have calcified nodule in the ligamentum flavum of C-4. Laminectomy was performed. Histological examination showed calcium pyrophosphate dihydrate crystals in the nodule. Images were of plain cervical spine radiographs and computed tomographic myelography.

INTRODUCTION

Calcium pyrophosphate dihydrate crystal deposition in the ligamentum flavum of the cervical spine is rare. It compresses the spinal cord, causing neurologic sign and symptoms. There have been several reports describing its histopathology, clinical and radiographic features. Most occured in United States of America and Japan.

We present a case of CPPD crystal deposition in the ligamentum flavum of the cervical spine in Thailand by plain radiograph and CT myelography.

CASE REPORT

A 73-year-old Thai female patient was requested for CT myelography of cervical spine. The patient was admitted with a 6-month history of progressive tetraparesis. She also had mild hypertension and DM. Examination revealed weakness in all extremities, more severe in lower extremities, and decreased pinprick sensation below the C-5 level. The deep tendon reflexes were 3+ and equal in all four extremities. The Babinski sign revealed a plantar extension. She had a positive Hoffman's sign.

Plain cervical spine radiographs showed minimal spondylotic change. A calcified nodule size about 10 mm. was found in left paramedian portion of the posterior spinal canal at C4-5 level. (Fig. 1)

CT myelography demonstrated a left posterolateral extradural oval- shaped densely calcified nodule size about 10 mm. at C-4 level compressing the spinal cord and displacing it to the right. (Fig. 2)

Laminectomy was performed at C-4. Histologically, the lesion consisted of CPPD crystal deposition in the ligamentum flavum. (Fig. 3)

[1] Section of Radiology, Trang Hospital, Trang, Thailand
[2] Section of Surgery, Trang Hospital, Trang, Thailand
[3] Department of Pathology, Faculty of Medicine, Prince of Songkla University, Songkhla, Thailand.

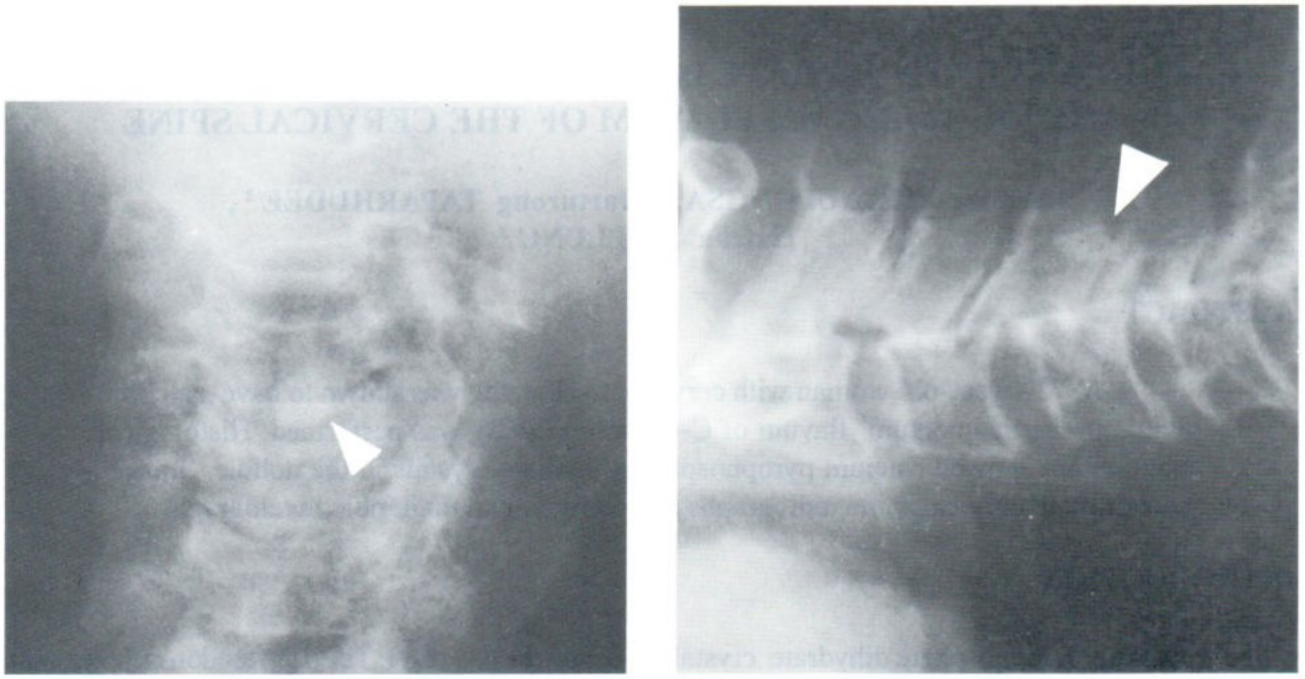

Fig.1 Plain radiographs of the cervical spine, AP and lateral views (A,B), showing radiopaque nodular shadow in posterior part of the spinal canal at C4 level.

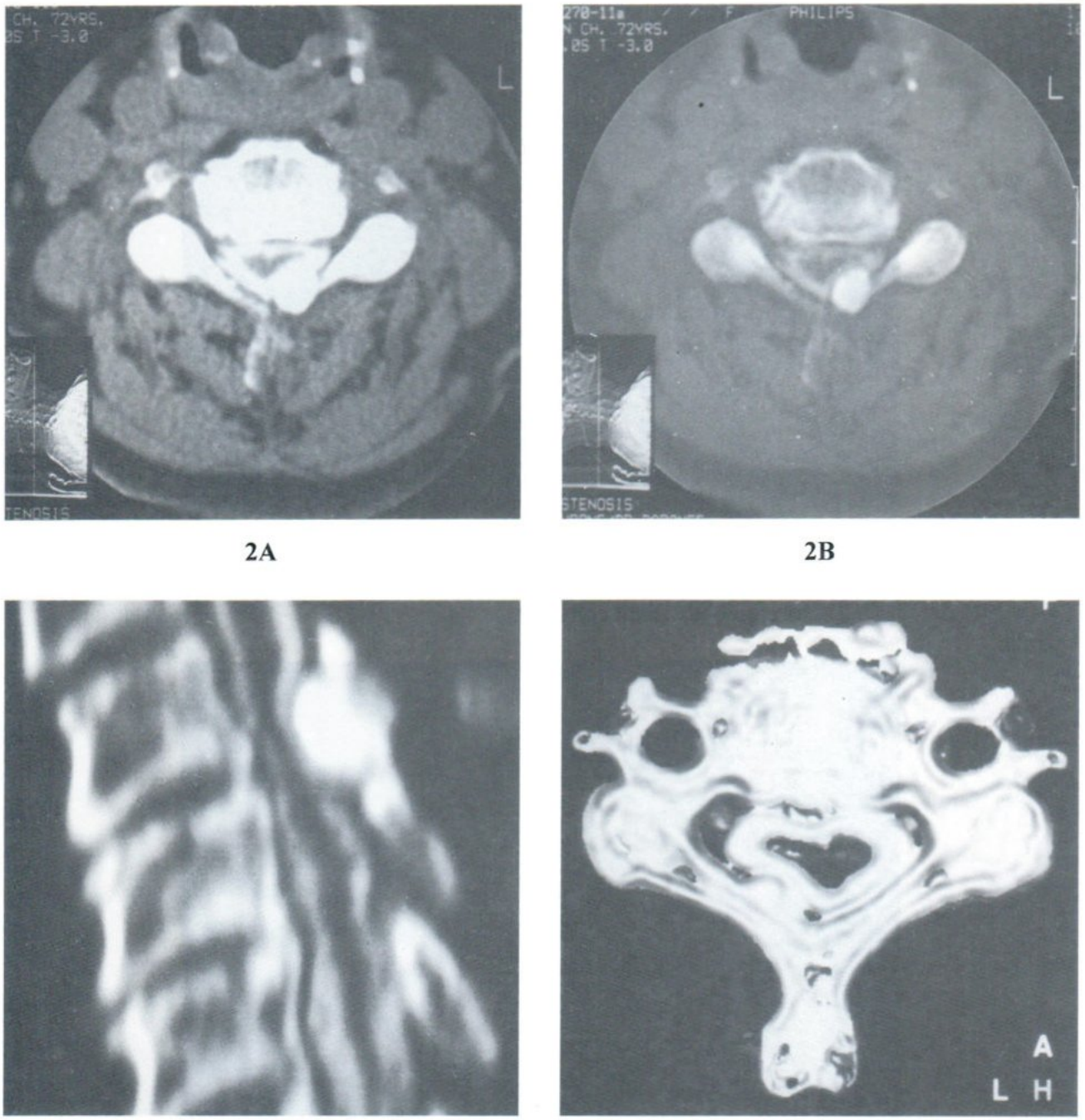

2A 2B

2C 2D

Fig.2 CT myelography, A. axial image – soft tissue window, B. axial image – bone window, C. Midline sagittal reconstruction, D. 3 D reconstruction, demonstrating a left posterolateral extradural calcified mass compressing the cervical cord.

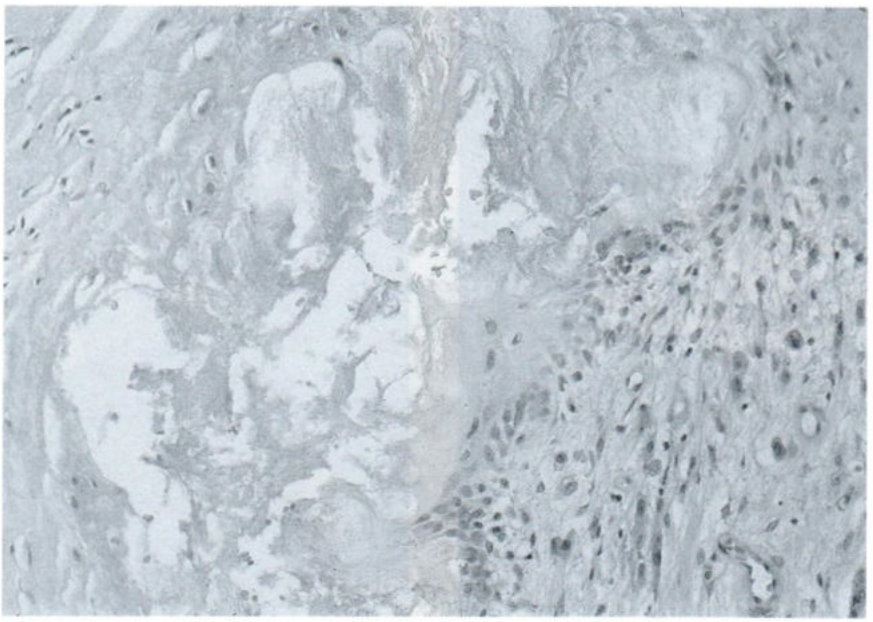

Fig.3A The granuloma consists of crystals and pink fibrinous material surrounded by epitheloid macrophages and a few foreign body giant cells (20x).

Fig.3B The center of granuloma contains rhomboid crystals of calcium pyrophosphate dihydrate and pink fibrinous material (40x).

DISCUSSION

Calcium pyrophosphate dihydrate (CPPD) crystal deposition disease is a general term for a disorder characterized by the presence of $Ca_2P_2O_7 \cdot 2H_2O_2$ (calcium pyrophosphate dihydrate or CPPD) crystals in or around joints.[1] CPPD crystal deposition disease affects both men and women and generally is observed in middle-aged and elderly patients.[1] Mc. Carty applied certain diagnostic criteria for CPPD : demonstration of crystal deposition by polarized light microscopy and chondrocalcinosis were required for a definite diagnosis; demonstration of crystal deposition or chondrocalcinosis provided a probable diagnosis; and the presence of a clinical syndrome consistent with pseudogout, a possible diagnosis.[1,5]

CPPD crystal deposition generally is first observed in articular cartilage, althrough deposits may be recognized in other articular tissues, such as synovium and capsule, as well as periarticular tissues, such as tendons and ligaments.[1,4,8] Rarely, the crystals are indentified at the dura mater or ligamentum flavum.[1]

Chondrocalcinosis and CPPD can involve the spine through a variety of mechanisms. Intervertebral discal calcifications are frequent, calcific collections resemble syndesmophytes of ankylosing spondylitis.[1,2,5] Vertebral body and intervertebral disc destruction causing disc space narrowing and vertebral sclerosis is a common finding.[1,5] Severe osseous destruction is unusual.[1] CPPD deposits in the ligamentum flavum causing myelopathy and cervicomedullary compression have been reported.[1,2]

Calcium crystal deposition rarely occurs in the ligamentum flavum of the cervical spine.[3,6] Crystal deposition in the cervical spine is most commonly a result of Calcium pyrophosphate deposition disease.[7] CPPD crystal deposition disease involved the cervical spine, usually in elderly woman without other systemic evidence of CPPD.

Most patients presented with progressive cervical myelopathy or radiculomyelopathy.[2,3,5,7,8,9,10] Most radioghaphic findings, including our case, showed focal enlargement of the ligamentum flavum due to oval CPPD deposits that compressed the spinal cord, causing neurologic sign and symptoms. The midcervical spine is most frequently involved.

CPPD deposition within the ligamentum flavum can be associated with significant spinal stenosis. Most patients described in the literature underwent laminectomy. These characteristics allow the radiologist to suggest a propable diagnosis of CPPD and to guide the pathologist to identify the CPPD crystals in the calcified deposits.

ACKNOWLEDGEMENT

We wish to thank Prof. Dr.Vorachai Sirikulchayanonta M.D., Department of Pathology, Ramathibodi Hospital, for helpful review the histologic slides and to Associate Prof. Dr.Patchrin Pekanan, Department of Radiology, Ramathibodi Hospital for reviewing the manuscript.

REFERENCES

1. Resnick D, Niwayama G. Calcium pyrophosphate dihydrate (CPPD) crystal deposition disease. In : Resnick D, editors. Diagnosis of Bone and Joint Disorders. 3rd ed. Philadelphia : WB Saunders ; 1995. P.1556-610.

2. Salcman M, Khan A, Symonds DA. Calcium pyrophosphate arthropathy of the spine : case report and review of the literature. Neurosurgery 1994;34:915-8.
3. Fye KH, Weinstein PR, Donald F. Compressive cervical myelopathy due to Calcium pyrophosphate dihydrate deposition disease. Arch Intern Med. 1999;159:189-93.
4. Ishida T, Dorfman HD, Bullough PG. Tophaceous pseudogout (tumoral calcium pyrophosphate dihydrate crystal deposition disease). Hum Pathol 1995;26:587-93.
5. Resnick D, Niwayama G, Goergen TG, et al. Clinical , radiographic and pathologic abnormalities in calcium pyrophosphate dihydrate deposition disease (CPPD) : pseudogout. Radiology 1977;122:1-15.
6. Babe H, Maezawa Y, Kawahara N, et al. Calcium crystal deposition in the ligamentum flavum of the cervical spine. Spine 1993;18:2174-81.
7. Ojemann JG, Grubb RL, Kyriakos M, et al. Calcium carbonate apatite deposition in the cervical spine with associated vertebral destruction. J Neurosurg 1997; 86:1022-6.
8. Brown TR, Quinn SF, D'Agostino AN. Deposition of calcium pyrophosphate dihydrate crystals in the ligamentum flavum : evaluation with MR imaging and CT. Radiology 1991;178:871-3.
9. Kawano N, Yoshida S, Ohwada T, et al. Cervical radiculomyelopathy caused by deposition of calcium pyrophosphate dihydrate crystals in the ligamenta flava. J Neurosurg 1980;52:279-83.
10. Norris JS, Hope DT. Cervical myelopathy caused by pseudogout. Br J Neurosurg 1995;9:103-5.
11. Fidler WK, Dewar CL, Fenton PV. Cervical spine pseudogout with myelopathy and charcot joints. J Rheumatol 1996;23:1445-8.

DESMOID TUMOR : A CASE REPORT

Kulthida SAKOLCHAIPONG,M.D.[1] Darunee BOONJUNWETWAT, M.D.[1]
Voranuch PUNYAVORAVUT, M.D.[2]

Extra-abdominal fibromatosis (desmoid tumor) is an uncommon soft tissue tumor. About two-third of cases occur in the extremities. We present a female 43-year-old case of multicentric desmoid tumor.

CASE REPORT

A 43-year-old woman came to the Chulalongkorn Hospital in June 1998 presenting with painless, non tender and slow growing masses at left calf and foot for a year. She had previous surgery of left thigh mass since she was 12 year-old. Physical examination revealed soft tissue mass, 15x10 cm in size at dorsum of left equinous foot, which was fixed, firm consistency and ulcerated on top. The lesion along left calf was composed of multiple small masses, about 1.5 cm. in size and a big mass, 8 cm. in size with the surgical scar on the skin. Neither neurological deficit nor vascular compromise was observed. There was no palpable node at both inguinal areas. The laboratory data were within normal limits. The plain radiographs of the left leg and foot revealed large soft tissue masses at dorsum of left foot and along posterior aspect of left leg. Multiple cortical bony projections of fibula and tarsal bones were identified being spicule-like appearance (Fig. 1 A,B). The tarsal bones showed well defined cystic changes due to pressure erosion (Fig. 2). Three times of tissue biopsies were taken. The first and second specimens revealed chronic inflammation and fibrosis. The last one showed fibroma of tendon sheath. Wide excision was performed subsequently. Pathologically, the lesion was poorly circumscribed and consisted of elongated spindle-shaped cells of uniform appearance which separated by abundant collagen. There was no cellular atypia. The constituent nuclei were small, pale staining, and had one minute nucleoli (Fig. 3 A, B).

DISCUSSION

Fibromatosis (desmoid tumor) refers to locally invasive tumor of connective tissue and its overlying fascia or aponeurosis. The biologic behavior is intermediate between that of benign fibrous lesion and that of fibrosarcoma, although never metastasize.[1-3] According to Enzinger and Weiss,[4] the fibromatoses are classified on the basis of their anatomic location as either superficial or deep. The superficial group includes palmar fibromatosis, plantar fibromatosis, penile fibromatosis and knuckle pads fibromatosis. The deep or musculoaponeurotic fibromatoses include extra-abdominal fibromatosis (aggressive fibromatosis), abdominal fibromatosis, and intra-abdominal fibromatosis.

Extra-abdominal fibromatosis typically presents in young adult between puberty and 40 years of age, with a peak incidence between 25 and 35 years. Reports in the literatures indicate

[1] Department of Radiology
[2] Department of Pathology Faculty of Medicine, Chulalongkorn University, Bangkok, THAILAND

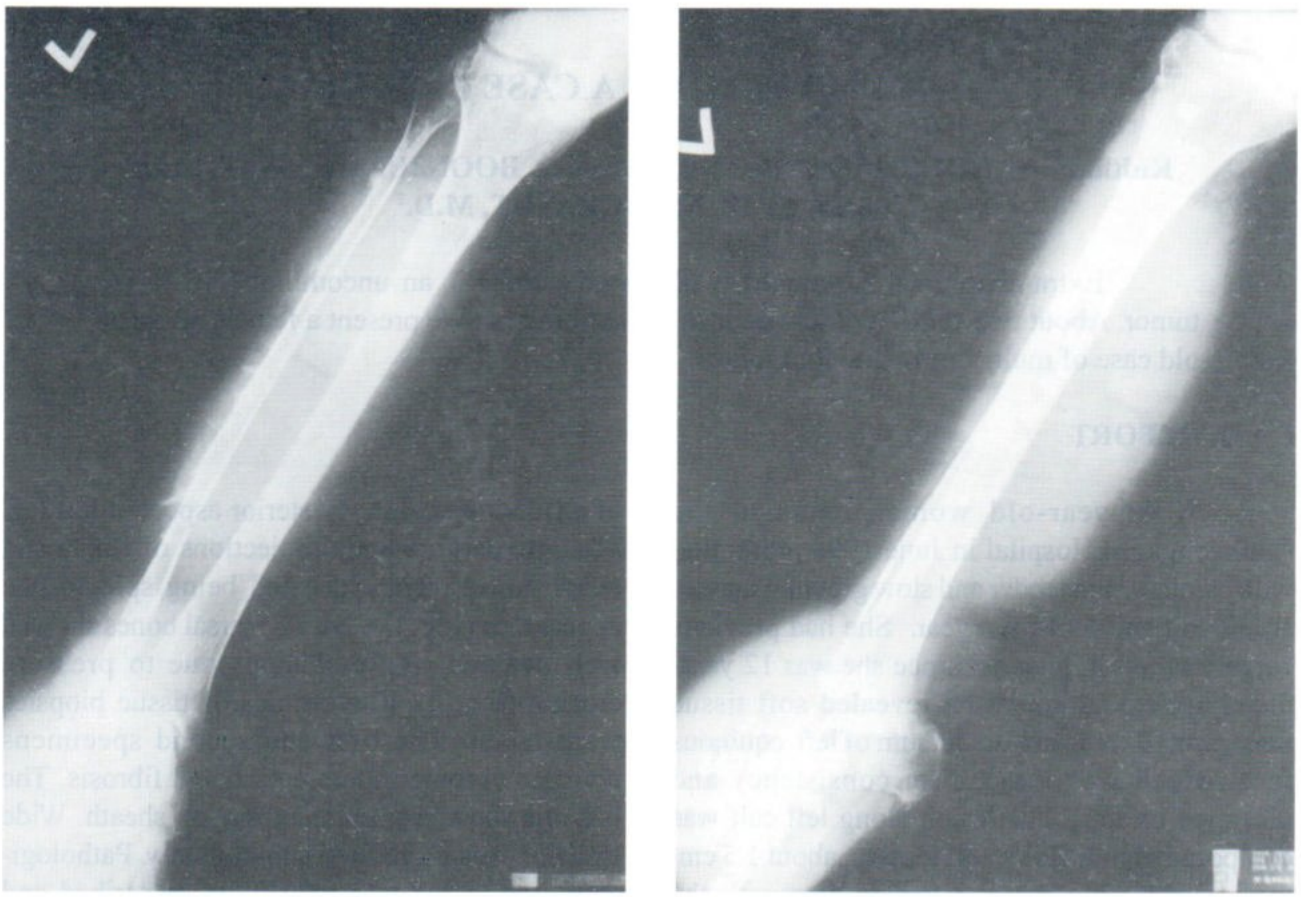

1A 1B

Fig. 1 A,B Plain radiographs of left leg (AP, lateral) showing large soft tissue masses at dorsal foot and calf with cortical spiculation of tibula and tarsal bone

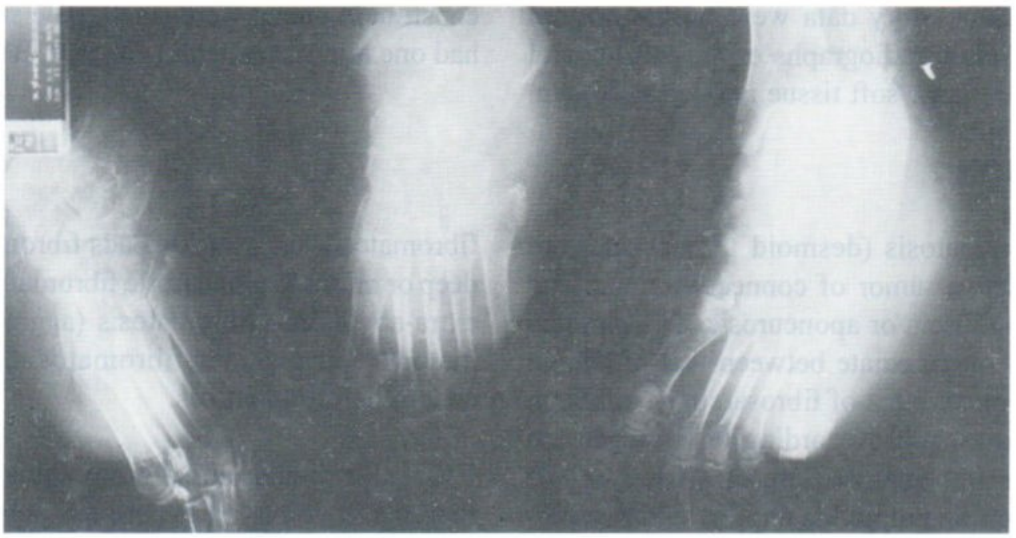

Fig. 2 Plain radiograph left foot (AP, lateral, oblique) showing soft tissue mass of dorsal foot with well defined cystic changes of tarsal bone or pressure erosion.

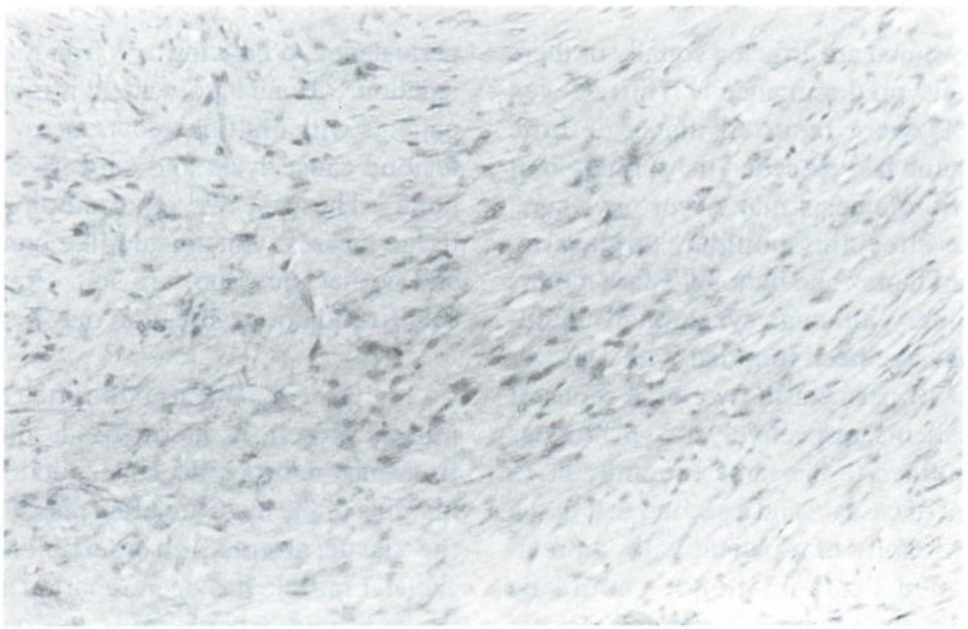

Fig. 3 A Low power picture showing interlacing bundles of fibroblasts separated by large amounts of collagen. (x 200)

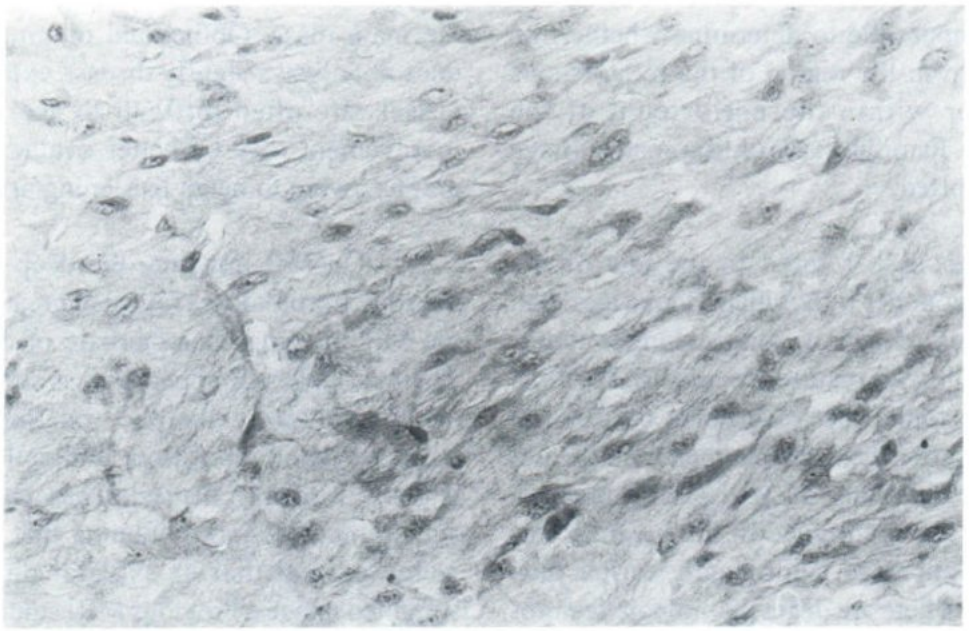

Fig. 3 B High power picture showing vesicular nuclei with minute nucleoli, rather indistinct cytoplasm, and interstitial collagen. (x 400)

that men and women are affected equally or there is 1.8 :1 female predominance.[1,5] Thirty seven patients (19%) were reported that a definite episode of trauma had preceded the formation of a mass. The fibromatosis may occur anywhere. The principle sites are shoulder, thigh, arm, posterior part of thorax and buttock. These tumors are usually solitary, although synchronous multicentric lesions have been reported with a prevalence of 10 to 15 per cent in two large series of 192 and 110 patients, respectively.[5-6] Synchronous lesions are confined to the same extremity in 75 to 100 per cent of cases[5-6] and a second soft tissue mass in the extremity of a patient with a previously confirmed desmoid tumor should be regarded as a second desmoid tumor until proved otherwise. Very rarely the lesion may be juxtacortical. Dong et al[7] reported a juxtacortical lesion in the forearm of a 14-year-old boy, noting that it was impossible to determine whether the tumor arose from the region of the interosseous membrane or within the periosteum of the adjacent bone. Familial cases of fibromatosis have also been reported.

Prognosis is related to the age of the patient, with younger individuals (those less than 20 to 30 years of age) having a longer tumor activity and a higher recurrence rate.[5] 68% of the patients were found that recurrence occurred at about 2 years after the first treatment and greater risk in female older than 30 year-old.[5] Romero et al[8] noted that the recurrence in the juvenile was multiple and appeared significantly earlier than adult patients. There are different biologic features between juvenile and adult patients with histologically same desmoid tumor.

Radiographs are usually nonspecific but roughly estimate of the size and location of the mass. Approximately 6 to 37 per cent of patients have evidence of bone involvement which is usually a pressure erosion, a scalloping without invasion or destruction or stimulation of the periosteum, producing a " frondlike" periosteal reaction.[5,9] Bone involvement is more common in patients with multiple recurrences.[5] Juxtacortical lesions cause lysis and saucerize the adjacent bone.[7] The case we reported showed the soft tissue masses with spicule-like bony projections and cortical pressure erosion. Rare cases with calcification or ossification may be seen.

On CT, extra-abdominal fibromatoses images present as a soft tissue mass, which is frequently nonspecific. Unless outlined by fat, the margins of the mass are often poorly defined,[3] and the tissue attenuation coefficient relative to skeletal muscle has been reported as hypodense, isodense and hyperdense.[2-3] Lesion is enhanced with intravenous contrast with better delineation.[2-3] CT afford the opportunity to discern the proximity of bone and neurovascular structure to the main mass. Obliterated intermuscular plane does not always signify disease extension. Small vessels are often difficult to see. Subtle bone involvement may be better evaluated on radiographs owing to beam hardening artifact.[3]

On MR imaging, the deep musculoaponeurotic fibromatoses revealed great variability of the MR imaging characteristic of the lesions.[3,11] Their variable MR appearance is similar to that of other soft tissue lesion, and this variability reflected the composition and cellularity of the lesion.[11] Typically, the lesion has a heterogeneous signal intensity approximating that of fat on T2-weighted and that of skeletal muscle on T1-weighted images. Previous MRI studies had shown that the signal characteristics of desmoids most closely resemble those of malignant neoplasm such as heterogeneity, poor margination and neurovascular encasement. Mass had areas of low signal intensity consistent with fibrosis on both T1- and T2 weighted images and a signal intensity in the non fibrous portion of the tumor that is less than of fat on T2 weighted image, desmoid should be a primary diagnostic consid-

eration.[12] Fibromatoses typically demonstrate moderate to marked enhancement following administration of the intravenous Gd-DTPA, with enhancement corresponding to the cellular portions of the lesion.[13] MRI provides clear delineation of abnormal tissue and its relation to adjacent vascular and nervous structures suggested that it is more useful than other currently available imaging methods in preoperative staging, planning the surgical approach and determining the potential for limb salvage. However, MRI can be difficult to distinguish reactive edema from malignant lesion on the basis of relaxation time determinations or other characteristics unique to MRI. Overall failure of MRI and CT in diagnosis is that of calcification, ossification and periosteal reaction are less easily evaluated than on plain radiographs.[10]

In conclusion we present an uncommon case of multicentric desmoid tumor with possibly recurrence as correlated with of previous surgery of thigh mass. Only plain radiograph was performed showing large soft tissue mass with pressure erosion and marked bony spiculation. Since no neurovascular symptom was evident so further CT or MRI was unnecessary for additional information owing to limited use of such studies as described.

REFERRENCES

1. Enzinger FM, Weiss SW. Soft tissue tumors. St Louise:CV Mosby, 1983;53-71
2. Francis IR, Dorovini-Zis K, Glazer GM, et al. The fibromatoses : CT- pathologic correlation. AJR 147:1063-1066, 1986
3. Hudson TM, Vandergriend RA, Springfield DS, et al. Agressive fibromatosis : Evaluation by computed tomography and angiography. Radiology 150; 495-501, 1984
4. Enzinger FM, Wiess SW Fibromatoses In : Enzinger FM, Weiss SW, eds. Soft tissue tumors. St. Louise : Mosby, 1988:136-163
5. Rock MG, Pritchard DJ, Reiman HM, et al. Extra-abdominal desmoid tumors. J Bone Joint Surg 66A:1369-1374, 1984
6. Disler DJ, Alexander AA, Mankin HJ, et al. Multicentric fibromatosis with metaphyseal dysplasia. Radiology 187 : 489-492, 1993
7. Dong PR, Seeger LL, Eckardt JJ, Mirra JM. Case report 847. Juxtacortical aggressive fibromatosis (desmo plastic fibroma) of the forearm. Skeletal Radiol 23 : 560-563, 1994
8. Romero JA, Kim EE, KIM CG, et al. Different biologic features of desmoid tumors in adult and juvenile patients : MR demonstration. J Comput Assist Tomogr 19 : 782-787, 1995
9. Abramowitz D, Zornova, Ayala AG, Romsdahl MM. Soft-tissue desmoid tumors : Radiographic bone changes. Radiology 146 : 11-13, 1983
10. Aisen AM, Martel W, Braunstein EM, et al. MRI and CT evaluation of primary bone and soft-tissue tumors. AJR 146 : 749-756, 1986
11. Quinn SF, Erickson SJ, Dee PM, et al. MR imaging in fibromatosis : Results in 26 patients with pathologic correlation. AJR 156 : 539- 542, 1991
12. Hartman TE, Berquist TH, Fetsch JH. MR imaging of extraabdominal desmoids : Differentiation from other neoplasms. AJR 158 : 581-585, 1992
13. Hawnaur JM, Jenkins JPR, Isherwood I : Magnetic resonance imaging of musculoaponeurotic fibromatosis. Skeletal Radiol 19 : 495-499, 1990

ขอขอบคุณ บริษัทต่อไปนี้ ที่ได้มีอุปการะคุณแก่

รังสีวิทยาสมาคมและราชวิทยาลัยรังสีแพทย์แห่งประเทศไทย ในการลงโฆษณาแก่รังสีวิทยาสารตั้งแต่พิมพ์เป็นภาษาไทย และ ASEAN JOURNAL OF RADIOLOGY ซึ่งพิมพ์เป็นภาษาอังกฤษ

คณะกรรมการรวมทั้งสมาชิกของรังสีวิทยาสมาคมและราชวิทยาลัยรังสีแพทย์แห่งประเทศไทย จะถือเป็นหน้าที่ซึ่งจะต้องระลึกถึงบุญคุณ และถ้ามีโอกาสจะช่วยเหลือกิจการของบริษัทต่างๆ ที่จะกล่าวนามต่อไปนี้ พวกเราจะไม่ละเลยหรือละเว้นที่จะช่วยเหลือด้วยความเต็มใจ

บริษัท แบร็คโค อินเตอร์เนชั่นแนล จำกัด
บริษัท อินเตอร์เนชั่นแนล ฟาร์มาซูติคัล จำกัด (BRACCO)
บริษัท ซี.เอ็ม.ซี. ไบโอเท็ค จำกัด (TOSHIBA)
บริษัท ฟิลิปส์ อิเล็กทรอนิกส์ (ประเทศไทย) จำกัด
ห้างหุ้นส่วน วิมิตรกิจ จำกัด
บริษัท เซริง (กรุงเทพฯ) จำกัด
บริษัท คงศักดิ์ เอกซเรย์การแพทย์อุตสาหกรรม จำกัด
บริษัท วรไทย เมดิคอล จำกัด (HOPE THAI)
บริษัท แปซิฟิคเฮลแคร์ (ไทยแลนด์) จำกัด
บริษัท ไทยเทคโนเมด จำกัด
บริษัท สุพรีม โพรดักส์ จำกัด
บริษัท กมลสุโกศล อีเล็คทริค จำกัด
บริษัท เบอร์ลี่ ยุคเกอร์ จำกัด (AGFA)
บริษัท รังสิภัณฑ์ จำกัด
บริษัท ยู.เอส.ส้มมิท (โอเวอร์ซีส์) จำกัด
บริษัท ฟูจิโฟโต้ฟิล์ม (ไทยแลนด์) จำกัด
บริษัท โกดัก (ประเทศไทย) จำกัด
บริษัท วิทยาคม จำกัด
บริษัท ซีเมนส์ จำกัด
บริษัท อ๊อกโซ่ เคมี (ประเทศไทย) จำกัด
บริษัท เคียววา ฮัคโค (ประเทศไทย) จำกัด
บริษัท เจ็บเซ่น แอนด์ เจ็สเซ่น มาร์เก็ตติ้ง จำกัด
บริษัท เมดิคอลอินเทนซีฟแคร์ จำกัด (M.I.C)
บริษัท ไทยโพลีเมดิค จำกัด
บริษัท ไอ.ซี.ซี. อินเตอร์เนชั่นแนล จำกัด (มหาชน)
บริษัท เทอรูโม (ประเทศไทย) จำกัด
บริษัท ซิลลิค ฟาร์มา จำกัด (ไนโคเมด)
บริษัท อุดมเมดิคอล อิควิปเม้นท์ จำกัด
บริษัท ซายน์เทค จำกัด
บริษัท เอส.ไอ.เมดิคอล จำกัด
บริษัท ไทยฮอทพิเทคส์ จำกัด
บริษัท เอส.เจ. เมดิคอล เทรดดิ้ง จำกัด
บริษัท ยี.อี. อินเตอร์เนชั่นแนล จำกัด
บริษัท ยูไนเตด 4 จำกัด
บริษัท ธเนศพัฒนา จำกัด
บริษัท ไบโอจีนีเท็คส์ จำกัด
บริษัท ทรานส์เมดิค จำกัด
บริษัท ยูนิเมด จำกัด
บริษัท โซวิค จำกัด
บริษัท บอร์เนียว (ประเทศไทย) จำกัด
บริษัท ไทยอินดัสเตรียลแก๊ส จำกัด
บริษัท เมดดิคอล อินดัสเซียล โดเมสติคส์ จำกัด
บริษัท ไทย จี แอล จำกัด
ห้างหุ้นส่วนจำกัด ปทุมการช่างเอกซเรย์
บริษัท บีกริม เฮลแคร์ จำกัด
บริษัท แองโกล-ไทย จำกัด
บริษัท จอนห์สัน แอนด์ จอนห์สัน (ประเทศไทย) จำกัด
บริษัท โอเร็กซ์เทรดดิ้ง จำกัด
บริษัท เมย์แอนด์เบเกอร์ จำกัด
บริษัท เดลตา แล็บบอราตอรี่ จำกัด
บริษัท นำสินเทรดดิ้ง จำกัด
ห้างหุ้นส่วน หริกุล จำกัด
บริษัท สยาม ฟาร์มาซูติคัส จำกัด
บริษัท 3เอ็ม (ประเทศไทย) จำกัด
บริษัท ไดมอนด์ ฟิลด์ จำกัด
บริษัท สเตอร์ลิง ดรั๊ค อินเตอร์เนชั่นแนล จำกัด
บริษัท เอส.บี. เมดิโค จำกัด
บริษัท พิคเกอร์ อินเตอร์เนชั่นแนล จำกัด
บริษัท ไทยยูนีค จำกัด
บริษัท ไทยก๊อส จำกัด
บริษัท ประมวลมิตร จำกัด
ห้างหุ้นส่วนจำกัด สุริยา แอนด์ แกแลคซี่ กรุ๊ป จำกัด
บริษัท ดีทแฮล์ม จำกัด
บริษัท เมดิคอลมีเดียโปรดักส์ จำกัด
บริษัท ไทยเมด-เทค จำกัด (SCHNEIDER)
บริษัท เจ.เอฟ.แอดวาน เมด จำกัด
บริษัท ไพร์ม เมดดิคอล จำกัด
บริษัท เอเป็กซ์เมดิคอล เทคโนโลยี่ส์ (ประเทศไทย) จำกัด
บริษัท เมดิท็อป จำกัด

CASE REPORT : RUPTURED CHOLEDOCHAL CYST IN INFANT AND CHILDREN ; 3 CASES

Chantima RONGVIRIYAPANICH [1], M.D., Sriprapai KEOROCHANA [1], M.D., Chana SATHORNKICH [2], M.D.

ABSTRACT

Choledochal cysts are uncommon and appear as cystic or fusiform dilatation of the biliary tract including both intra- and extra-hepatic sites. They are usually diagnosed in infancy and childhood. Ruptured choledochal cyst is a rare complication of choledochal cyst. The etiology of ruptured choledochal cyst remain obscure but it may be associated with blunt trauma, cholelithiasis, an additional anatomical abnormality such as ductal stenosis distal to the cyst, or pancreaticobiliary malunion, and inspissated bile. However the cause of rupture is unknown in many cases and is considered to be spontaneous. The perforation site may be single or multiple and mostly in the posterior wall of the cyst. In this report, there were 3 female patients admitted in our hospital with ruptured choledochal cyst type 1. The first and second patients were 3 years old and complained of fever, abdominal pain, and nonbilious vomiting. The third patient, 19 days old, was presented by obstructive jaundice and clinical sepsis. The operative findings of exploratory laparotomy in all 3 patients were saccular dilatation of CBD with intraabdominal bilelike fluid, leading us to make the postoperative diagnosis of ruptured choledochal cyst. The possible causes of ruptured choledochal cyst in the three patients of this report could be cholelithiasis, blunt trauma with a long common channel of the pancreaticobiliary system and inspissated bile respectively. All 3 patients had choledochal cyst type1 and were treated by cyst excision in the first operation and Roux-en-Y hepaticojejunostomy in the second operation with good result and no complication.

CASE 1

A 3-year-old girl was admitted with complaints of RUQ abdominal pain, nonbilious vomiting, and fever for 20 days. After admission there were worsened abdominal pain with a palpable RUQ abdominal mass. A right upper quadrant soft tissue density mass was seen in the plain abdomen, an exploratory laparotomy was underwent. The operative findings were saccular dilatation of choledochal cyst about 5 cm in size and dilated gallbladder with no stone, bile fluid collection about 10 ml at supracolic gutter but no perforation site of bile leakage was detected. So a postoperative diagnosis of concealed rupture of choledochal cyst type 1 with bile leakage to supracolic gutter was made and then T-tube choledochostomy was performed. Postoperative results were good and recovered 2 weeks after the operation. T-tube cholangiography showed saccular dilatation of the common hepatic duct and proximal common bile duct; measuring about 2.7x4.5 cm consistent with choledochal cyst.

[1] Department of Radiology
[2] Department of Surgery Siriraj Hospital, Mahidol University, Bangkok, Thailand

She was then referred to Siriraj Hospital. Laboratory studies on admission showed hemoglobin level of 12.1 g/dL, WBC of 7,000/mL, serum alkaline phosphatase level of 329 U/L, serum glutamic-oxaloacetic transaminase (SGOT) level of 62 U/L, serum glutamic-pyruvic transaminase (SGPT) level of 119 U/L with normal bilirubin level.

The second operation with total excision of choledochal cyst and Roux-en-Y hepaticojejunostomy were performed. Histopathologic findings were choledochal cyst type1, 3.5 cm in length, 1.5 cm in circumference with recent and old hemorrhage and nonspecific chronic inflammation at the cyst wall whereas the gallbladder contained pigmented stones with congestion and focal hemorrhage. Postoperative results were good and no complication after follow-up for 1 year and 2 months.

CASE 2

A 3-year-old girl was presented with RUQ abdominal pain, nonbilious vomiting and diarrhea for 4 days which firstly she was diagnosed and treated as acute gastroenteritis. Two days later, she had fever with progressive vomiting and abdominal pain so she was admitted in Siriraj Hospital. There was a history of preceeding blunt abdominal trauma of falling from bicycle one week ago.

Physical examination revealed a body temperature of 38.8 °C, generalized abdominal tenderness, rebound tenderness, guarding with a maximal tender point in RUQ and decreased bowel sound. Laboratory studies showed a hemoglobin level of 12.3 g/dL, WBC of 2,630/mL, neutrophil 73%.

She had undergone exploratory laparotomy for peritonitis with suspected of ruptured appendicitis or ruptured liver abscess. The operative findings were bile-stained purulent peritoneal fluid about 300 ml, dilated gallbladder, contusion and dilatation of CBD about 2 cm in diameter with no perforation site seen, unusually firm pancreas, small perforation at the mid-portion of appendix with minimal fluid in lesser sac. Postoperative diagnosis were traumatic contusion and minute perforation of CBD, pancreatitis and ruptured appendicitis. Then cholecystostomy with T-tube drainage, transperitoneal drainage and appendectomy were performed. Histopathologic findings of appendix were compatible with acute appendicitis. T-tube cholangiography showed choledochal cyst type1 about 3x5 cm in size with distal CBD narrowing and a long common channel of the pancreaticobiliary junction. Followed up laboratory studies showed serum amylase level of 401 U/L, GGT 75 U/L, SGOT 88 U/L, SGPT 62 U/L, serum alkaline phosphatase 142 U/L with normal bilirubin level. After operation, she was given antibiotic and postoperative care. Then she recovered well and could be discharged 2 weeks after operation. Later the second operation was done with excision of the choledochal cyst (just beneath the confluence of Rt. IHD and Lt. IHD to 1 cm from the pancreaticobiliary junction) and Roux-en-Y hepaticojejunostomy was done successfully without complication.

Histopathologic findings were choledochal cyst about 2x5 cm in size and a short distal duct o.5 cm in length and 1 cm in diameter with chronic cholecystitis.

The result after 4-month follow-up was good.

CASE 3

A 19-day-old female infant was admitted because of jaundice, acholic stool, abdominal distension and clinical sepsis.

Laboratory studies showed a hemoglobin level of 13.1 g/dL, WBC of 16,550/mL, neutro-

phil 56%, lymphocyte20%, monocyte10%. The liver function test showed a total bilirubin level of 8.8 mg/dL, direct bilirubin level of 4.8 mg/dL, GGT 403 U/L with normal SGOT and SGPT levels. Radiologic examinations including plain * IHD = Intrahepatic Duct abdomen and abdominal ultrasound were performed. Plain abdomen showed ascites with bowel ileus. Abdominal ultrasound revealed ascites and a RUQ cystic mass communicating with the biliary system but no normal gallbladder could be identified. So the differential diagnosis was choledochal cyst or dilated gallbladder from sepsis. Peritoneal tapping was performed showing bilious ascites. Therefore exploratory laparotomy with peritoneal toilet and cholecystostomy were performed. The operative findings were intraperitoneal bile about 500 ml with fusiform dilatation of CBD about 5 cm in size consistent with ruptured choledochal cyst type 1. Later the second operation with excision of choledochal cyst and Roux-en-Y hepatico-jejunostomy were done with operative findings of bile plug in the choledochal cyst and perforation at the posterior wall of the choledochal cyst. She recovered well without complication after operation.

Histopathologic findings were compatible with choledochal cyst about 1.3x1.3x1 cm in size without stone formation.

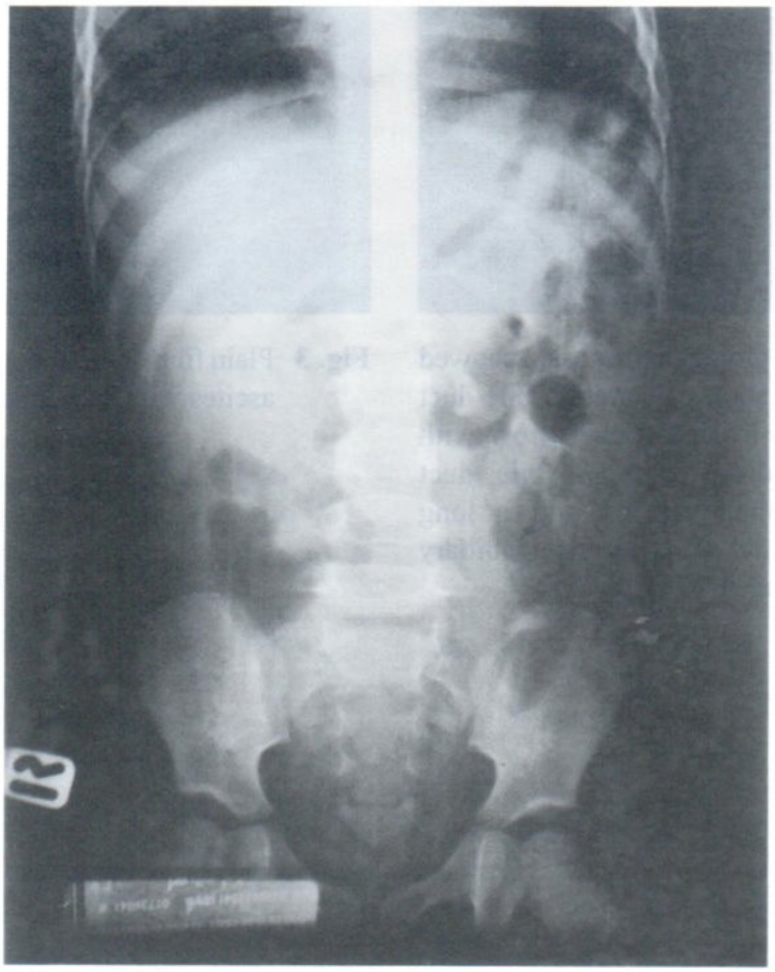

Fig. 1 Plain film of the abdomen in case 2 showed bowel ileus.

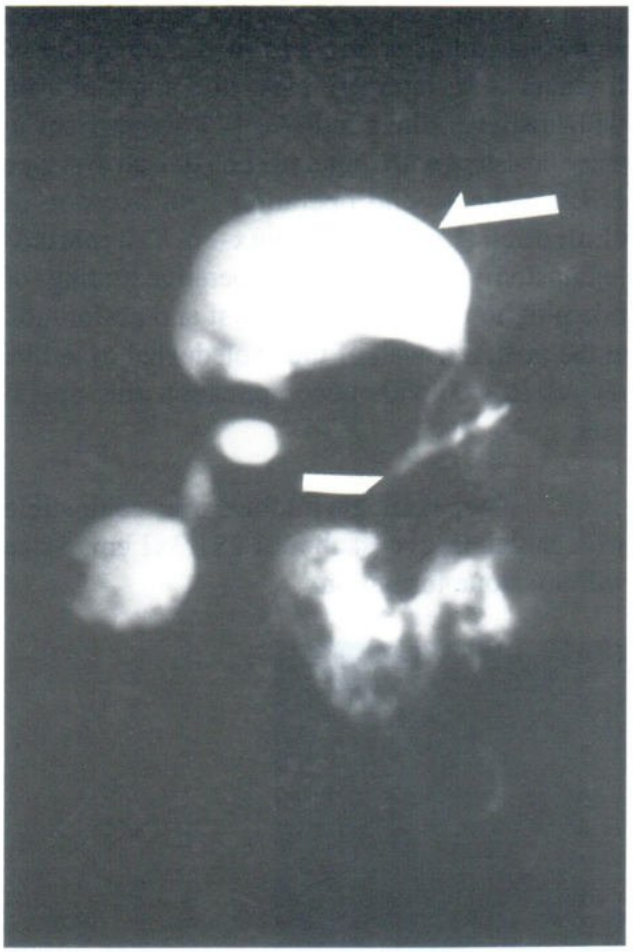

Fig. 2 T-tube cholangiography in case 2 showed fusiform dilatation of common bile duct about 3x5 cm in size (Long arrow with head) with distal common bile duct narrowing (Short Arrow) and a long common channel of the pancreaticobiliary junction. (Long Arrow)

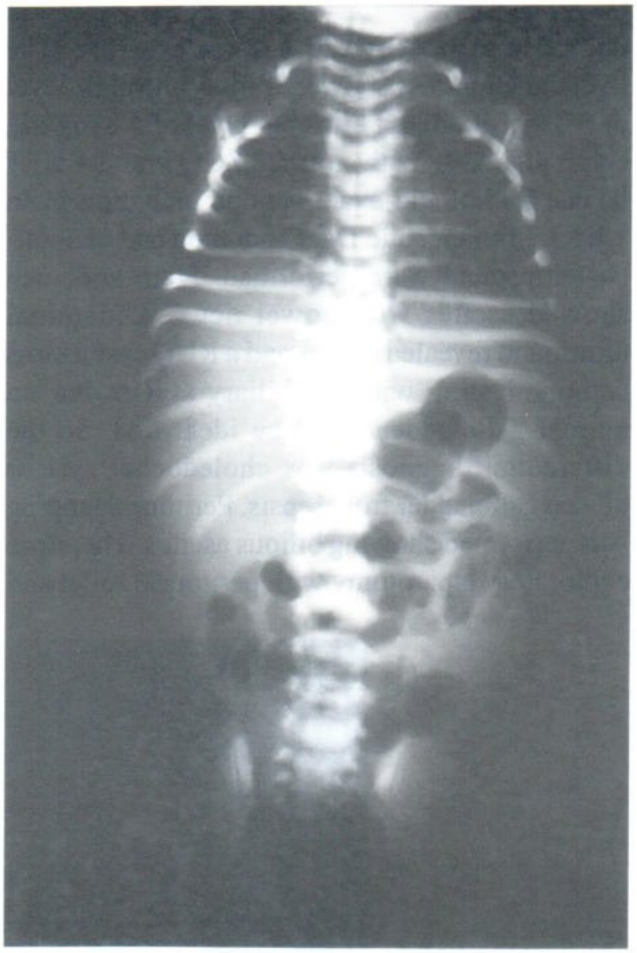

Fig. 3 Plain film of the abdomen in case 3 showed ascites with bowel ileus

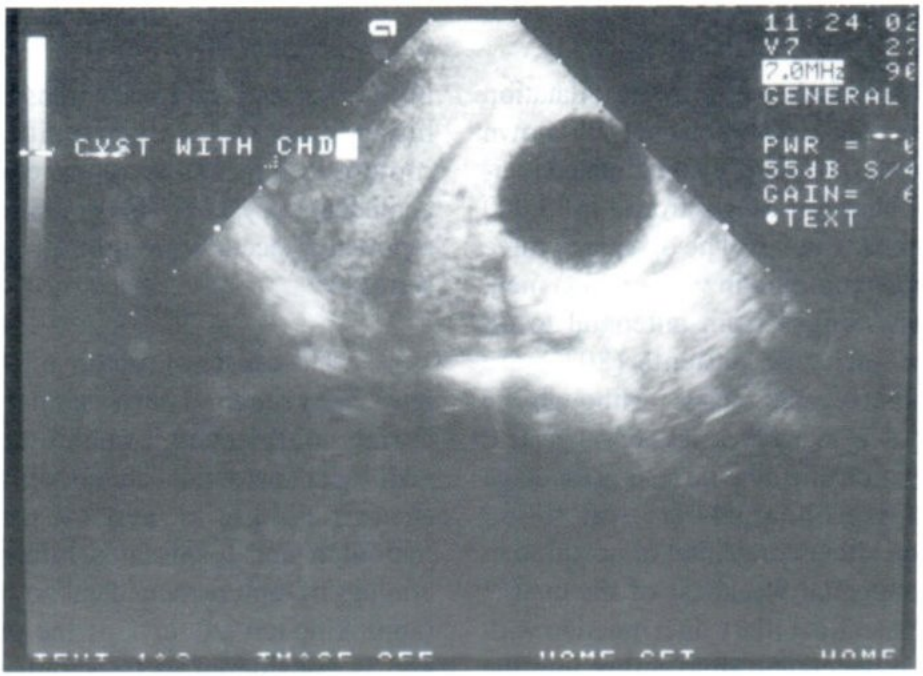

Fig. 4

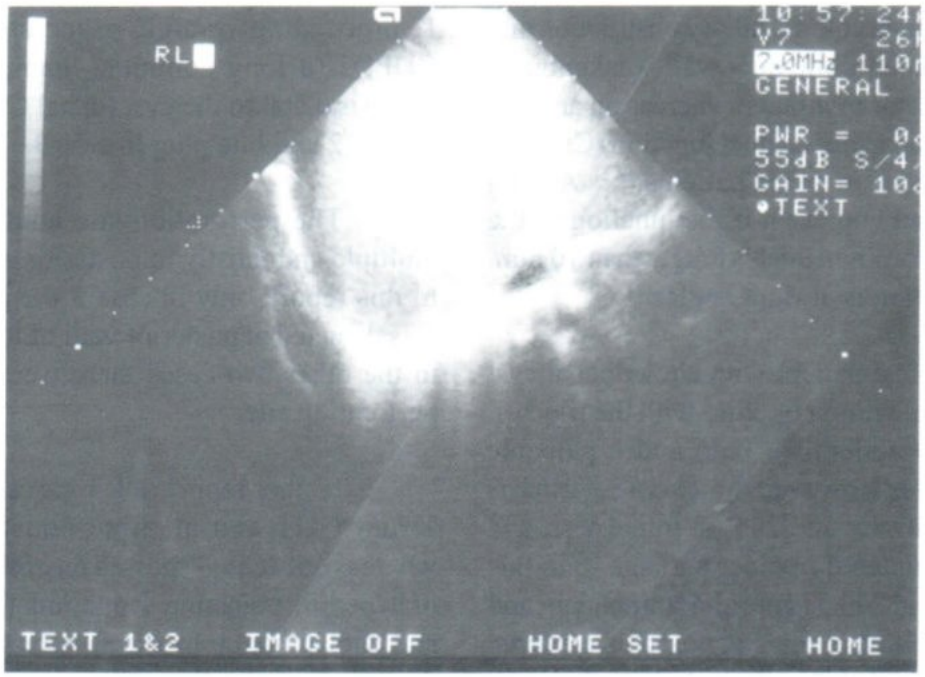

Fig. 5

Fig. 4 & 5 Abdominal ultrasound in case 3 showed ascites and a RUQ cystic mass communicating with biliary system but no visualization of a normal gallbladder

DISCUSSION

The choledochal cyst, a cystic dilatation of the biliary tree, is an uncommon but well-known cause of obstructive jaundice. The estimated incidence of choledochal cyst ranges from 1 in 13,000 to 1 in 2 million patients.[15,16] The disease is three to four times more common in women than men. Age at diagnosis ranges from antenatal to 68 years.[14] The majority of patients (80%) are diagnosed before 10 years of age. Although the etiology is unknown, many theories are suggested. Unequal proliferation of epithelial cells at the stage when the primitive bile ducts are still solid,[6] distal obstruction either congenital or acquired in additional to congenital weakness of the duct,[6,7] an abnormal pancreaticobiliary duct junction with resultant chronic pancreatic fluid reflux into the biliary tree,[8] and the ischemia of the bile duct[9] are among the proposed theories. Some authors have suggested that embryologic biliary obstruction and subsequent common bile duct wall weakening is an important factor in infants, whereas an anomalous choledochopancreatic duct junction (CDPDJ) is more important in older patients.[18-21] A long common channel is present if the junction of the pancreatic and common duct is longer than 10 mm. Often this junction is at right angles.[22]

The typical patient with choledochal cyst has been a female infant or child with the triad of, jaundice, RUQ abdominal pain and a palpable abdominal mass. However the classical triad is encountered only 15% to 25% at initial visit and is usually encountered in older patients.[1-6] In this report, case 1 and 2 had acute abdominal pain and peritonitis which were misdiagnosed as ruptured appendicitis. So the ruptured choledochal cyst should be considered as an unusual cause of acute abdomen in children similar to the previous study.[13] The patients may present with the complications of choledochal cysts such as ascending cholangitis, recurrent pancreatitis, progressive biliary cirrhosis and portal hypertension, stones in the cyst and malignant transformation in the biliary tract.[3-6] Bile peritonitis secondary to rupture is one of the rarest complications of choledochal cysts.[1,2] This complication has been reported to occur at rates of 1.8%- 2.8% in large series.[1,8-12]

The causes of rupture of choledochal cyst have been reported such as after blunt trauma[1], during confinement,[10] cholelithiasis,[22] with an additional anatomical abnormality such as ductal stenosis distal to the cyst,[7] or pancreaticobiliary malunion and inspissated bile.[22] However the etiology of rupture remain unknown in many cases (approximately 20-46% of the published cases) and is considered to be spontaneous.[13,22] This report showed the possible causes of ruptured choledochal cyst including cholelithiasis in case 1, preceeding trauma, associated anomalous CDPDJ (a long common channel) and ductal stenosis distal to the cyst (distal CBD narrowing) in case 2 and bile plug in case 3.

The perforation site could be single or multiple and mostly in posterior wall of the cyst. In this report, only in case 3 the perforation site was detected at posterior wall of the cyst whereas in the other two cases there were no detectable perforation site.

In this report, all 3 cases had increased serum GGT and alkaline phosphatase levels whereas only case3 showed an obstructive pattern of hyperbilirubinemia. Abdominal ultrasound, CT and cholangiography are all effective in defining the presence of biliary dilatation and in the diagnosis of choledochal cyst.[4-6,8] It has been generally accepted that abdominal ultrasound is the most useful diagnostic tool for detection of choledochal cyst. Cholangiography is essential in differentiating the type of choledochal cyst and in planning the extent of operative resection. Preoperative

percutaneous cholangiography has been the preferred mode of cholangiography to endoscopic retrograde cholangiography because it has the ability to define the proximal extent of biliary dilatation and this information can be used in the preoperative plan for resection. Endoscopic retrograde cholangiography is best to visualize the pancreaticobiliary junction but the superior intrahepatic extent of the cysts may be not defined if the cysts are redundant and sequester large amount of contrast material.[14]

An abdominal ultrasound was performed in only case 3 showing RUQ cystic mass communicating with biliary tract but no visualization of a normal gallbladder. The differential diagnosis could be either a choledochal cyst or a distended gallbladder due to sepsis. Plain abdomen showed ascites and bowel ileus, possibly from perforation of GI tract or a ruptured choledochal cyst. However bile-stained peritoneal fluid after peritoneal tapping was helpful and suggestive of biliary tract pathology. Although spontaneous perforation of choledochal cyst is rare, it can sometimes be the initial manifestation of choledochal cyst and should be considered in the presence of bilelike peritoneal fluid. In the presence of bile peritonitis, it is important to differentiate spontaneous perforation of the bile duct with a wall-off bile collection, from a ruptured choledochal cyst. Spontaneous perforation of the extrahepatic bile duct occurs almost exclusively in infants less than 20 weeks of age, and most often occurs at junction of the cystic and common hepatic ducts.[2,12]

Differentiation between these two entities is definitely required because a perforated bile duct could be cured and spontaneously close after simple surgical drainage whereas a ruptured choledochal cyst would require cyst excision and Roux-en-Y choledochoenterostomy.[2] On the other hand, intestinal anastomosis to the site of perforation or sac under the misdiagnosis of a ruptured choledochal cyst is generally lethal.[12] Preoperative diagnosis of bile leakage from spontaneous rupture of the extrahepatic bile duct could be differentiated from ruptured choledochal cyst in which a definite preoperative diagnosis could be made by hepatobiliary scan.[11] If bile duct pathology has not been considered preoperatively, the presence of any fluid suggestive of bile should urge the surgeon to evaluate the biliary tree for the possibilities of spontaneous perforation of bile duct or ruptured choledochal cyst.

The definite diagnosis of ruptured choledochal cyst may be difficult even at laparotomy. The main reasons for this difficulty are the lack of history suggesting a choledochal cyst, overlooking the cyst because of the collapse following the perforation, the rupture of a relatively small cyst, and the usual location of the perforation on the posterior wall of the cyst.[13] Perioperative cholangiography has been suggested to be helpful for the diagnosis of biliary pathology[4,8,9,12] and may be useful especially in the absence of apparent ruptured choledochal cyst or perforation of bile ducts.

Currently, excision of the cyst and Roux-en-Y hepaticojejunostomy are considered to be appropriated for most patients with a choledochal cyst type 1.

REFERENCES

1. Chen WJ, Chang CH, Hung WT: Congenital choledochal cyst; with observations on rupture of the cyst and intrahepatic ductal dilatation. J Pediatric Surg 8:529-538,1973
2. Treem WR, Hyams JF, McGowan, et al: Spontaneous rupture of a choledochal cyst: clue to diagnosis and etiology. J Pediatric Gastroenterol Nutr 13:301-306,1991
3. Chijiiwa K, Koga A: Surgical management and long-term follow-up of patients with choledochal cysts. Am J Surg 165:238-242,1993

4. Shian WJ, Wang YJ, Chi CS: Choledochal cysts: A nine year review. Acta Pediatr 82: 383-386,1993
5. Sherman P, Kolster E, Davies C, et al: Choledochal cysts: Heterogenity of clinical presentation. J Pediatr Gastroenterol Nutr 5:867-872,1986
6. Crittenden SL, McKinley MJ: Choledochal cyst-Clinical features and classification. Am J Gastroenterol 80:643-647, 1985
7. Suda K, Matsumoto Y, Miyano T: Narrow duct segment distal to choledochal cyst. Am J Gastroenterol 86:1259-1263,1991
8. Ohkawa H, Takahashi H, Maie M: A malformation of the pancreatico-biliary system as a cause of perforation of the biliary tract in childhood. J Pediatr Surg 12:541-546,1977
9. Lloyd DA, Mickel RE: spontaneous perforation of the extrahepatic bile ducts in neonates and infants. Br J Surg 67:621-623,1980
10. Friend WD: Rupture of choledochal cyst during confinement. Br J Surg 46:155-157, 1958
11. Levine GM, Sziklas JJ, Spencer RP: Bile leak from choledochal cyst in a child. Clin Nucl Med 9:678-679,1991
12. Lily JR, Weintraub WH, Altman RP: Spontaneous perforation of the extrahepatic bile ducts and bile peritonitis in infancy. Surgery 75:664-673,1974
13. Ibrahim Karnak, F.Cahit T, Nebil B, Akgun H: Spontaneous rupture of choledochal cyst; an unusual cause of acute abdomen in children. J Pediatr Surg 32:736-738, 1997
14. Pamela A. Lipsett, Henry AP, Paul MC, John KB, John LC: Choledochal cyst disease; a changing pattern of presentation Ann Surg 220:644-652
15. Yamaguchi M.: Congenital choledochal cyst; analysis of 1,433 patients in Japanese literature. Am J Surg140: 653-657,1980
16. Todani T, Watanabe Y, Narusue M, et al: Congeneital bile duct cysts: classification, operative procedures, and review of thirty-seven cases including cancer arising from choledochal cyst. Am J Surg 134:263-269, 1977
17. Young W, Blane C, White SJ, Polley TZ: Congenital biliary dilatation; a spectrum of disease detailed by ultrasound. Br J Rad 63:333-336,1990
18. Okada A, Nakamura, Higaki J, et al: Congenital dilatation of the bile duct in 100 instances and its relationship with anomalous junction. Surg Gynecol Obstret 171: 291-298,1990
19. Rattner DW, Schapiro RH,Warshaw AL : Abnormalities of the pancreatic and biliary ducts in adult patients with choledochal cysts. Arch Surg 118:1068-1073, 1983
20. Iwai N, Yanagihara J, Tokiwa K, et al: Congenital choledochal dilatation with emphasis on pathophysiology of the biliary tract. Ann Surg 215:27-30,1992
21. Wong KC, Lister J.: Human fetal development of the hepatopancreatic duct junction — a possible explanation of congenita dilatation of the biliary tract. J Pediatr Surg 16:139-145,1981
22. Haruo Ohkawa, Hideyo Takahashi, Masahiko Maie: A malformation of the pancreaticobiliary system as a cause of perforation of biliary tract in childhood J Pediatr Surg 12: 541-546,1977

COMPARISON BETWEEN ULTRASONOGRAPHIC FINDINGS OF WILM'S TUMOR AND NEUROBLASTOMA

Anchalee LEEPOOLSUP, MD, Jiraporn SRINAKARIN, MD

OBJECTIVE

The purpose of this study was to compare the differences of the ultrasonographic findings between Wilm's tumor and neuroblastoma and to determine whether there are ultrasonographic patterns which are characteristic features for both entities.

MATERIALS AND METHODS

Fifteen patients with Wilm's tumor and 17 patients with neuroblastoma who underwent transabdominal ultrasound imaging during January 1992 - December 1997 were retrospectively reviewed. All cases of Wilm's tumor and 8 cases of neuroblastoma were pathologically proved. The diagnosis of remaining 9 cases of neuroblastoma was made by positive urine vanillylmandelic acid plus bone marrow involvement (n=7), bone marrow involvement plus leptomeningeal metastasis (n=1) and bone marrow involvement plus leptomeningeal metastasis plus bilateral retrobulbar mass (n=1). The tumor echogenicity, cystic component, tumor border, pseudocapsule, midline crossing, presenting of calcification and lymphadenopathy were reviewed and analyzed.

RESULTS

Statistically significant ($p< 0.05$) finding that was often seen on ultrasound of Wilm's tumor was cystic component ($p = 0.0006$) while the neuroblastoma often revealed calcification ($p = 0.013$). There was no statistically significant in echogenicity ($p = 0.397$), tumor border ($p = 0.086$), midline crossing ($p = 5.26$), ipsilateral caliectasis ($p = 1.177$) or lymphadenopathy ($p = 0.055$) between Wilm's tumor and neuroblastoma.

CONCLUSION

Initial ultrasonography in children presenting with palpable abdominal mass was non-invasive and useful. The mass with cystic component was more specific for Wilm's tumor than neuroblastoma. The mass contained calcification was statistically significant for neuroblastoma.

Department of Radiology, Faculty of medicine Khon Kaen University, Khon Kaen, Thailand.

Correspondence Anchalee Leepoolsup Department of Radiology, Faculty of medicine, Khon Kaen University, Khon Kaen, Thailand Telephone, Fax 043-348389

INTRODUCTION

Wilm's tumor and neuroblastoma represent the two most common solid abdominal masses of infant and childhood. One can usually determined whether the mass is intrarenal or extrarenal by means of an intravenous pyelogram. This distinction at time may be difficult, and an incorrect diagnosis may result.

Ultrasonography is a useful method to evaluate abdominal mass in children because of its readily availability, non-invasive and no exposure to radiation. So ultrasonogram is prefered as primary screening.

Many previous reports have described the ultrasonographic appearance and emphasized the use of ultrasonography in the evaluation of echogenicity, size, consistency and extent of the tumor. But the characteristic findings of each disease have not been documented. Distinguishing an intrarenal huge mass from extrarenal location is difficult. Each tumor may have invasive behavior and extents outside its compartment.

The purpose of this paper is to compare the ultrasonographic pattern of 15 cases of Wilm's tumor and 17 cases of neuroblastoma, to evaluate the ability of ultrasound in distinguishing between these two neoplasms, and to determine characteristic features of each disease.

MATERIALS AND METHODS

Technically adequate gray-scale ultrasonograms of 15 cases of Wilm's tumor and 17 cases of suprarenal neuroblastoma from Srinagarind hospital between January 1992-December 1997 were retrospectively reviewed. All cases of Wilm's tumor were pathologically proved. For 17 cases of neuroblastoma: 8 cases were proven pathologically, 7 cases had positive bone marrow aspiration plus urine VMA, 1 case had positive bone marrow plus leptomeningeal metastasis and 1 case had positive bone marrow aspiration plus leptomeningeal metastasis plus bilateral retrobulbar masses with periorbital echymosis.

The tumor echogenicity, cystic component, tumor border, midline crossing, presence of calcification, caliectasis of ipsilateral kidney and lymphadenopathy were reviewed and analyzed.

Fisher's exact test was used to established two-tailed p values. The differences between ultrasound finding in patients with Wilm's tumor and neuroblastoma were considered statistically significant when the p value was less than 0.05.

RESULTS

The peak age incidence of Wilm's tumor is at less than 1 year and another peak is at 4 years (range 1 month-8 years). The peak incidence of neuroblastoma is at 4 years old (range 1 month-9 years). Fourteen Wilm's tumor patients presented with palpable abdominal mass and one patient with hematuria. Neuroblastoma cases had variable presenting symptoms: palpable abdominal mass 10 patients, exophthalmos and periorbital echymosis 4 patients, spinal cord compression 1 patient, hemoperitoneum 1 patient and bone pain 1 patient.

Ultrasonographic findings of Wilm's tumor and neuroblastoma were compared and analyzed as shown on table 1. The Fisher's exact test was used to establish two-tailed p value for each of the ultrasonographic finding. Statistically significance is considered at p value < 0.05.

Wilm's tumor had predominate cystic component that presented in 8 of 15 patients which could be a single large cystic area or multiple small discrete cysts while neuroblastoma was not dem-

onstrated this finding (p value = 0.0006) (Graph 1, Fig 1,2). Neuroblastoma was shown to have calcified component in 11 of 17 patients but this character was not found in Wilm's tumor (p value = 0.0136) (Graph 2) . The calcified component in neuroblastoma ranged from fine granular to large dense calcification (Fig 3A,B, 4).

Both neoplasms had heterogeneous hyperechogenicity. The size of Wilm's tumor ranged from 5 cm to 19 cm, while neuroblastoma was 2.9 cm to 16 cm. The diameter of both tumors were mostly 5-10 cm and showed no statistically significant difference.

Wilm's tumor had well-defined border in 12 of 15 cases while neuroblastoma had only 3 of 17 cases (Fig 5). Caliectasis of ipsilateral kidney was observed in 1 case of Wilm's tumor and 4 cases of neuroblastoma (Fig 6).

Six of 17 cases of neuroblastoma had metastatic nodes at first presentation while Wilm's tumor had only one. (Fig 7)

Metastases at presentation was found in 12 patients of neuroblastoma (4 pulmonary, 1 liver, 6 brain and 6 skeleton). Only one pulmonary metastasis was found in Wilm's tumor.

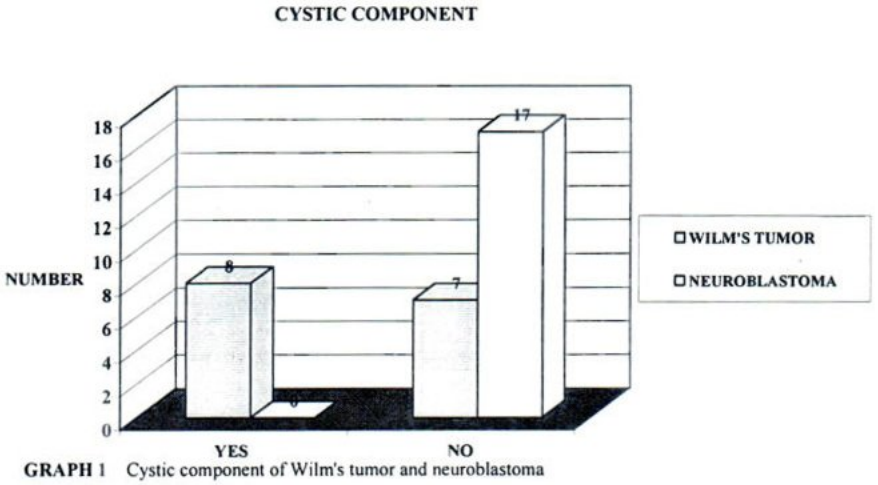

GRAPH 1 Cystic component of Wilm's tumor and neuroblastoma

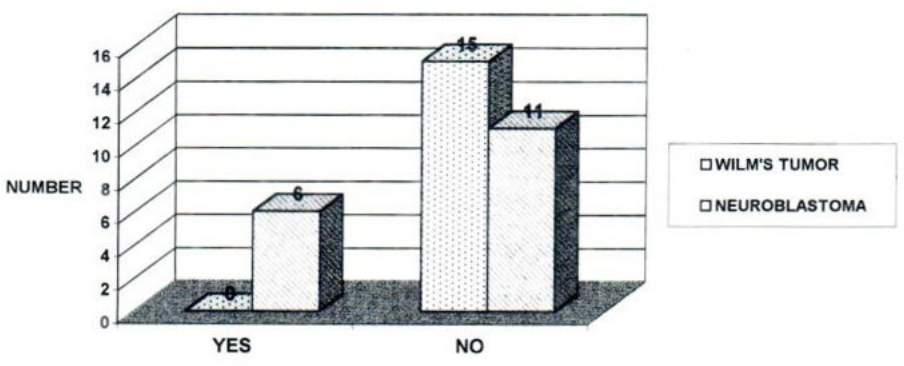

GRAPH 2 Calcification of Wilm's tumor and neuroblastoma

Table 1 Ultrasonographic findings of Wilm's tumor and neuroblastoma, statistical analysis.

FINDINGS	WILM'STUMOR	NEUROBLASTOMA	P VALUE
HETEROGENEOUS ECHO	13	15	0.397
HYPERECHOGENICITY	14	15	0.411
CYSTIC COMPONENT	8	0	0.0006
CALCIFICATION	0	6	0.0136
WELL-DEFINED BORDER	12	9	0.086
SIZE> 10 CM	6	3	0.12
MIDLINE CROSSING	10	7	5.26
CALIECTASIS	1	4	0.177
LYMPHADENOPATHY OR METASTASIS	1	14	0.000003

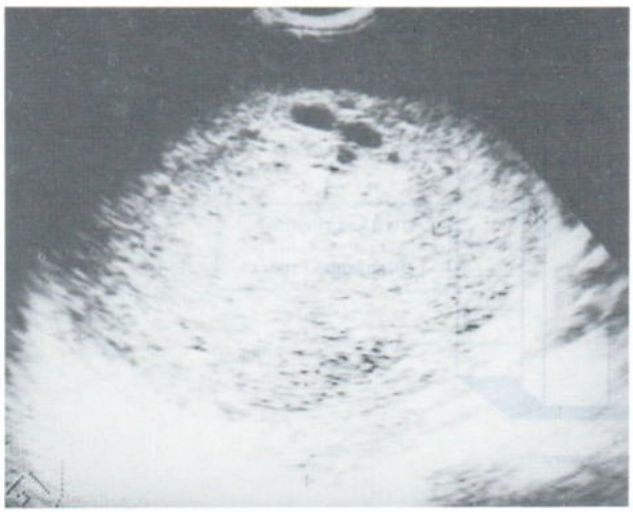

Fig. 1 Wilm' tumor in a 2 year-old-boy. Transverse ultrasonographic image of Rt. flank shows a solid renal mass with small cystic areas at the periphery of the tumor.

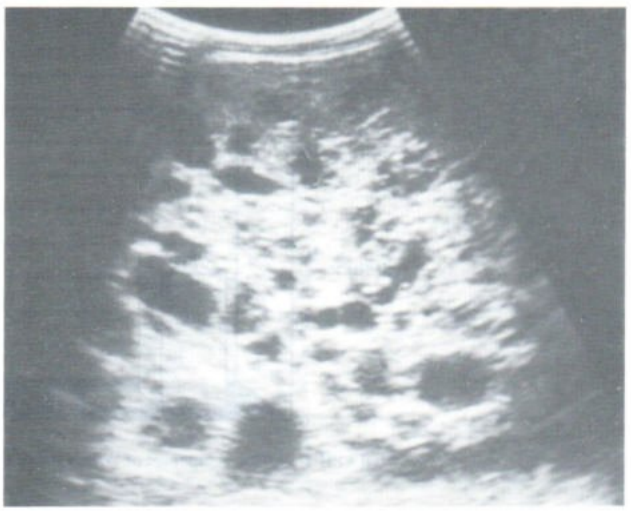

Fig. 2 Wilm's tumor. Longitudinal ultrasonographic image of this 2 year-old boy shows a large Lt. abdominal mass. Multiple small cystic areas, varying in size distributed in the entire mass.

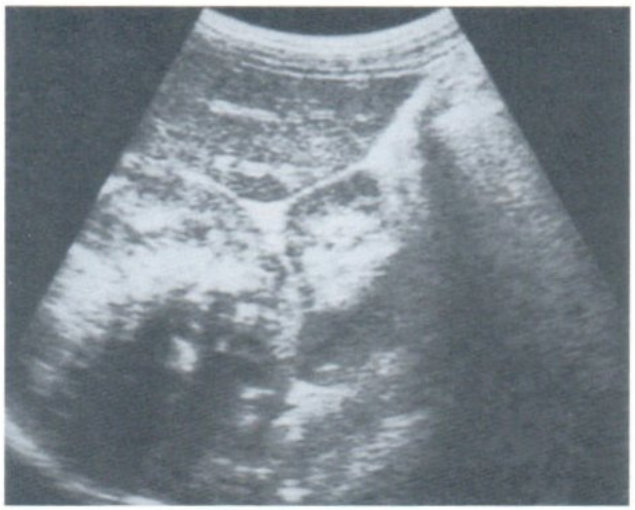

Fig. 3A

Fig. 3A Longitudinal ultrasonogram of Rt. upper quadrant in a 4 year-old boy with Rt. adrenal neuroblastoma. There is a round-shaped mass with isoechogenicity compared to the adjacent liver parenchyma, containing a large area of calcification. Pressure effect to upper pole of Rt. kidney is also demonstrated and confirmed the extrarenal in origin of the tumor.

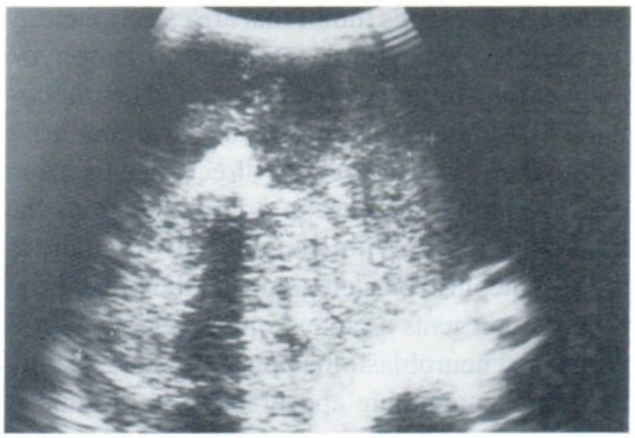

Fig. 4 Transverse ultrasonogram in a 9 year-old girl with huge Rt. adrenal neuroblastoma. The neoplasm shows inhomogeneous high echogenicity containing conglomerated area of calcifications.

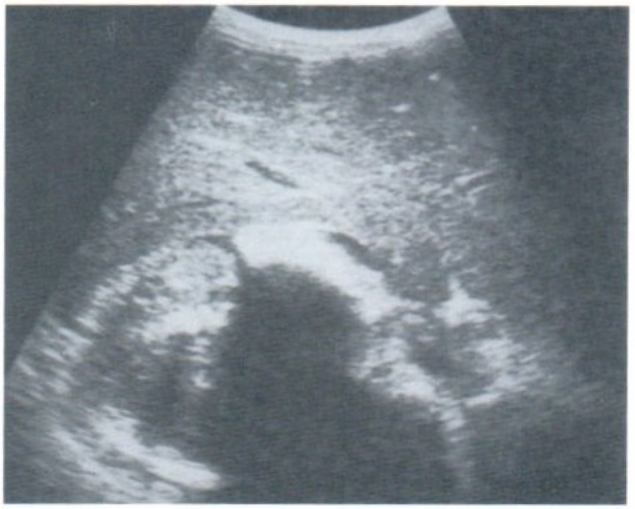

Fig. 3B

Fig. 3B Another area of the same patient shows dense calcification.

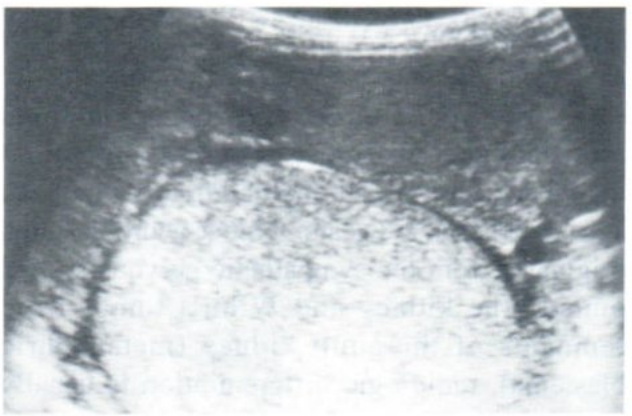

Fig. 5 Wilm's tumor in 5 month-old girl with palpable Rt. flank mass. Longitudinal ultrasonogram of Rt. upper abdomen shows a large well demarcated homogeneous hyperechoic mass. Hypoechoic rim of the compressed renal parenchyma or pseudocapsule surrounding the tumor mass is also observed.

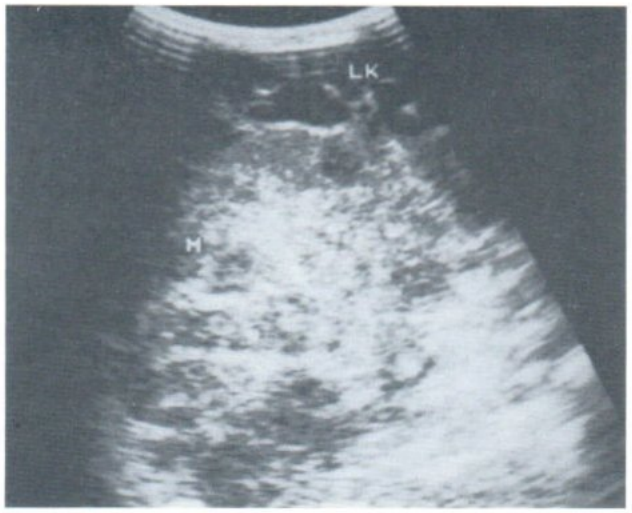

Fig. 6 Neuroblastoma. Longitudinal ultrasonogram of Lt. upper abdomen in a 4 year-old-girl presented with Lt. abdominal mass. There is a large poorly demarcated heterogeneous hyperechoic mass anterior to the kidney. Caliectasis of the ipsilateral kidney is shown.

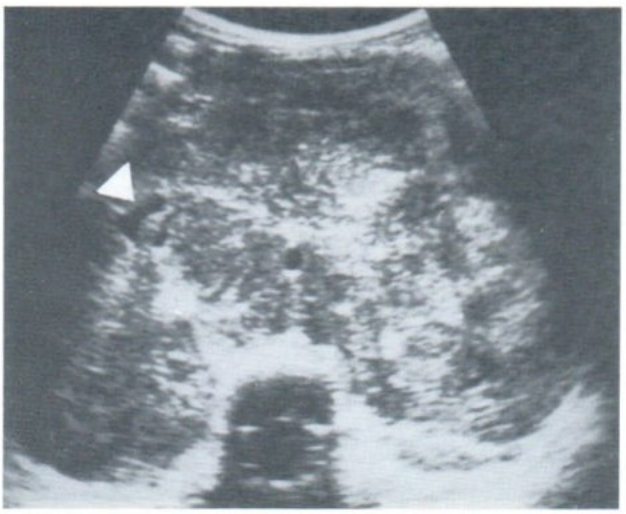

Fig. 7 Neuroblastoma. Transverse ultrasonogram of upper abdomen in a 4 year-old-girl presented with Lt. upper quadrant mass. There is a large poorly defined heterogeneous hyperechoic mass at Lt. renal fossa. Enlarged paraaortic lymphnode causing encasement of abdominal aorta, lateral displacement of IVC (arrowhead) with luminal narrowing is also demonstrated.

DISCUSSION

Wilm's tumor and neuroblastoma represent the two most common abdominal malignancies in infant and children with a peak age incidence at 2-3 years.[2-4] Since neuroblastoma originates from the sympathetic nervous system outside the kidney and Wilm's tumor from remnants of the adult kidney (metanephric blastema), radiologic differentiation is usually possible by determining whether the mass is intrarenal or extrarenal. It is well known that ultrasonography is helpful in establishing this relationship.[5-6]

Occasionally, however, despite technically good urograms and ultrasonograms, it is impossible to determine the origin of the mass. Rarely, a diagnosis made solely on the basis of this intrarenal or extrarenal distinction will be incorrect. A Wilm's tumor that arises peripherally within the kidney and grows in an exophytic manner may mimic with an extrarenal neuroblastoma.[3,4] Although neuroblastoma does not arise within the kidney, those with direct renal invasion often resemble neoplasms originating from the kidney.[1,7] Rarely, Wilm's tumor may originate in the metanephric blastema outside the kidney and therefore presents as an extrarenal mass.[1] Wilm's tumor and neuroblastoma appear to have distinctive ultrasonographic appearances, ultrasound is usually able to differentiate between the two malignancies independent of their relation to the kidney and thus can overcome these difficulties in most cases.[1]

A knowledge of the pathology of these two tumors is helpful in understanding the difference

in their ultrasonic appearance. The typical Wilm's tumor is sharply marginated, compressing the renal tissue and forming a pseudocapsule. Focal hemorrhage and necrosis may be encountered but are seen less frequently than in neuroblastoma. On microscopic examination there is typically admixture of three components: stroma, epithelial and blastematous elements.[6] Neuroblastoma, however, may be sharply marginated in some regions but is often locally invasive and fades into the adjacent tissue. Unlike the Wilm's tumor, the neurob lastoma has a much more variably echogenic pattern on ultrasonographic examination. Hemorrhage, necrosis and dystrophic calcification are common. Microscopically, the tumor is very cellular without much collagenous stroma.[8]

Ultrasonographic findings of Wilm's tumor in our study was a well-marginated, large heterogeneous hyperechoic mass with cystic component predominate. Neuroblastoma was a large heterogeneous hyperechoic mass with predominate calcific component. Few cases of Wilm's tumor (1 case) and neuroblastoma (4 cases) showed caliectasis of ipsilateral kidney. The reason of few cases of the caliectasis may be due to both kinds of the tumors presented with large masses (> 10 cm in diameter) which caused distortion or entirely involved the kidneys.

In 1992, David S. Hartman[1] reported that Wilm's tumor had evenly fair echogenic or evenly echoigenic with discrete holes that represent necrosis, and neuroblastoma showed heterogeneous echogenicity which result from quite cellular and extensive area of hemorrhage with necrosis and microcalcification.[1] In this study, the authors also found predominate cystic component in Wilm's tumor (p value = 0.006) but no statistically significant in heterogenicity.

In 1985, George O. Atkinson reported 3 cases of cystic neuroblastoma as a rare form of Neuroblastoma.[9] In 1992 D.P. Croitoru, A.B. Sinsky also reported a case of cystic neuroblastoma with multiple septation.[10] However, there was no cystic component in neuroblastoma in our study.

Many studies reported that calcification is more common in neuroblastoma.[12,13] And our study also found that calcification is a characteristic finding of neuroblastoma (p value 0.0136). In 1995,Sandra K. Fernbach et al[11,12,13,14] reported 5% of Wilm's tumor had calcification, but in our study, no calcification was found in ultrasonogram of Wilm's tumor.

Lymphadenopathy or other organ metastasis were found in 14 cases of neuroblastoma. One patient with pulmonary metastasis was observed in Wilm's tumor but no lymphadenopathy was detected. Metastasis at first presentation was predominated in neuroblastoma with statistical significant (p value 0.000003).

From previous documents, midline crossing is more frequent in neuroblastoma.[12] In our study, Wilm's tumors cross midline 10 of 15 cases while, neuroblastoma had 7 of 17 cases. This finding may depends on tumor size, as we found tumor larger than 10 cm in 6 of 15 cases of Wilm's tumor and 3 of 17 cases of neuroblastoma.

CONCLUSION

Ultrasonography is a useful, non-invasive method in differentiation between Wilm's tumor and neuroblastoma. Wilm's tumor has predominated cystic component while calcification is specific finding for neuroblastoma. Metastasis at presentation is another clue for diagnosis of neuroblastoma. No statistical significant in the differences of tumor echogenicity, tumor border, midline crossing or caliectasis of ipsilateral kidney is observed.

ACKNOWDEGEMENT

Tula Diensiri, MD,
Suwanna Arunpongpaisarn, MD

REFERENCES

1. David S. Hartman, Roger C Sanders: Wilm's tumor versus Neuroblastoma: Usefulness of Ultasound in Differentiation. J ultrasound Med 1:117-122, April 1982.
2. Fried AM, Hatfield DR, Ellis GT, et al: Extrarenal Wilm's tumor: Sonographic appearance. J Clin ultrasound 8:360, 1980.
3. Jaffe MH, White SJ, Silver TM, et al: Wilms tumor: Ultrasonic features, pathologic correlation, and diagnostic pitfalls. Radiology 140:147, 1981.
4. Susan J. White, Karen J. Stuck : Sonography of Neuroblastoma. AJR 141:465-468, September 1983
5. Coldcleugh DJ, Miller JH, Hindman BW: The utilization of ultrasound in the initial evaluation and follow-up of children with neuroblastoma. Presented at the 24th annual meeting of the Association of Ultrasound Technical Specialists, American Institute of Ultrasound in Medicine. August, 1979. Montreal, Canada. Paper No. 334.
6. Teele RL: Ultrasonography of the genitourinary tract in children. Radiol Clin North Am15:109, 1977.
7. Benington JL, Beckwith JB. Atlas of Tumor Pathology. Second Series. Fascicle 12. Tumor of the Kidney, Renal pelvis, and Ureter. Washington, DC, Armed Forces Institute of pathology, 1975, p 57
8. Nancy S. Rosenfield, MD, John C. Leonidas, MD, Kenneth W. Barwick, MD: Aggressive Neuroblastoma Simulating Wilms Tumor. Radiology 1998: 165-167.
9. Harkin JC, Reed RJ: Atlas of Tumor pathology. Second Series. Fascicle 3. Tumors of the Peripheral Nervous System. Washinton, DC, Armed Forces Institute of Pathology, 1969, pp 137-144
10. George O. Atkinson, Jr, Ghazi S. Zaatari : Cystic Neuroblastoma in Infacts: Radiographic and pathologic Features. AJR 146: 113-117, January 1986
11. D.P. Croitory, A.B. Sinsky, and J.M. Laberge: Journal of pediatric Surgery, vol 27, No 10, pp 1320-1321, October, 1992.
12. George H. Myers, Jr: Tumors of genitourinary tract, pp 1680-1686, EMMET
13. Stark DD, Moss AA, Brasch RC, et al: Neuroblastoma: Diagnostic imaging and staging. 148:101-105,Radiology 1983.
14. Sandra K. fernbach and Kate A. Feinstein : Renal tumor in children: Seminar in roentgenology, Vol xxx, No 2:200-217, April, 1995
15. White KS, Grossman H: Wilm's and associated renal tumors of childhood. Pediatr Radiol 21:81-88, 1991.
16. Cushing B, Slovis TL: Imaging of Wilm's tumor: What is important! Urol Radiol 14:241-251, 1992
17. Reiman TAH, Siegel MJ, Shackelford GD: Wilm's tumor in children: Abdominal CT and US evaluation. Radiology 160:501-505, 1986

THE CORRECTION OF ELECTRON OUTPUT AT EXTENDED SSD

L. TUNTIPUMIAMORN[1], V. POLWATSATIAN[1]

ABSTRACT

Correction of electron output at extended treatment distance in Mitsubishi ML-15 MIII Linear Accelerator that available with the solid closed-sided applicator was performed. Comparison of electron outputs from inverse square law (ISL) correction with the outputs from direct measurement in electron field 4x4 to 14x14 cm^2, 101-115 cm SSDs with energies at 8,10,12, and 15 MeV revealed that ,with a nominal SSD ,the ISL calculation will provide the corrected output that fitting within $\pm$ 3 % of the measured output if the field size is equal to or larger than 10x10 cm^2 in all gaps and all energies. While with the effective SSD, the calculated outputs were found to agree with all the measured doses in all field sizes, all SSDs, and all energies in the study.

INTRODUCTION

Due to the limitation of the electron applicator or cone and sites of treatment such as head and neck, groin and vulva, extended source to surface distance (SSD) electron beam treatments are occasionally performed. Corrections to dose rate or output at extended SSD do not follow the inverse square law (ISL) if the nominal value of SSD (usually 100 cm.) is used. Because the interactions of electron with the components of accelerator head and the applicator differ from the photon. Therefore, the electron point source does not exist at the accelerator window as in the case of photon.[1] It is desirable to represent the extended electron point source so that divergence correction formulae such as ISL can be applied. Two methods of characterizing electron point source are virtual point source[2-4] and effective point source.[5] Either method is considered acceptable for calculating output at extended treatment distance. Except that the use of virtual SSD to predict dose variation with distance requires another correction factor in addition to ISL relationship while the effective SSD does not.[6] Moreover, because the electron output are strongly affected by the scatter from the cones. Thus, in this study we would like to investigate that with the closed-sided electron applicators that are available in our linear accelerator, nominal or effective SSD will be suitable in correcting electron output at extended SSD treatment.

MATERIALS AND METHODS

Three solid closed-sided square and rectangular electron applicators were shaped into 4x4, 6x6, 8x8,10x10,12x12 and 14x14 cm^2 fields by inserting the lead cut-outs that have suitable thickness for electron energies at 8,10,12, and 15 MeV.

Then, the depth of dose maximum (d_{max}) in each electron field and beam energy will be determined from the film isodose measurements. Type of film using are Kodak X-OMAT TL Ready pack film. All films were processed by Kodak X-

[1] Division of Radiotherapy, Department of Radiology, Faculty of Medicine, Siriraj Hospital, Mahidol University, Bangkok-10700, THAILAND

OMAT Auto Processor M-35 and the optical density was read by the X-Rite 301 black and white densitometer that the aperture is 1mm. in diameter.

After that, the measurements of output at d_{max} were undertaken in water phantom by Farmer Dosemeter Type 2571 ionization chamber and electrometer. The measurements were made in a given electron field and beam energy at various SSD values ranging from 100-115 cm. These electron outputs from direct measurements at various SSDs will be compared with the electron outputs from the ISL calculation that the equation was shown following

$$Dose_g = Dose_0 \{(SSD + d_{max})/ (SSD+ d_{max} + Gap)\}^2 \quad \ldots\ldots(1)$$

$Dose_g$ and $Dose_0$ are the outputs at gap g and at the standard nominal SSD 100 cm., d_{max} is the depth of dose maximum for a given electron field and energy.

The SSD value in an equation (1) could be either a nominal SSD 100 cm. (SSD_{NOM}) or effective SSD (SSD_{EFF}) as shown in equation (2) and (3) below.

$$Dose_g = Dose_0 \{(SSD_{NOM} + d_{max})/(SSD_{NOM} + d_{max} + Gap)\}^2 \quad \ldots\ldots(2)$$

and

$$Dose_g = Dose_0 \{(SSD_{EFF} + d_{max})/(SSD_{EFF} + d_{max} + Gap)\}^2 \quad \ldots\ldots(3)$$

The method to obtain the value of effective SSD was proposed by Khan et al (1978).[5] Q_0 is the ionization charge reading at d_{max} at the standard nominal SSD and Q_g is the charge reading at d_{max} at various gaps (in this study the gaps from applicator end to phantom surface, g =1,2,3, 6,9,12,and15 cm respectively). The value of effective SSD for a given electron field and energy then be determined from the value of the slope of the curve plotting between the ratio of $(Q_0/Q_g)^{1/2}$ and gap g as shown in an equation (4). Figure 1 is an example to determine the effective SSD in electron field 10x10 cm^2, 10 MeV energy by this method.

$$SSD_{EFF} = 1/slope - d_{max} \quad \ldots\ldots(4)$$

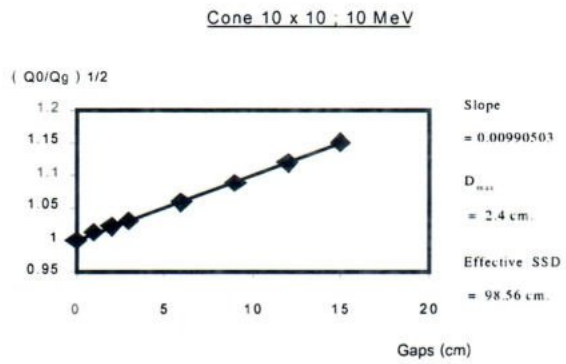

Fig.1 The curve plotting $(Q_0/Q_g)^{1/2}$ as a function of gaps in electron field 10x10 cm^2,10 MeV energy

Data will be analyzed by comparing the percentage of dose difference or variation between the calculated dose both with a nominal SSD and effective SSD in the ISL calculation to the dose from direct measurement.

$$\% \text{ Dose variation} = \frac{\text{Calculated dose} - \text{Measured dose}}{\text{Measured dose}} \times 100$$

RESULTS

The values of effective SSD in each electron field and beam energy that determined from a set of measurements are presented in Table 1.

Table 1. Effective SSD for various field sizes and beam energies

Field size (cm^2)	Effective SSD (cm) 8Mev	10MeV	12 MeV	15 MeV
4x4	59.14	65.88	69.66	75.18
6x6	66.83	73.94	78.69	86.48
8x8	84.98	90.46	98.25	93.36
10x10	91.28	98.56	95.48	100.65
12x12	96.44	102.53	100.91	102.85
14x14	98.93	101.50	103.39	95.87

The data in Table 1 clearly showed that the values of effective SSD in small fields prominently increased with the beam energy and also are much lower than the value of the nominal standard SSD. While in the large fields, the values are close to a nominal SSD and not depend on beam energy.

Comparisons of the output correction both with a nominal SSD and effective SSD in the ISL calculation with the output from direct measurement are simply presented by curves that plotting between the percentage of dose variation and gap distances as shown in Fig.2-Fig.7

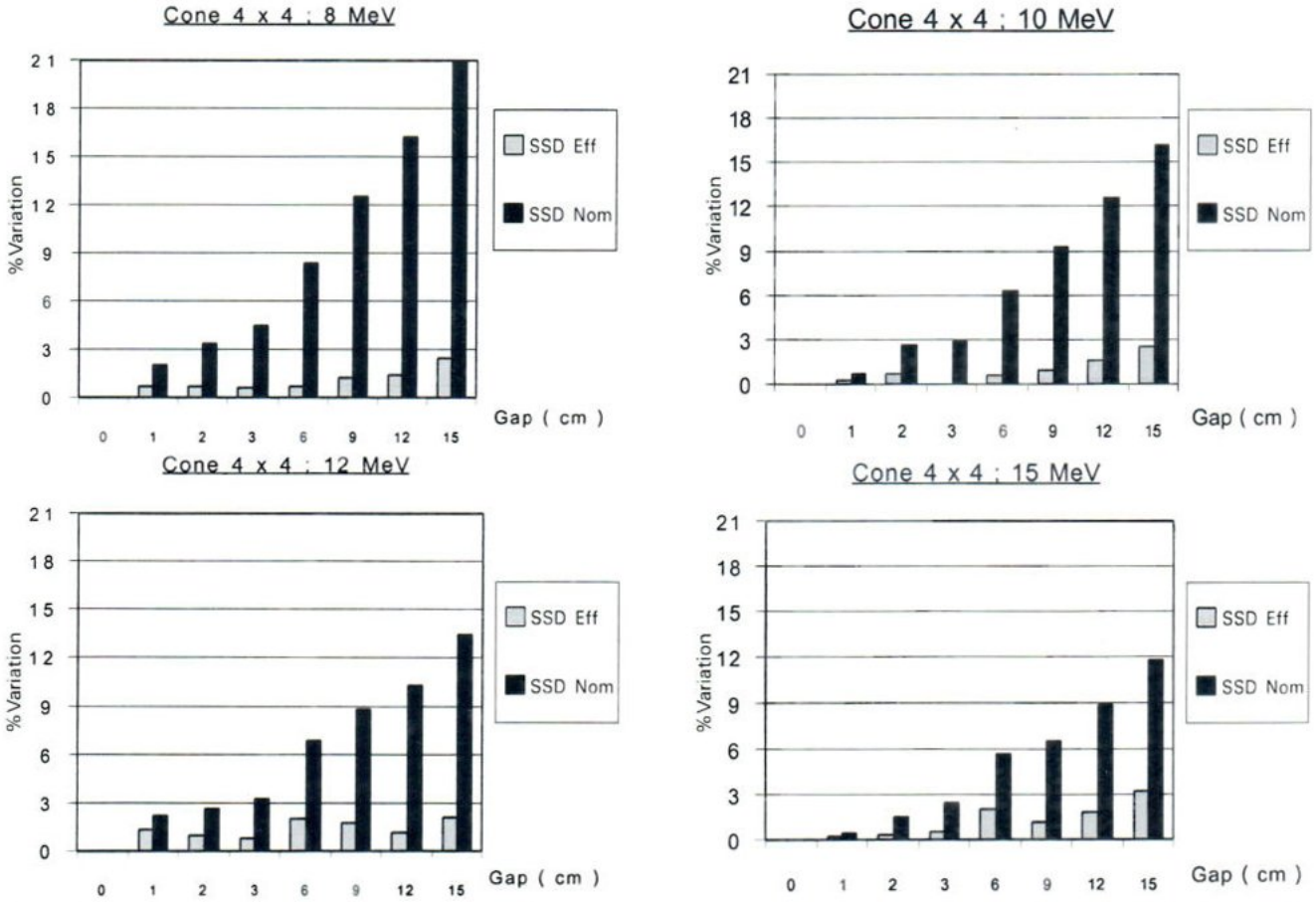

Fig. 2 Curve plotting the percentage of dose variation as a function of gaps in electron field 4x4 cm^2 at all energies

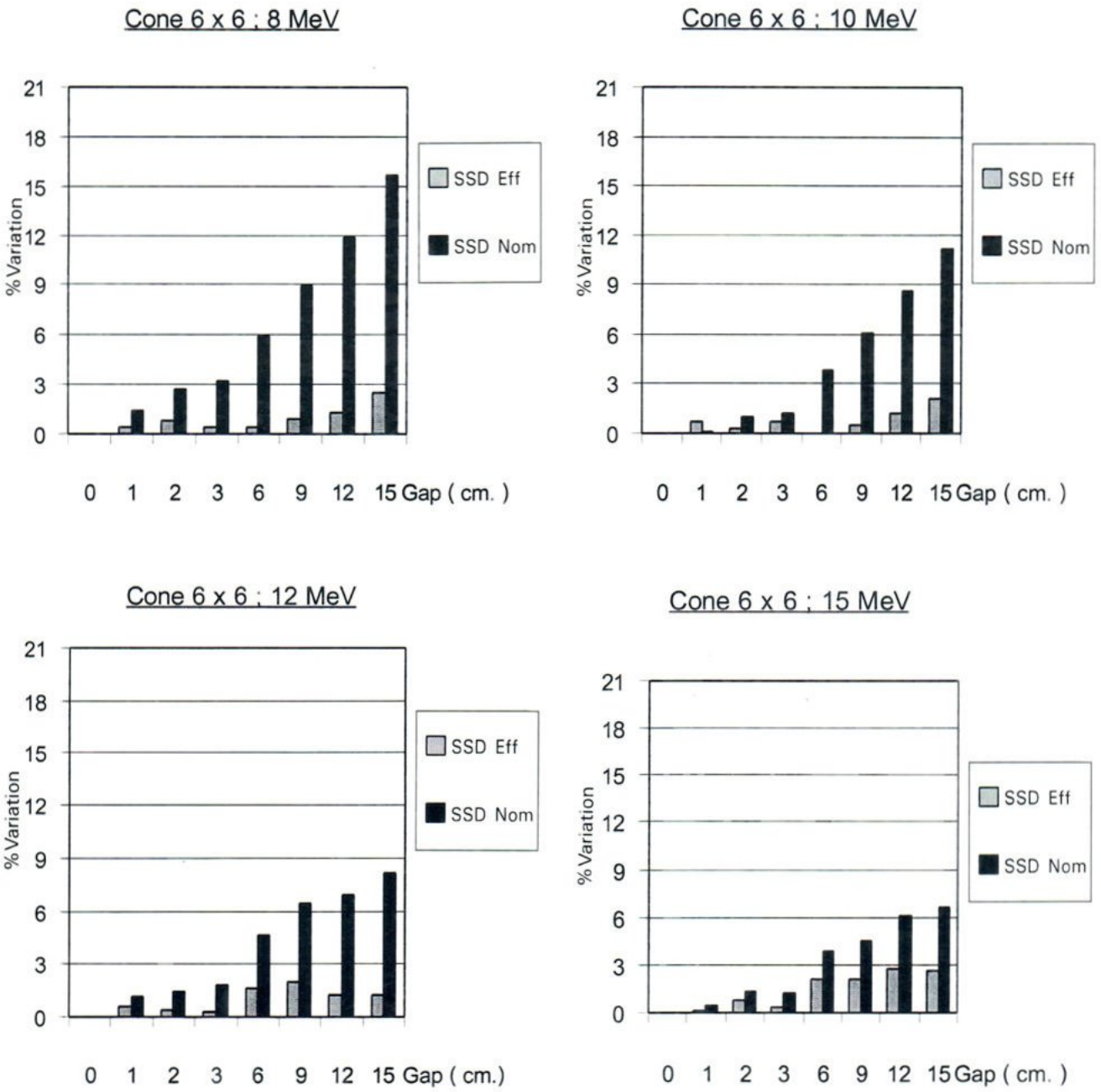

Fig. 3 Curve plotting the percentage of dose variation as a function of gaps in electron field 6x6 cm^2 at all energies

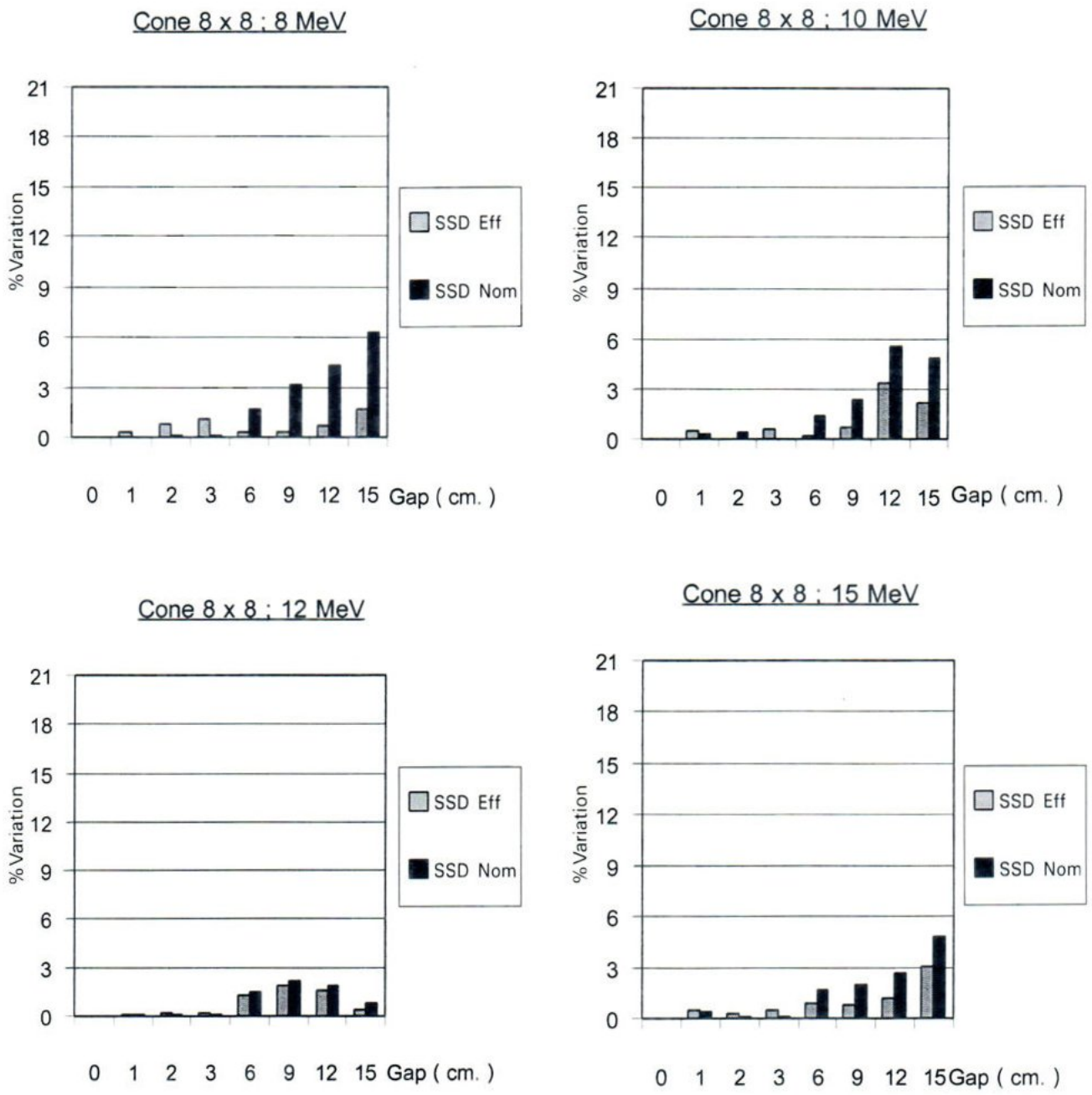

Fig. 4 Curve plotting the percentage of dose variation as a function of gaps in electron field 8x8 cm^2 at all energies

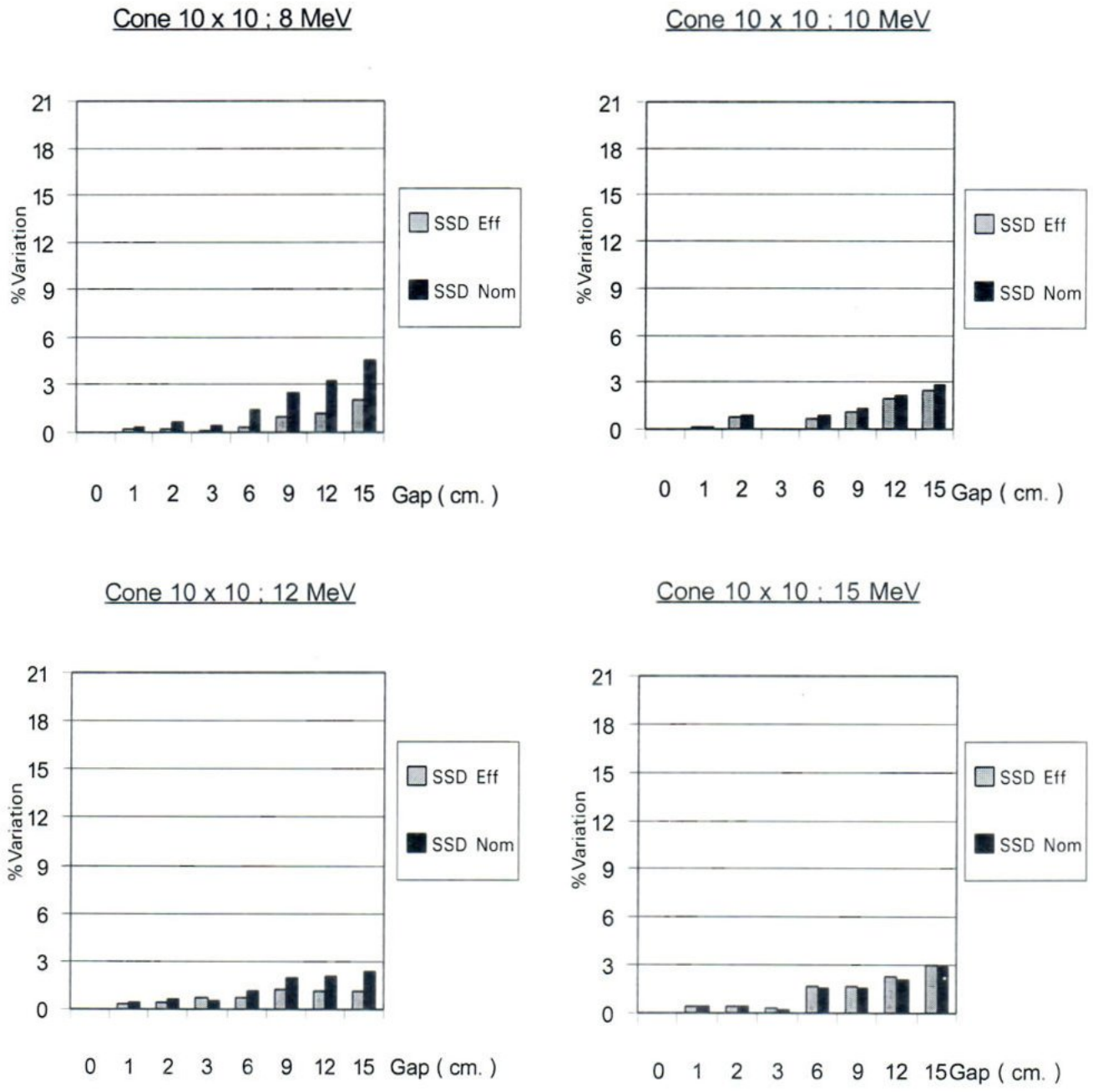

Fig. 5 Curve plotting the percentage of dose variation as a function of gaps in electron field 10x10 cm^2 at all energies

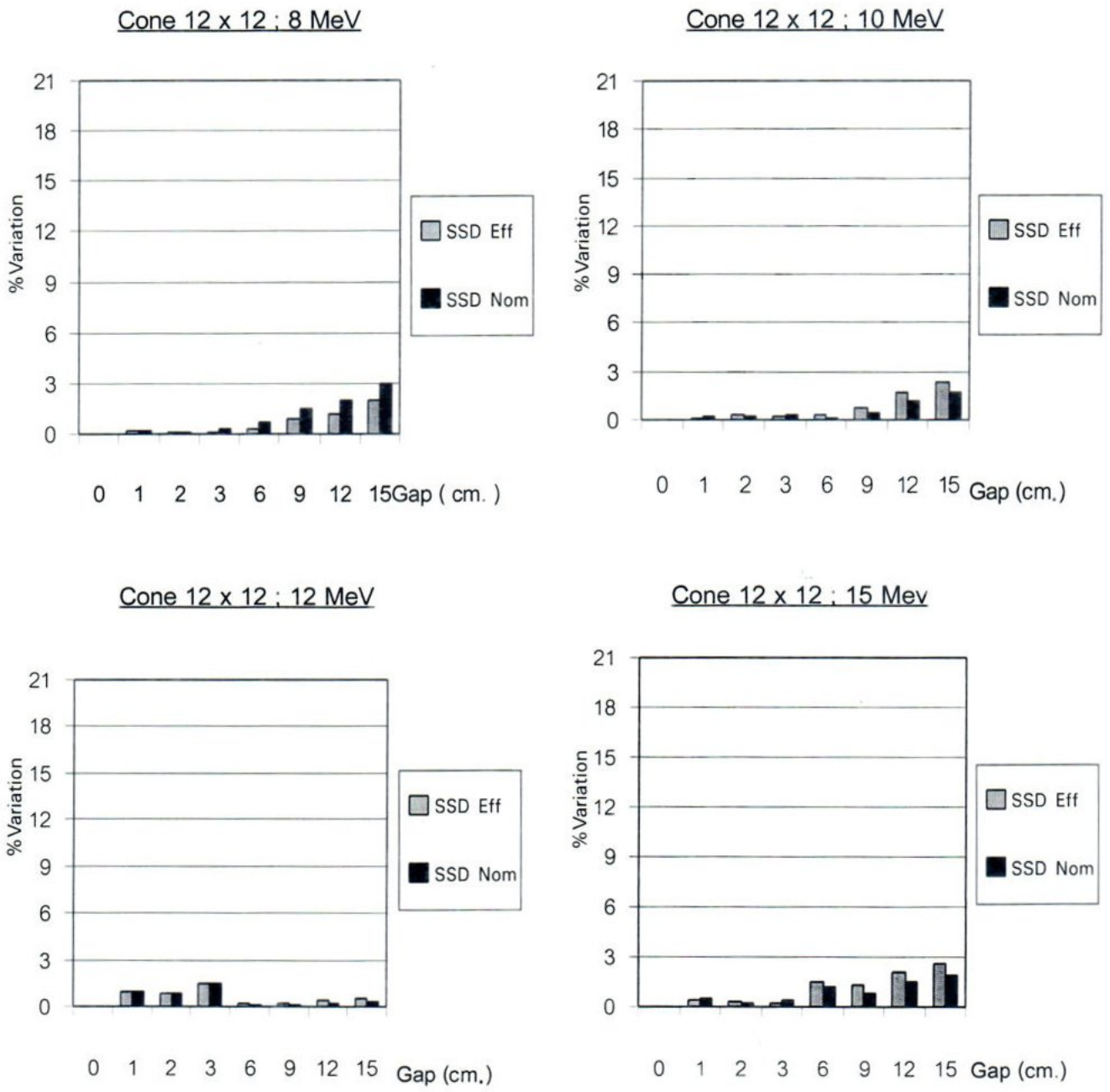

Fig. 6 Curve plotting the percentage of dose variation as a function of gaps in electron field 12x12 cm^2 at all energies

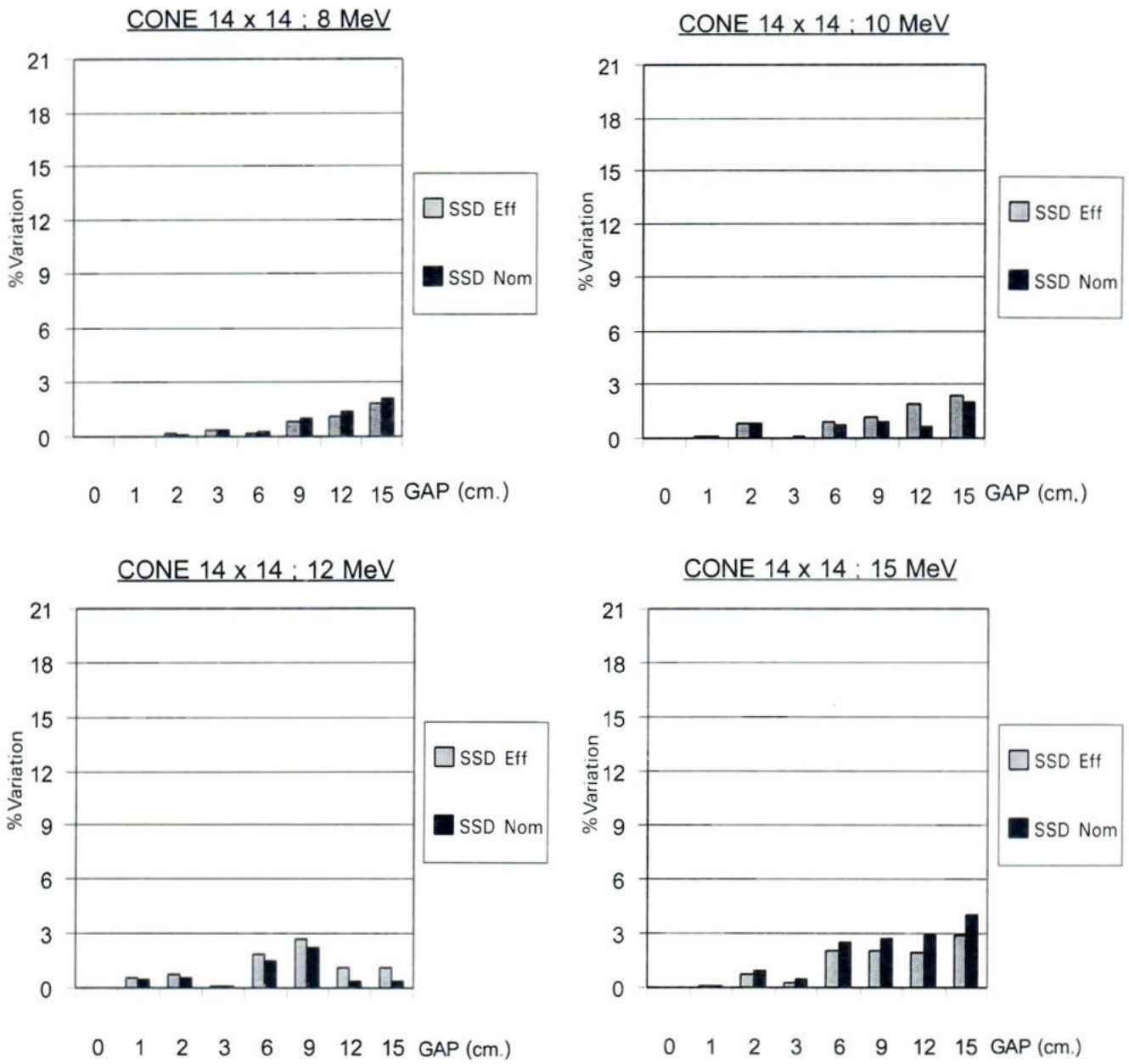

Fig. 7 Curve plotting the percentage of dose variation as a function of gaps in electron field 14x14 cm^2 at all energies

Based on Figure 2 to Figure 7, it could be seen that if the effective SSD is in the ISL calculation, the corrected dose will be fitted within ±3% of the measured dose in all field sizes, all SSD distances and all energies in the study. In contrast with the nominal SSD, the percentage of dose difference will be significantly high in small fields such as 4x4 and 6x6 cm^2 and in large gaps. But it will decreased rapidly with the beam size.As it was seen in 10x10 cm^2 field ,at almost energies, that the dose variation were in ±3% of the measured dose at all gaps. However, nominal SSD in the ISL dose correction are also found to be valid in small fields with in some small gaps. We summarized the maximum gap available for dose correction when a nominal SSD is in the ISL calculation as presented in Table 2.

Table.2 Maximum gap available when a nominal SSD is in the ISL dose correction at extended SSD

Field size (cm^2)	Energy (MeV) 8 MeV	10 MeV	12 MeV	15MeV
4x4	2	3	3	3
6x6	3	3	3	3
8x8	9	9	15	12
10x10	12	15	15	15
12x12	15	15	15	15
14x14	15	15	15	15

DISCUSSION AND CONCLUSION

In this study, we characterize the extended electron point source with the effective SSD method because of its advantages over the method of virtual point source. The effective SSD is measured under more realistic conditions of collimation and phantom scatter. Moreover, it is independent from depth, so the effective SSD that normally determined at d_{max} would be adequate for correcting dose at all depths.[5]

Effective SSD is known to vary with field sizes and strongly depend on the accelerator characteristics. For a given energy, the effective SSD depends strongly on the collimator opening and for a given collimator opening, the effective SSD depends on the energy of the beam.[5,7-9] This investigation, with the difference in electron applicator design, the results agreed with the previous studies in small fields only. In large electron fields (≥ 8x8 cm^2), it showed that the effective SSD were independent from both field size and beam energy.

It can be concluded from this study that, with the effective SSD, the inverse square law correction agreed for all field sizes, all SSDs and all energies. With the nominal SSD , the corrected dose will agree in all gaps, all energies in the study if the field size is equal to or larger than 10x10 cm^2. However, in small fields such as 4x4 and 6x6 cm^2, if the gap in the treatment is not too large, the nominal SSD are found to be valid in dose correction also. Use of the effective SSD or nominal SSD in correcting electron output at extended SSD treatment depends on clinical situation.

REFERENCES

1. ICRU Report 35. Radiation dosimetry: Electron beams with energies between 1 and 50 MeV. International commission on radiation units measurements. Issued 15 September,1984
2. Pohlit W. Dosimetric Zur Betatron-therapie. (Georg Thieme Valag, Stuttgart) 1965
3. Schroder- Babo P. Determination of virtual electron source in a betatron. Acta Radiol 1983; suppl 364:7-10
4. Meyer JA, Palta JR, Hogstrom KR. Determination of relative new electron dosimetry measurements techniques on the Mevatron 80. Med Phys, 1984; 11(5): 670-677
5. Khan FM, Sewchand W, Levitt SH. Effec t of air space on depth dose in electron beam therapy. Radiology, 1978; 126: 249-252
6. Khan FM, Doppke KP, Hogstrom KR, Kutcher GJ, Nath R, Prasad SC, Purdy JA, Rosenfeld M and Werner BI. Clinical electron beam dosimetry: Report of AAPM radiation therapy committee task group No. 25. Med Phys, 1991;18:73-109
7. Jamshidi A, Kuchnir FT, Reft CS. Determination of the source position for the electron beams for a high energy linear accelerator. Med Phys, 1986; 13: 942-948
8. Roback DM, Khan FM, Gibbons JP, Sethi A. Effective SSD for electron beams as a function of energy and beam collimation. Med Phys, 1995; 22: 2093-2095
9. Sweeney LE, Gur D, Bukovitz AG. Scatter component and its effect on virtual source and electron beam quality. Int J Radiat Oncol Biol Phys, 1981;7:967-971

EARLY DETECTION OF BREAST CANCER BY IMAGING

Darunee BOONJUNWETWAT, M.D.[1]

Breast cancer is common among cancers of women and comes the second rank in Thai women. The incidence is increasing in these recent years especially in the fourth to sixth decades. Breast cancer is a major cause of morbidity and mortality. In order to reduce the death rate, breast cancer must be treated at a small size and early stage. This requires that the breasts should be evaluated before there are signs and symptoms to suggest the presence of malignancy. Self breast examination (SBE) and clinical breast examination (CBE) may not help to detect early lesion until it grew large enough to be felt by women and her physician. Imaging modalities are effective tools in early detection of breast cancer including mammography, sonography, magnetic resonance imaging and scintimammography.

Screening mammography has been proved to be the most effective method for early detection of breast cancer. Success or failure of screening depends on the detection time when the tumor is cured or defered death. Many studies have repeatedly shown that prognosis is directly related to the size of the cancer, then the goal of screening mammography is to detect the lesion at early stage when the metastatic disease is free. Early lesion is the status of early growth usually lower than 1 centimeter which could not be evident by palpation. Each tumor does not have synchronized growth, the time for the preclinical phase to clinical event called "Sojourn time". Time between screening is critical importance. The ideal for early detection is to have the screening interval being short. On the other hand, the cost in screening is high that effect the economic status. The American cancer society (ACS) and the National cancer institution (NCI) promote for all women to have screening mammography at a favourable peroid of 40-80 years. They suggest that a high screening frequency results in more life time gained especially at relatively young ages. For the high risk groups are recommened to have screening at the age 35 years. Genetic, envivonmental, and gene-environvmental interactions are factors which induced breast cancer.

The major risk factors for breast cancer are these followings.

- Age after 35
- Early menarch
- Late menopause
- Nulliparity
- Late age at first full term pregnancy (after age 30)
- Affected first degree relative (mother, sister, or daughter)
- Previous history of breast cancer
- Biopsy proof of atypical epithetial proliferation
- Biopsy proof of lobular carcinoma in situ

Mammography should be performed in the right way by the trained technologists in order to obtain good image. Basically, two standard views are required for each breast including mediolateral obilique and craniocaudial views. Additional views including spot compression, cone down or magnification may be necessary for the doubtful lesion. The received radiation dose is low which is in the safety limit. Women should be better informed about the risks of mammographic screening especially for the low dose radiation gained, the compressive effect from the technique and the uncertainty in the diagnosis of carcinoma in situ.

1 Department of Radiology, Faculty of Medicine, Chulalongkorn University, Bangkok THAILAND.

Now a days, the mammographic equipment has been developed by advanced technology in order to reduce the radiation dose and to get very good detail of internal structures. Advanced digital mammography is promising in the future for the quantitative analysis of the radiographic features of microcalcifications and masses that may help the radiologists to improve their specificity. Noteworthy the important factors influenced the early cancer detection are :

1. Good equipment
2. Good technique
3. Good interpretation

BREAST ULTRASOUND

Since the sensitivity of mammographic detection of lesion is reduced in women with dense breasts. The Asian women usually have smaller and dense breasts than the Western women. The normal mammographic breast patterns of Thai women of Chulalongkorn hospital were studied and the result was that 80% of women in the ages of 40 to 60 years have dense breasts. Breast ultrasound has been accepted to be the primary imaging modality in early detection of breast cancer in dense breasts, and widely used in Chinese women. Basically, breast ultrasound is used strictly for diagnosis, the benefits are to distinguish between solid and cystic mass, and to differentiate benign versus malignant lesion. On the otherhand, the microcalcifications can not be detected by ultrasound, then the early cancer presenting with microcalcifications would be missed. Several studies have been reported that 10 to 30% of women who have breast cancer have negative mammograms and for the women who went for biopsy, only 20% to 40% have breast cancer. The major goal of breast ultrasound is to give a more specific diagnosis but not for cancer screening. The development of the advanced ultrasound equipments that provide the excellent resolution and superb color doppler study, help to gain much more informations of the lesion. The main purposes of performing breast ultrasound are :

1. to prevent unnecessary biopsy
2. to obviate "short term" follow up
3. to judge the indeterminate lesion for biopsy
4. to guide needles procedures

MRI is one of the imaging tool in evaluating breast lesion with the requirement of contrast enhancement. Although mammography is accepted to be an effective method of early breast cancer detection, there are some weaknesses that limit the sensitivity and specificity. The factor masking the tumors are including the histologic tumor type, the absence of microcalcifications and the presence of dense breasts. MRI is used as a second level screening technology that may be able to detect early cancers with clinically and mammographically occult cancers. MRI give the additional capability for the diagnostic problem cases, these include :

1. Suspected leaks from silicone implants
2. Follow up multiple known mammographic or sonographic lesions.
3. Women with radiation phobia
4. Strong familial history of breast cancer with dense breasts
5. Metastases thought to be of breast origin but negative mammography

SCINTIMAMMOGRAPHY

PET (position emission tomography) plays an important role in breast imaging providing anatomical imaging method as well as function information with dynamic imaging. Many kinds of radiophamaceutical agents used for scintimammography including ^{201}Tl Cl, Tc^{99m} sesta MIBI and Tc^{99m} MDP were proved to increase the sensitivity and specificity in the cases of palpable masses. The sensitivity and specificity of mammography are lower in young patients, dense breasts, fibrocystic change, dysplasia, implantation, and evaluation after biopsy, surgery or radiotherapy. Scintimammography is introduced for these conditions. The mechanisms of increased uptake in the lesion are hypothesized as :

- changes in secretory function and cell metabolism with calcium accumulated in the necrotic degenerative tissue and modification of permeability.
- increased vascularization, inflammatory change and angiogenesis
- active mitochondria in neoplasm
- hormonal effect

The scintimammograms of breast cancer and some benign conditions with hypercellularity such as fibrocystic disease and fibroadenoma show abnormal increased uptake. To distinguish benign and malignant lesion depends directly on the calculated value of the tumor uptake ratio. A comparative study of breast cancer detection between the scintimammography and mammography in a group of patients of Chulalongkorn hospital, the results confirmed that scintimammography gave more specificity and accuracy for detection of breast cancer larger than 1 centimeter. Scintimammography should be used as a complementary to mammography, especially for the indeterminated lesion, in order to avoid the unnecessary biopsies.

REFERENCES

1. Issues in Breast Imaging. Lippincott's primary care practice 2(2) : 141-8, 1998
2. Kollias J. Sibbering DM, B Lamey RW, Holland PA, Obuszko Z, Wilson AR. Screening women aged less than 50 years with a family history of breast cancer European Journal of cancer. 34(6):878-83, 1998
3. New methods for imaging the breast : techniques, findings, and potential. American Journal of Roentgenology. 164 (1):19-30, 1995
4. Daudt A, Albery AJ, Helzlsouer KJ. Epidemiology, prevention, and early detection of breast cancer. Current opinion in Oncology. 8(6):455-61, 1996
5. Griffiths RI, McGrath MM, Vogel VG. Economic savings and costs of periodic mammographic screening in the work-place. Oncology 10(3):285-9 : discussion 289-94, 1996
6. May DS, Lee NC, Nadel MR, Isenson RM, Miller DS. The National Breast and cervical cancer early detection program : report on the first 4 years of mammography provided to medically underserved women. American Journal of Roentgenology. 170(1):97-104, 1998
7. Napoli M. What do women want to know. Journal of national cancer Institute. Monograph. (22):11-3, 1997
8. Jansen JT, Zoetelief J. Assessment of lifetime gained as a result of mammographic breast cancer screening using a computer model. British Journal of Radiology. 70(834):619-28, 1997
9. Schilling RB, Cox JD, Sharma SR. Advanced digital mammography. Journal of Digital Imaging. 10 (3 Suppl 1):133-5, 1997
10. Mah Z, Bryant HE. The role of past mammography and future intentions in screening mammography usage. Cancer detection and prevention. 21(3):213-20, 1997
11. Lopes MJ, Smart CR. Twenty-year follow up of minimal breast cancer from the breast cancer detection demonstration project. Surgical Oncology Clinics of North America. 6(2):393-401, 1997
12. Newman J. Early detection techniques in breast cancer management. Radiologic technology. 68(4):309-24 fiz 325-8, 1997
13. Weinberg AD, Cooper HP, Lane M, Kripalani S. Screening behaviors and long-term complicence with mammography quidelines. American Journal of preventive Medicine. 13(1):29-35, 1997
14. Hogge JP, Artz DS, Freedman MJ. Update in digital mammography. Critical Reviews in Diagnostic Imaging. 38(1):89-113, 1997

15. Champion V, Miller AM. Recent mammography in women aged 35 and older : predisposing variables. Heath care for women international. 17(3):233-45, 1996
16. Brakelmans CI, Van Gorp JM, Peeters, Collette HJ. Histopathology and growth rate of internal breast carcinoma. Characterization of different subgroups. Cancer 78(6):1220-8, 1996
17. Peer PG, Berbrek AL, Mravnnac M, Hendrites JH, Holland R. Prognosis of younger and older patients with early breast cancer. British journal of cancer. 73 (3):382-5, 1996
18. Roubidoux MA, Lai NE, Paramajul C, Joynt LK, Helvie MA. Mammographic appearance of cancer in the opposite breast : Comparism with the first cancer. American journal of Roentgenology. 16 (11):29-31, 1996
19. Foulkes WD, Narod SA. Hereditary breast cancer and ovarian cancer : epidermiology, genetics, screening and predictive testing. Clinical & investigative Medicine. Medicine clinique at Experimentate. 18(6):473-83, 1995
20. Leitch AM. Controversies in breast cancer screening. Cancer 76 (10 Suppl) : 2064-9, 1995
21. Houn F, Elliott ML, McCrohan JL. The mamography Quality standards Act of 1992. History and philogophy radiologic clinic of North America. 33(6):1059-65, 1995
22. Ronbidoux MA, Helvie MA, Lai NE, Paramagul C. Bilateral breast cancer : early detection with mammography. Radiology 196(2) : 422-31, 1995
23. Jackson VP. The role of US in breast imaging. Radiology 177 : 305, 1990
24. Kolb JM, Lichy J, Newhouse JH. Occult cancer in women with dense breasts. Detection with screening US. Diagnostic yield and tumor characteristics. Radiology 207:191, 1998
25. Jacksm VP, Hendrich RE, Feig SA. Imaging of the radiographically dense breast. Radiology 188:297, 1993
26. Hall FM. Sonography of the breast. Centroversies and opinions. AJR 169: 1635, 1997
27. Chao TC, Lo YE, Chen SC, Chen MF. Prospective sonography study of 3093 breast tumors. Journal ultrasound Med. 18:363-370, 1997
28. Safir J, Zito JL. Gershwind ME, Faegenburg D, Tobin CE, Cayea PD, Wortman WJ, Sclafani LM, Maures VE. Contrast enhanced breast MRI for cancer detection using a commercially available system a perspective. Clinical imaging 22 (3) 162-79, 1998
29. Hulka CA, Kopans DB. Magnetic Resonance Imaging. Breast imaging 2nd ed. By Daniel B, kopans. Lippin cott Raven. Publishers, Philadephia P. 617-635
30. Flanagan FL, Dehdashti F, Siegel BA. PET in breast cancer seminars in nuclear medicine 28(4):290-320, 1998
31. Salvatore M, Del Vecchio S. Dynamic imaging. Scintimammography. European Journal of Radiology 27 Suppl 2:3 259-64, 1998
32. Khalkali I, Iraviha S, Cutrone JA, Diggles LE, Klein SR. Scintimammography with Tc^{99m} sesta MIBI
33. Rebollo AC, Torres - Avisbal M, Espinosa A, Diaz C, Vallejo JA, Pacheco C, Pera C, Mateo A. Evaluation of pulpable breast masses with ^{201}Tl scintigraphy. The British journal of radiology 68:1052-1056, 1995
34. Piccolo S, Lastoria S, Mainolfi C, Muto P, Bazzicalupo L, Salvatore M. Tc99m Methylene Diphosphonate scintimammography to image primary breast cancer. Journal of nuclear medicine 36:5,718-724, 1995

THE CRAZY–PAVING PATTERN; A NONSPECIFIC SIGN ON HRCT CHEST

Piyaporn Limanond; M.D., Orasa Chawalparit; M.D., Trongtum Tongdee; M.D., Poonsook Jitnuson; M.D., Pornpim Fuangtharntip; M.D. and Kobkun Muangsomboon; M.D.

ABSTRACT

Purpose : To report the crazy–paving pattern on High Resolution Computed Tomography (HRCT) chest found in our institute which were caused by various processes other than pulmonary alveolar proteinosis (PAP)

Materials and Methods : From June 1998 to August 1999, 4 patients (3 male and 1 female, mean age 38.5 years, range 23-52 years) with crazy-paving pattern on HRCT chest were diagnosed by 2 radiologists. Retrospective review of the imagings was performed with clinical and pathologic correlation.

Results : The crazy-paving pattern in our institute was caused by various processes, including 1 bronchioloalveolar carcinoma, 1 lipoid pneumonia, 1 PAP and 1 pulmonary hemorrhage.

Conclusion : From our findings, we can conclude that the crazy–paving pattern is only a nonspecific sign on HRCT chest, resulted from multiple causes. Clinical and pathologic correlation are necessary for differential diagnosis.

INTRODUCTION

The crazy–paving pattern on High Resolution Computed Tomography (HRCT) chest was previously known as a characteristic sign of pulmonary alveolar proteinosis (PAP), consisting of geographic areas of ground-glass alveolar infiltration with superimposed smooth thickening of interlobular septa.

Based on open lung biopsy, well-demarcated geographic areas of ground-glass consolidation are explained by filling of alveolar spaces with PAS-positive phospholipoprotein materials whereas superimposed smooth interstitial thickening reflects septal edema and alveolar wall infiltration by lymphocytes and macrophages.

We report 4 cases of crazy-paving pattern on HRCT chest; found in our institute with clinical and pathologic proving not to be caused by only PAP but various causes.

MATERIALS AND METHODS

From June 1998 to August 1999, 4 patients (3 male and 1 female); age range from 23 – 52 years (mean age 38.5 years); showed crazy-paving pattern on HRCT chest. The imagings were blindly reported by 2 radiologists without patho-

Department of Radiology, Faculty of Medicine Siriraj Hospital, Mahidol University, Bangkok 10700, THAILAND

logic correlation.

The HRCT chest of these patients were performed by Philips Tomoscan AVE 1, using 1-mm collimation, high-spatial frequency reconstruction algorithm, 1-second scan time, 120-140 kVp, 150-175 mA and 512x512 matrix size.

Retrospective review with clinical and pathologic proving of these 4 patients were done, showing variation of causes.

RESULTS

Case 1 : a 33-year-old man presented to his primary physician with chronic cough and blood-tinged sputum. A chest radiograph showed minimal fibronodular infiltration at RUL, that was diagnosed to be pulmonary tuberculous infection. He had received anti-TB drugs for 6 months but no clinical improvement. A 1-year subsequent chest radiograph revealed progression of RUL infiltration with an irregular-walled cavity at RUL. The HRCT chest (Fig. 1) demonstrated a geographic area of ground-glass consolidation at the posterior segment of RUL with superimposed smooth thickening of interlobular septa (crazy-paving pattern). A large cavity about 5 x5 cm was demonstrated nearby the consolidation. It had thick irregular wall with internal septation. Bronchoscope and transbronchial biopsy showed bronchogenic carcinoma, non-small cell type.

Case 2 : A 23-year-old man presented with productive cough and progressive dyspnea for 2 months. A chest radiograph showed bilateral alveolar infiltration. Subsequent HRCT chest (Fig. 2) revealed diffuse ground-glass opacity with smooth interlobular septal thickening (crazy-paving pattern) in both lung fields. The pathologic findings from lung biosy highly suggested lipoid pneumonia with interstitial fibrosis.

Case 3 : A 52-year-old man presented with dyspnea for 1 month, showing bilateral interstitial infiltration in chest radiograph. The HRCT chest (Fig. 3) demonstrated discrete geographic ground-glass consolidation with superimposed interlobular septal thickening (crazy-paving pattern) in both lung fields, a highly suggestive sign for PAP. Bronchoscopic and bronchoalveolar larvage findings also supported the diagnosis.

Case 4 : A 46-year-old woman presented to her chest physician with cough and blood-tinged sputum for 3-4 days. No history of weight loss or previous trauma was interviewed. Her chest radiograph showed normal findings but subsequent HRCT chest (Fig. 4) revealed a small area of crazy-paving pattern at the anteromedial basal segment of LLL. Her first bronchoscope revealed an organized hematoma at the basal segment of LLL bronchus without cytologic or histologic evidence of malignancy. Her symptoms were spontaneously improved without any treatment. A 1-week-subsequent bronchoscope showed resolving hematoma with nearby dilated bronchial vessels. Her chest physician believed that the crazy-paving pattern was due to pulmonary hemorrhage from spontaneous rupture of dilated bronchial vessels.

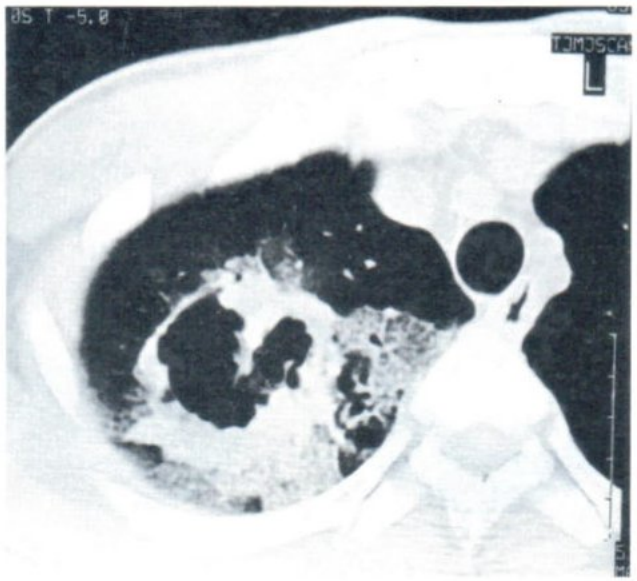

Fig. 1 Bronchogenic carcinoma, non-small cell type. HRCT chest of a 33-year-old man, who presented with chronic cough and blood-tinged sputum, revealed the crazy-paving pattern at the posterior segment of RUL with a nearby large cavity showing thick irregular wall and internal septation. Transbronchial biopsy showed bron chogenic carcinoma, non-small cell type.

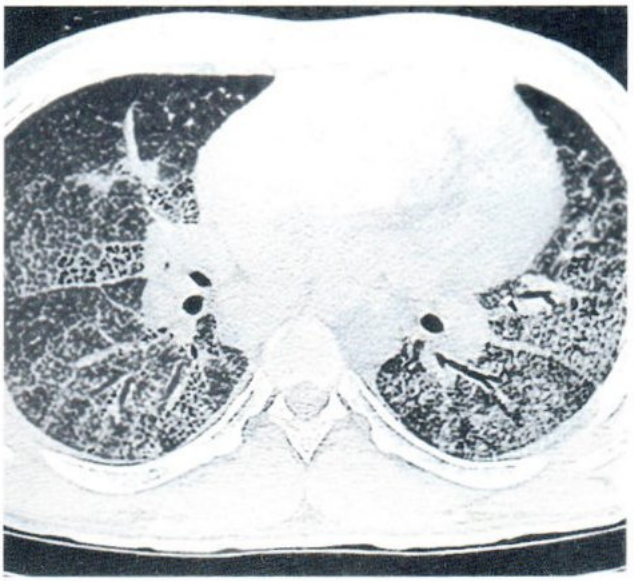

Fig. 2 Endogeneous lipoid pneumonia. HRCT chest of a 23-year-old man, who presented with productive cough and progressive dyspnea for 2 mo., revealed diffuse crazy-paving pattern in both lungs fields. The pathologic findings highly suggested to be lipoid pneumonia.

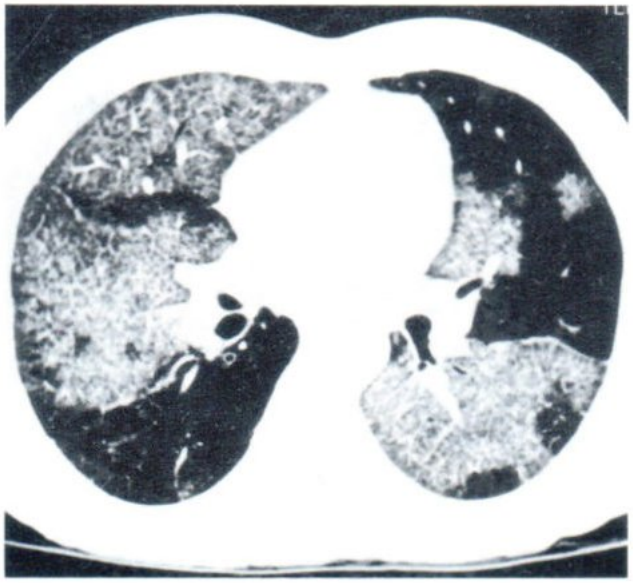

Fig. 3 PAP. HRCT chest of a 52-year-old man, who presented with dyspnea for 1 mo., demonstrated discrete geographic areas of crazy-paving pattern in both lung fields. Pathologic findings supported the diagnosis of PAP.

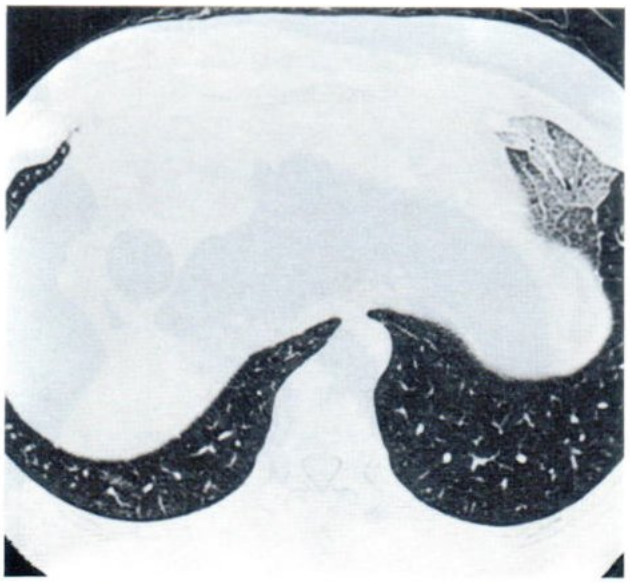

Fig. 4 Pulmonary hemorrhage. HRCT chest of a 46-year-old woman, who presented with cough and blood-tinged sputum for 3-4 days and had spontaneous improvement without any treatment, demonstrated a small area of crazy-paving pattern at the anteromedial basal segment of LLL. Two bronchoscopic studies showed an organized hematoma at the basal segment of LLL bronchus which rapidly dissappeared in 1 wk. and nearby dilated bronchial vessels.

DISCUSSION

Pulmonary alveolar proteinosis (PAP) is an idiopathic disease which associates with dust exposure (silicoproteinosis) and other immunodeficiency. Its pathophysiology is overproduction of surfactant by pneumocyte type 2 with defective clearance of surfactant by alveolar macrophage. Surfactant-filling alveoli cause sharp-demarcated geographic areas of ground-glass consolidation on HRCT chest. The typical pattern of alveolar infiltration in pulmonary alveolar proteinosis is rather symmetrical ground-glass pattern in bilateral lung fields, possibly diffuse or bilateral perihilar areas (bat-wing appearance) with tendency to be prominent at lung bases. Superimposed smooth thickening of interlobular septa are pathologically proved to be septal edema and alveolar wall infiltration by inflammatory cells. Ground-glass consolidation and superimposed interlobular septal thickening cause a well known radiologic sign on HRCT chest called Crazy-Paving Pattern which was previously known as a characteristic sign for PAP. Although Webb et al.[1] suggested that the crazy-paving pattern can be found in other diseases such as pneumocystis and cytomegalovirus infection; until now there is a little information about other causes.

Previously, Tan and Kuzo[3] reported the crazy-paving pattern in a patient with bronchioloalveolar carcinoma; a well differentiated primary lung cancer that associates with preexisting pulmonary scar and fibrosis. Bronchioloalveolar carcinoma arises along peripheral bronchiolar and alveolar walls with absence of an intrinsic bronchial tumor. It has a tendency to spread locally; using lung structure as a stroma (lepedic growth) without disrupting lung architecture. Bronchioloalveolar carcinoma has various radiologic and CT findings such as a single mass, multiple nodules or diffuse (pneumonic) form. Crazy-paving pattern is also one of its findings. Ground-glass opacity reflects alveolar filling of glycoprotein materials from mucous-producing cells. Superimposed interlobar septal thickening represents lepedic growth of tumor cells or lymphatic edema.

Franquet et al.[4] recently reported the crazy-paving pattern in 3 patients with exogeneous lipoid pneumonia. They had a history of aspiration or inhalation of oily substance and subsequent pulmonary inflammation. The CT-pathologic correlation showed that areas of ground-glass consolidation with negative Hounsfield units represented alveolar filling with oily substance and lipid-laden macrophages. Interlobular septal thickening reflected interstitial infiltration with inflammatory cells and variable amount of fibrosis. Due to aspiration cause, the common areas of pulmonary involvement in exogeneous lipoid pneumonia are gravity-dependent areas such as RML and lower lobes. On the contrary, endogeneous lipoid pneumonia has an unknown etiology and not associates with history of external oil used. Pulmonary involvement of endogeneous lipoid pneumonia are also not gravity-dependent areas. Our patient (case 2) had no history of external oil used and showed diffuse crazy-paving pattern in his HRCT chest, compatible with endogeneous lipoid pneumonia.

In case of pulmonary hemorrhage; ground-glass opacity reflected alveolar filling by hemolyzed blood. Interlobular septa in area of consolidation appear thicker and denser than normal, explained by excellent contrast resolution of pulmonary interstitium stand out prominently from the background of low-density material filled alveoli.

We report 4 cases of patients with crazy-paving pattern in HRCT chest, found in our institute which have a variation of causes (1 non-small cell lung cancer, 1 lipoid pneumonia, 1 PAP and 1 pulmonary hemorrhage). Although a small number of patients were included in this study, we can prove that the crazy-paving pattern is only a nonspecific finding which can be found in various processes. Ground-glass opacity represents alveolar filling of low density materials (PAS-positive phospholipoprotein materials in PAP, glycoprotein in bronchioloalveolar carcinoma, oily substance in lipoid pneumonia and hemolyzed blood in pulmonary hemorrhage). Superimposed smooth interlobular septal thickening reflects tumor or inflammatory cell infiltration, septal edema and fibrosis. So pathologic correlation is sometimes important for definite diagnosis. However, there are some clues which can be helpful for differentiation such as previous history, distribution of pulmonary involvement, other associated CT findings and the progression of disease.

Pulmonary alveolar proteinosis (PAP) associates with history of dust exposure (silicoproteinosis) or other immunodeficiency. It has a gradual onset of symptoms with a slow progression of disease. The pattern of ground-glass opacity in PAP are usually symmetrical which is helpful in the differential diagnosis from other diseases. It is common to involve bilateral perihilar areas, prominent at lung bases.

Bronchogenic carcinoma is suspected in elderly patient with preexisting pulmonary scar or fibrosis. Asymmetrical involvement, associated lymph nodes and pleural effusion are helpful in the differentiation from PAP.

Exogeneous lipoid pneumonia is highly suspicious in patient who has a history of aspiration or inhalation of oily substance, contrasting with endogeneous lipoid pneumonia. Clinical course of lipoid pneumonia has a gradual onset and a slow progression like PAP. Exogeneous lipoid pneumonia usually involves asymmetrical gravity-dependent areas such as RML and lower lobes. However endogeneous lipoid pneumonia such as our patient (case 2) was different. He had diffuse ground-glass opacity in both lung fields. Lipoid pneumonia sometimes demonstrates areas of low-attenuated consolidation with negative Hounsfield units (oily substance). However due to reactive inflammation and subsequent fibrosis, oily substance is sometimes obscure and so did our patient.

A remarkable feature of pulmonary hemorrhage is rapid resolution. It sometimes enlarges in early 48-72 hours after its onset (possible having a history of previous trauma) and usually has complete resolution in 2 – 10 days.

CONCLUSION

Crazy-paving pattern is an infrequent finding on HRCT chest. Previously, it was reported as a characteristic finding in pulmonary alveolar proteinosis (PAP). However the more HRCT chest is performed; the more crazy-paving pattern is found. Now it is no longer being a specific sign for PAP but has a variation of causes. Other than pathologic correlation; clinical history, distribution of pulmonary involvement and associated CT findings are necessary for a definite diagnosis.

REFERENCES

1. Webb WR, Müller NL, Naidich DP. High resolution CT of the lung, 2nd edition. 1996
2. Dähnert W. Radiologic review manual, 4th edition. 1999
3. Tan RT, Kuzo RS. High resolution CT findings of mucinous bronchioloalveolar carcinoma : a case of pseudopulmonary alveoar proteinosis. AJR 1997;168:99-100
4. Franquet T, Giménez A, Bordes R et al. The crazy-paving pattern in exogeneous lipoid pneumonia : CT-pathologic correlation. AJR 1998;170:315-317
5. Lee KS, Müller NL, Hale V, Newell JD Jr, Lynch DA, Im JG. Lipoid pneumonia : CT findings. J Comput Assist Tomogr 1995;19 (1):48-51

Message from

Professor Dr. Kawee Tungsubutra

Editor-in-Chief, The Asean Journal of Radiology

Dear Friends ,

This is the 2nd Number of Vol VI of the Asean Journal of Radiology. It has passed the goal of 5 years of regular publication so that our journal will be eligible to be entered into the Index Medicus. The 10th AAR Congress of Radiology has taken place in Bangkok, Thailand on 23-25 March in the year 2000. I have taken the Chair of the President of Asean Association of Radiology which was handed over from Singapore.

I will continue to be the editor of the AAR journal so that it will be admitted into the Index Medicus. After that I am sure that other member committee in the Royal College of Radiology will be able to continue to do the task and improve to the perfection and satisfaction.

I would like to thank to Bracco International for providing the educational grant for starting the Journal in 1955. I would like to thank in person to Dr. Zaini Ibrahim, Dr. Paul Synaeve, Dr. Maria C. Cedrini for his and her kind considerations. I would also like to thank to every body involved in the publishing of the AAR journal to be successful as it is.

Kawee Tungsubutra.

Kawee Tungsubutra
May - August 2000.

AAR Journal of Radiology.
Instructions for Authors.

1. The AAR Journal of Radiology publishes the papers on Radiological Sciences, such as research work, review articles, case reports, innovations in Medical Sciences related to all branches of Radiology, and letters to the editor. The aforementioned materials can be written in English only.

2. The authors have to submit 2 copies of the manuscript and a diskette: **to Prof. Dr. Kawee Tungsubuttra.** 318 Kaweevej Hospital, Taksin Road, Dhonburi, Bangkok 10600, Thailand.

3. The original copy to be submitted must be typed in a double space on one side of the page of 8.1/2" x 11.1/2" paper.

4. The format of the article must include :

a. Title page and address of the author (s)
b. Abstract
c. Introduction (Background)
d. Material and Method
e. Results and discussion (Tables and Illustrations)
f. Acknowledgement (if any)
g. References (Follow the Vancouver style developed by ICMJE)

5. We will provide 25 copies of reprints for the author (s) who submit (s) an article for publication in the AAR Journal.

6. The illustrations and tables must be clearly prepared with legends in English as they are the art works to be reproduced.

7. The authors are reponsible for the contents of the article as to its facts and findings.

8. Ethics.

Paper reporting studies which might be interpreted as human experimentation (e.g. controlled trials) should conform to the standards of the Declaration of Helsinki (see British Medical Journal 1964:2:177) and should indicate that, approval that such studies may proceed, has been granted by the local or hospital Ethics Committee.

When reporting experiments on animals indicate whether the institution's or the National Research Council's guide for, or any national law on, the care and use of laboratory animals was followed.

บริษัท กรงศิลป์วรรณ จำกัด
SONGSITTIVAN CO.,LTD.
Tel. 910-1999 Fax : 910-1888

Research that's more than just state-of-the-*art*

X-ray MRI Ultrasound

Schering offers a wide range of innovative products in all major diagnostic areas.

Our aim is to give you the full benefits of technological advance.

When it comes to MRI, X-ray and Ultrasound, Schering knows how.

Schering Diagnostics

From seeing to understanding

SCHERING (BANGKOK) LTD.
28/19 Changwattana Rd., Pakkred Nonthaburi 11120, Thailand Telephone : (662) 573-0053 (7 Lines) Fax No. : (662) 573-6938, 573-1171